

# STUDY ON NONLINEAR ELASTICO-VISCOUS PULSATILE NANOFLUID SLIP FLOW OVER POROUS CHANNEL STRETCHING SHEET

Thesis Submitted in Fulfilment of the Requirement for the Award of the Degree

of

Doctor of Philosophy

in

Applied Mathematics

by

Md Enamul Karim

Under the Supervision of

Professor Dr. Md. Abdus Samad

and

Professor Dr. Mohammad Ferdows



Department of Applied Mathematics, University of Dhaka  
Dhaka-1000, Bangladesh

Registration No.: 27, Session: 2020-21 (Re-registration)

## CERTIFICATE

This is to certify that the thesis titled "Study on Nonlinear Elastico-Viscous Pulsatile Nanofluid Slip Flow over Porous Channel Stretching Sheet" submitted by PhD researcher Md. Enamul Karim at University of Dhaka, Dhaka is a record of the research work of good faith carried out by him under our supervision and guidance at the Department of Applied Mathematics, University of Dhaka. Mr. Md. Enamul Karim has worked for four years, starting from March 2019, to prepare his thesis in this department as a full-time candidate, and the thesis is, in our opinion, worthy of consideration for the award of the degree of Doctor of Philosophy in Applied Mathematics in accordance with the rules and regulations of this university. The results contained in this thesis have not been submitted elsewhere for the award of another degree.



**Supervisor**

Professor Dr. Md. Abdus Samad

Department of Applied Mathematics, University of Dhaka, Dhaka-1000.




**Joint-Supervisor**

Professor Dr. Mohammad Ferdows

Department of Applied Mathematics, University of Dhaka, Dhaka-1000.

## DECLARATION

I, Md Enamul Karim, hereby confirm that the contents of the recent thesis represent my own work, and all the results organised here are original works. Any ideas or techniques taken from the published works of others have been appropriately acknowledged in accordance with the standard referencing practices. Furthermore, the thesis has never before been submitted for academic review in support of a degree or diploma at another university.

Signed: 

Date: 22-05-23

## **ABSTRACT**

In 1959, Richard Feynman, a renowned physicist, shared the idea of micro-machines at the yearly American Physical Society meeting. Today, it is worth reconsidering these forecasts to see that reality has exceeded imagination. Conversely, this journey to today's ultrathin devices is not expected to continue unabated. Already, designers of mechanics, electronic and computer devices are feeling the bottleneck they have reached. Unexpectedly, the bottleneck is not electronic or mechanical but thermal. The movement towards machines that operate at increasing speed results in greater and greater heat flow. Remarkably, the problem of heat dissipation is not only a microscale but also a macroscale issue. The problem of heat transfer is similar in controlled bioreactors, high- and medium-temperature fuel cells, and large transport vehicles. Consequently, the cooling requirements of cutting-edge technologies necessitate a radical new approach at this pivotal moment in heat transfer technology's history.

Because refrigerants are such poor heat conductors, all previous efforts to develop cooling technology have been, in a nutshell, "penny wise and pound stupid." This is because, while every effort has been made to advance transport processes. This inherent insufficiency of coolants indicates that it is expected that the current level of heat removal can be significantly improved by designing more conductive fluids. Particles in nanofluids are so small and make up such a small percentage of the total volume that they don't interact with one another, so they're completely stable and don't cause any issues with heat transfer. This finding sparked a flurry of research in the area, with scientists primarily using experimentation to back up the huge potential of nanofluids and also making theoretical attempts to explain the phenomenon.

The enthusiasm of the research community in the nanofluid area was evident from the number of papers published. The main focus of the current research is on nanofluids. Some relevant articles or kinds of literature, which are studied, explored and reviewed cautiously, have been arranged in Chapter 1. Some elementary information and introductory text have been incorporated in Chapter 2 describing non-Newtonian nanofluids, giving an adequate background in

these areas. The other important issue is the incorporation of basic numerical techniques to solve BVPs. The rest of chapters 3-6 are the discussions of some nanofluid models incorporating non-Newtonian viscoelastic phenomena. The large number of references related to this thesis has been organised as an appendix which can assist as a glossary for the research community.

## **ACKNOWLEDGEMENTS**

First, I would like to convey my sincerest gratitude to my supervisor, Professor Dr. Md. Abdus Samad, Department of Applied Mathematics, and Dean, Faculty of Science, University of Dhaka, Dhaka-1000, Bangladesh, for his guidance and advice that carried me through all the stages of my research. His profound perceptions and encouragement helped to make my effort successful.

I would also like to give special appreciation to my joint supervisor, Professor Dr. Mohammad Ferdows, Department of Applied Mathematics, University of Dhaka, Dhaka-1000, Bangladesh, for his constructive ideas and discussions in developing the current project.

Furthermore, I am thankful to all the departmental teachers, particularly Professor Dr. Md. Shawkat Ali, Chairman, Department of Applied Mathematics, University of Dhaka, for helping me to carry out my work triumphantly.

I wish to utter my honest gratitude to colleagues Dr Md. Abdulla Al Mahbub, Md. Maruf Hasan, and Zillur Rahman, Department of Mathematics, Cumilla University, for sharing their support and helpful suggestions throughout my work.

Especially, I am delighted to the Ministry of Science and Technology, Government of the People's Republic Bangladesh, for awarding me a National Science and Technology (NST) research fellowship for PhD research.

Finally, I must state my deep acknowledgements to my parents and my spouse for providing me with dedicated support and endless inspiration throughout my study time and through researching and writing this thesis.

## TABLE OF CONTENTS

### List of Tables

### List of Figures

<b>Chapter 1:</b>	<b>Introduction</b>	1
1.1	Literature Review . . . . .	1
1.2	Research Objective . . . . .	6
1.3	Thesis Framework . . . . .	7
<b>Chapter 2:</b>	<b>Research Background</b>	10
2.1	Fluid Terminologies . . . . .	10
2.1.1	Fluids . . . . .	10
2.1.2	Boundary Layer Concept . . . . .	13
2.1.3	Magnetohydrodynamics (MHD) . . . . .	16
2.1.4	Application of MHD . . . . .	17
2.1.5	Heat Transfer . . . . .	18
2.1.6	Nanofluids . . . . .	21
2.1.7	Thermal Transport Properties of Nanofluids . . . . .	24
2.1.8	Application of Nanofluids . . . . .	29
2.1.9	Mass Transfer . . . . .	35

2.1.10	Newton's Law of Viscosity . . . . .	35
2.1.11	Newtonian Fluids . . . . .	37
2.1.12	Non-Newtonian Fluids . . . . .	38
2.2	Governing Principles of Physical Aspects . . . . .	40
2.2.1	Formation of the Model Equations . . . . .	42
2.2.2	Magnetic Field Effect . . . . .	43
2.2.3	Hall Current Effect . . . . .	44
2.3	Viscoelastic Fluid Model . . . . .	46
2.3.1	Second-Grade Fluid Model: . . . . .	46
2.3.2	Upper Convected Maxwell (UCM) Fluid Model . . . . .	49
2.3.3	Couette Parallel Flow . . . . .	54
2.4	Dimensional Analysis . . . . .	54
2.5	Boundary–Layer Approximation . . . . .	57
2.6	Dynamic Similarity Analysis . . . . .	57
2.6.1	Lie Symmetry Analysis . . . . .	58
2.7	Dimensionless Parameters . . . . .	60
2.8	Numerical Technique . . . . .	66
2.8.1	Finite Difference Method (FDM) . . . . .	66
2.8.2	Boundary Value Problem Solver <i>bvp4c</i> in MATLAB . . . . .	72
2.8.3	Nachtsheim-Swigert Shooting Method . . . . .	74
<b>Chapter 3:</b>	<b>Magneto Hall Effect on Unsteady Elastico-Viscous Nanofluid Slip Flow in a Channel in Presence of Thermal Radiation and Heat Generation with Brownian motion</b>	<b>81</b>



3.1	Introduction . . . . .	81
3.2	Mathematical Formulation . . . . .	83
3.3	Results and Discussion . . . . .	87
3.4	Conclusions . . . . .	92
<b>Chapter 4:</b>	<b>Numerical Study of the Effect of Variable Viscosity on Unsteady Pulsatile Nanofluid Flow through a Couette Channel of Stretching Wall with Convective Heat Transfer</b>	<b>93</b>
4.1	Introduction . . . . .	93
4.2	Mathematical Model . . . . .	95
4.3	Numerical Analysis . . . . .	99
4.4	Results and Discussion . . . . .	100
4.5	Conclusions . . . . .	106
<b>Chapter 5:</b>	<b>Analysis for Elastico-viscous Nanofluid Flow in a Channel Integrating Thermal Relaxation Time Using Two Parameters Lie Group Transformation</b>	<b>107</b>
5.1	Introduction . . . . .	107
5.2	Model Equations . . . . .	111
5.3	Method of Transformations . . . . .	116
5.4	Numerical Method . . . . .	119
5.5	Results and Discussion . . . . .	119
5.6	Conclusions . . . . .	127
<b>Chapter 6:</b>	<b>Effect of Brownian Diffusion on Squeezing Elastico-viscous Nanofluid Flow with Cattaneo-Christov Heat Flux Model in a Channel with Double Slip Effect</b>	<b>128</b>

6.1	Introduction . . . . .	128
6.2	Mathematical Model . . . . .	131
6.3	Numerical Method . . . . .	135
6.4	Results and Siscussion . . . . .	136
6.5	Conclusions . . . . .	142
<b>Chapter 7:</b>	<b>Conclusion</b>	<b>144</b>
7.1	Summary . . . . .	144
7.2	Future study . . . . .	145
<b>Appendix A:</b>	<b>Nomenclature</b>	<b>147</b>
<b>Appendix B:</b>	<b>Research contribution from the current thesis</b>	<b>150</b>
<b>References</b>		<b>170</b>

## LIST OF TABLES

2.1	Thermo-physical properties of base fluids and nanoparticles . . . . .	28
2.2	Dynamical viscosity of base fluids . . . . .	28
2.3	Entities commonly used in fluid mechanics and their dimensions . . . . .	56
3.1	Skin friction coefficients $C_{fx}$ , $C_{fz}$ , the local Nusselt number $Nu$ and Sherwood number $Sh$ for several parameters. . . . .	91
4.1	Thermophysical properties of water as the base fluid and silver as the nanoparticles	97
4.2	Comparison of different values of $Bi$ and $\beta$ taking $\varphi = 0$ , $\varepsilon = 0$ , $\gamma = 0$ , $M = 0$	100
4.3	Physical properties of $Ag$ -water nanofluid for different $\varphi$ . . . . .	101
4.4	Skin Friction and Nusselt Number with parameters variations: $Pr = 6.2$ , $Le = 1$ , $Nb = 0.4$ , $Nt = 0.16$ , $Ec = 1$ , $Bi = 1$ , $M = 0.5$ , $\gamma = 0.1$ , $A = 2$ , $\varepsilon = 2$ , $\Omega = 15^\circ$ for different values of $\varphi$ and $\beta$ for pulsatile pressure gradient . . . .	106
5.1	Thermophysical properties of water and different nanoparticles . . . . .	114
5.2	Comparison of local Nusselt number for several values of $\varphi$ . . . . .	119
5.3	Heat transfer ( $Nu$ ) in $Ag$ -water nanofluid for different values of $\beta_S$ and $\beta_T$ . .	125
5.4	Heat transfer ( $Nu$ ) in $TiO_2$ -water nanofluid for different values of $\beta_S$ and $\beta_T$ .	125
6.1	Comparison for skin friction coefficient, local Nusselt number and local Sherwood numbers for different values of $Sq$ when $Pr = Ec = \gamma_u = 1.0$ , $\delta = 0.1$ .	136
6.2	Skin friction ( $C_f$ ) for different values of $Sq$ and $\beta_S$ at the upper ( $\eta = 1$ ) and lower ( $\eta = 0$ ) plates for classical Fourier ( $\beta_T = 0$ ) and Cattaneo Christov ( $\beta_T = 0.3$ ) heat fluxes . . . . .	142
6.3	Nussult number ( $Nu$ ) for different values of $Sq$ and $\beta_S$ at the upper ( $\eta = 1$ ) and lower ( $\eta = 0$ ) plates for classical Fourier ( $\beta_T = 0$ ) and Cattaneo Christov ( $\beta_T = 0.3$ ) heat fluxes . . . . .	142

## LIST OF FIGURES

2.1	Boundary layer at a flat plate at zero incidences (schematic). . . . .	14
2.2	Boundary layer formulation. . . . .	15
2.3	Geometrical configuration of viscosity . . . . .	36
2.4	Newtonian and Non-Newtonian Fluid . . . . .	39
2.5	Space-Time index notation . . . . .	68
2.6	Finite difference space grid . . . . .	71
2.7	Finite difference space grid . . . . .	74
2.8	Algorithm of Nachtsheim-Swigert shooting method . . . . .	80
3.1	Physical model . . . . .	84
3.2	Primary velocity profile for $K$ . . . . .	88
3.3	Secondary velocity profile for $K$ . . . . .	88
3.4	Temperature profile for $Q$ . . . . .	89
3.5	Volume fraction profile for $Q$ . . . . .	89
3.6	Primary velocity profile for $\alpha$ . . . . .	89
3.7	Secondary velocity profile for $m$ . . . . .	89
3.8	Temperature profile for $R$ . . . . .	90
3.9	Volume fraction profile for $R$ . . . . .	90
3.10	Primary velocity profile for $N_B$ . . . . .	90
3.11	Temperature profile for $N_B$ . . . . .	90
3.12	Volume fraction profile for $N_B$ . . . . .	91
3.13	Concentration profile for $N_B$ . . . . .	91
4.1	Physical configuration and coordinate system . . . . .	95
4.2	Velocity profiles for $\tau$ at different space . . . . .	102
4.3	Velocity profiles for different $\varphi$ . . . . .	102
4.4	Velocity profiles for different $\beta$ . . . . .	102

4.5	Velocity profiles for different $\gamma$ . . . . .	102
4.6	Temperature profiles for different $\varphi$ . . . . .	103
4.7	Temperature profiles for different $\beta$ . . . . .	103
4.8	Temperature profiles for different $Bi$ . . . . .	103
4.9	Temperature profiles for different $\gamma$ . . . . .	103
4.10	Concentration profiles for different $\varphi$ . . . . .	104
4.11	Concentration profiles for different $\beta$ . . . . .	104
4.12	Concentration profiles for different $Bi$ . . . . .	104
4.13	Concentration profiles for different $\gamma$ . . . . .	104
5.1	Physical model . . . . .	112
5.2	Temperature profiles for different water-based nanofluids . . . . .	120
5.3	Temperature profiles for nanoparticle shape factor $n$ . . . . .	120
5.4	Temperature profiles for nanoparticle volume fraction $\varphi$ . . . . .	120
5.5	Velocity profile for Maxwell number $\beta_S$ . . . . .	120
5.6	Temperature profile for Maxwell number $\beta_S$ . . . . .	121
5.7	Velocity profile for magnetic field parameter $M$ . . . . .	121
5.8	Temperature profile for magnetic field parameter $M$ . . . . .	122
5.9	Velocity profile for momentum slip parameter $\varepsilon_u$ . . . . .	122
5.10	Temperature profile for momentum slip parameter $\varepsilon_u$ . . . . .	123
5.11	Temperature profile for thermal slip parameter $\varepsilon_T$ . . . . .	123
5.12	Temperature profile for Biot number $Bi$ . . . . .	124
5.13	Nusselt number at $\eta = 0$ for thermal relaxation parameter ( $\beta_T$ ) . . . . .	126
5.14	Nusselt number at $\eta = 1$ for thermal relaxation parameter ( $\beta_T$ ) . . . . .	126
5.15	Temperature profile for thermal relaxation parameter ( $\beta_T$ ) . . . . .	126
6.1	Physical model . . . . .	133
6.2	$N_B$ effect on the profiles of (a) temperature and (b) concentration . . . . .	137
6.3	$Sq$ effect on the profiles of (a) primary velocity and (b) transverse velocity. . . . .	137
6.4	$Sq$ effect on the profiles of (a) temperature and (b) concentration. . . . .	138
6.5	$\beta_S$ effect on the profiles of (a) primary velocity and (b) secondary velocity. . . . .	138
6.6	(a) $\varepsilon_u$ effect on transverse velocity profile and (b) $\gamma_u$ effect on primary velocity profile. . . . .	139
6.7	$\gamma_u$ effect on the profiles of (a) transverse velocity and (b) temperature. . . . .	140

- 6.8  $\varepsilon_u$  effect on the profiles of (a) primary velocity and (b) secondary velocity. . . . 141
- 6.9 (a)  $\varepsilon_u$  effect on the temperature profile and (b)  $\varepsilon_T$  effect on the temperature profile. 141

# CHAPTER 1

## INTRODUCTION

### 1.1 Literature Review

The study of fluid motion is known as fluid dynamics. Gases, liquids, and ionised gases (plasma) are all considered fluids. As a branch of plasma physics and continuum mechanics, Magneto-hydrodynamics (MHD) combines the study of the flow of liquids called hydrodynamics and the study of electromagnetism. Although the concepts of magnetism and fluid dynamics were developed early in the 20th century, MHD did not emerge as a distinct field of study until the late 1930s and early 1940s. Thus, while physicists like Faraday [1] conducted a few unique experiments in the 19th century attempting to measure the voltage across the Thames persuaded by its wave through the earth's magnetic field, the subject lagged until the turn of the century when astrophysicists appreciated how pervasive magnetic fields and plasmas are throughout the earth. In his classic paper published in 1942, engineer-astrophysicist Alfvén [2] devised the term MHD, heralding the birth of a fully formed MHD. He found MHD waves emanating from the sun. These waves are the result of disturbances that travel through a conducting fluid and a magnetic field at the same time.

The current development for applying magnetofluid dynamics is towards a strong magnetic field (so that the influence of the electromagnetic force is noticeable) and towards a low gas density (as in spaceflight and nuclear fusion research). At roughly the same time, geophysicists began to hypothesise (first proposed by Larmor [3] in 1919) that the earth's magnetic field was created by a dynamo action within the liquid metals of its core. Ostrach [4], the originator of the convection flow theory, used an integral approach for the similarity solution of transient free convection flow over a semi-infinite perpendicular wall and wrote a technical note about it. Goody [5] considered the influence of radiative transfer on a neutral fluid. For incompressible

constant property flat plate boundary layer flow, Rossow [6] published the first academic work on the topic. His research showed that applying a transverse magnetic field to the fluid significantly decreased skin friction and heat transmission.

Sakiadis [7] studied the flow of a boundary layer over a moving solid wall. The entrainment of ambient fluid makes this boundary layer flow situation very different from the classical Blasius problem of boundary flow over a semi-infinite plane plate. Crane [8] seemed to initiate the study of boundary layer flow due to an elongating plate in an ambient fluid. By extending a flat sheet with a velocity that varies linearly with distance from a fixed point, he provided a closed analytical form of a similarity solution for the steady boundary layer flow. Sparrow and Chess [9] described a parameter called the Rosseland approximation for describing the radiation heat flux in the energy equation. The MHD forced and free convection past a vertical porous plate was analysed by Soundalgekar *et al.* [10]. Using numerical methods, Raptis and Perdikis [11] investigated free convection flow in a porous medium bounded on all sides by a vertical, semi-infinite porous plate. Laminar boundary layer flow with suction/injection was investigated by Mansour [12] over a horizontal, continuously moving sheet with mixed convection and thermal radiation interacting. Heat transfer from a burgeoning exterior with a varying heat flux was precisely solved by Lin and Chen [13].

Jha [14] investigated how a homogeneous transverse magnetic field interacts with natural convection to produce an unsteady Couette flow. Pop *et al.* [15] investigated the flow over a stretching sheet near a stagnation point, taking the effect of thermal radiation. Ferdows *et al.* [16] showed a similarity solution for MHD flow through the vertical porous plate with suction. They applied a uniform magnetic field normal to the plate and investigated the effect of various parameters on the velocity and temperature fields across the boundary layer. Jordán [17] studied radiation and dissipation effects on MHD unsteady free convection over the vertical porous plate using the Network Simulation Method. Samad and Mohebujjaman [18] examined the relationship between mass transfer and MHD boundary layer flow in a porous medium subjected to a constant heat flux from an adjacent vertical wall. In the presence of a magnetic field and



convective heat exchange at the plate with the surroundings, Makinde [19] researched the MHD boundary layer flow with heat and mass transfer past an advancing erected plate.

Efficient, accurate and stable numerical methods for solving fluid flow problems, heat and mass transfer processes, chemical reactions and turbulent phenomena are highly important in many industrial applications. Nowadays, computer-based computation of complex issues may provide a cost-effective, quick and sufficiently reliable method in many cases. Sometimes, the computational approaches may also be an alternative or a complement to experimental investigations. Pavar *et al.* [20] discussed the convective MHD flow carried over a permeable exponentially prolonging surface, giving importance in clinical and medical research to generate 3D anatomical images from nuclear magnetic resonance signals. Li *et al.* [21] investigated the axisymmetric transient squeezing MHD flow of the Newtonian non-conducting fluid through a porous system retaining the slip condition at the plate boundary.

Ultrahigh-performance cooling in engineering and industrial technologies is a vital part of the imperative issues in research today. With the mounting demand for resourceful cooling systems, more effective coolants are essential to maintaining the temperature of heat-generating engines and engineering devices such as electronic machinery below protected limits. Most common industrial fluids such as water, ethylene, glycol, toluene or oil generally have poor heat transfer characteristics owing to their low thermal conductivity [22]. As competition grows on a global scale, industries will need to upgrade modern heat transfer fluids to have much higher thermal conductivities than are currently on the market. Nanofluids are newly invented industrial fluids with developed thermal conductivity at deficient particle concentrations than conventional fluids [23]. These artificial fluids are made by stably suspending and uniformly dispersing a few metallic or nonmetallic particles, which are ultrafine and nanostructured, in ordinary heat transfer fluids. The most important point is that nanostructured materials exhibit different and unique thermal properties as compared to bulk materials with the same compositions [24]. Choi [25] first established the concept of nanofluids in 1995 to generate engineering fluids with enhanced transport properties and higher heat transfer performance. Undoubtedly, the nanofluids

have superior wetting, spreading, and dispersal properties on a solid surface and are more stable than conventional fluids [26]. Many researchers have investigated nanofluids for thermal conductivity enhancement [27, 28, 29, 30]. An experimental study conducted by Lomascolo *et al.* [31] revealed that the thermal conductivity also depends on the concentration, size, shape and material of the nanoparticles.

In recent times, the flow analysis of nanofluids has been the topic of extensive research due to its characteristic of increasing thermal conductivity in the heat transfer process. Consequently, a new advanced branch of science, called Nanoscience, is revealed by discussing the materials on an atomic or molecular scale by synthesis, characterisation, exploration or exploitation of nanostructured materials [32, 33, 34, 35]

In general, the heat transfer features of nanofluids can be predicted by employing two main approaches, namely the single-phase model (e.g., homogeneous nanofluid model) and the two-phase mixture model (e.g., non-homogeneous nanofluid model). In the case of the single-phase model proposed by Tiwari and Das [36], the homogenous distribution of volume fraction for nanofluids express their thermos-physical features as functions of the thermo-physical properties of the base fluids and the nanoparticles [37, 38]. Hence, this model provides the solutions to the conservation equations for nanofluids. Moreover, the nanoparticles are assumed to be in thermal equilibrium with the base fluid, distributed uniformly within the base fluid and move with the same velocity, in which the nanoparticle dynamics are neglected completely. Furthermore, the single-phase model adopts the momentum and energy balance equations of the base fluid as those of the nanofluid, only with the modification of thermo-physical properties caused by the nanoparticles [39, 40].

In Buongiorno, two-phase non-homogeneous model [41], the significant enhancement in the heat transfer rate is due to the improvement of the thermal conductivity, caused by the combined influence of fluid particle slip mechanisms, Brownian diffusion and thermophoresis. In the two-phase approach, the particle relations are added to the fluid conservation equations in which the nanofluid can be treated as a two-component non-homogeneous mixture, including the base fluid

and the nanoparticles. [42, 43, 44, 45]. Various purposes of nanofluids originated in industrial and engineering premises, primarily in the heat conversation devices design, accelerators, MHD generators, etc. [46, 47, 48].

Fluids that do not obey Newton's law of viscosity are called non-Newtonian fluids. A fascinating and unsettled tribological subject entails the viscoelasticity impact on thin-film flows. The preparation of mixing polymers with mineral lubricants, known as multi-grade lubricants, has been renowned since the mid-1990s [49, 50, 51]. These mixtures drive the consequential oils to behave like non-Newtonian fluids by performing a viscosity dependency on the shear rate. The classic Newtonian prototype covering the Navier-Stokes equations is unable to exhibit the extremely non-linear bondings between tangential stress and strain rate of non-Newtonian lubricants. Oldroyd [52], Beard and Walters [53], and Rajagopal *et al.* [54] are the pioneers of second-grade viscoelastic fluid models. They have developed the boundary layer theory for second-grade fluids and have motivated researchers to explore these kinds of fluids with various conditions and situations. Rajagopal *et al.* [55] presented an investigation of incompressible second-order fluid flow over a stretching plate. The problem had a bearing on some polymer processing applications, such as the continuous extrusion of a polymer sheet from a die.

A study of the series solution of unsteady 2nd-grade nanofluid towards a stretching plate is prepared by Ramzan, and Bilal [56], taking the effects of mixed convection and thermal radiation into account. It was observed that temperature and solutal distributions show similar behaviour for the thermophoresis diffusion, but the opposite tendency is noted in the case of Brownian motion diffusion. Majeed *et al.* [57] analysed the Soret and Dufour effects on the two-dimensional flow of second-grade fluid due to stretching cylinder subjected to thermal radiation. Yavuz *et al.* [58] proposed a qualitative study for the fractional second-grade fluid described by the classical Caputo fractional operator.

Lie group symmetry analysis is an effective technique to find similarity solutions to given model equations.  $m$  independent variables of a PDE are reduced to  $(m - 1)$  independent variables using Lie group analysis. Norwegian mathematician Sophus Lie (1842-1899) developed

a classic Lie group transformation scheme to discover invariant and similarity solutions [59]. A power-law fluid's transient flow was analysed by Akgül and Pakdemirli [60] using Lie group symmetry. The boundary layer flow of a Powell-Eyring fluid was characterised by Jalil and Asghar [61] using the Lie group symmetry analysis. To analyse the heat and mass transfer in a Powell-Eyring fluid flow across a stretched wall, Rehman *et al.* [62] used the scaling group of transformations, a special case of the Lie group symmetry. Researchers Afify and El-Aziz [63] looked into the scaling group for the flow and heat transfer behaviour in a power-law nanofluid. Roşca *et al.* [64] examined MHD double-diffusive convection through a vertically stretching and contracting permeable sheet using the Lie group symmetry approach. Ogunseye *et al.* [65] investigated the heat transfer in a Powell–Eyring nanofluid flow over an elongating plate using the nanofluid viscosity and thermal conductivity models derived from experimental data, applying Lie group analysis to reduce the model equations to a system of coupled differential equations.

## 1.2 Research Objective

Researchers have examined nanofluids and viscoelastic fluids in a wide variety of geometries, including flat, porous, and stretching sheets. However, to our knowledge, a few research works have been found on the nanofluids flow in a squeezing parallel plate. Therefore, the main objective of the recent thesis is a theoretical investigation of non-linear elastico-viscous pulsatile nanofluid boundary layer flow and heat transfer over a porous squeezing channel having a stretching wall in the presence of a magnetic field.

### Aims:

The specific aims of the study are as follows:

- To investigate the unsteady, laminar, incompressible nanofluid flow.
- To incorporate:
  - i) magnetic field effect
  - ii) viscoelastic non-Newtonian fluid

- iii) convective boundary surface
  - iv) Brownian motion and thermophoresis diffusion
  - v) Cattaneo-Christov heat flux
  - vi) pulsatile pressure
  - vii) unsteady squeezing channel.
- To construct the physical model considering Cartesian coordinates.
  - To derive mathematical models with different flow geometries for viscoelastic nanofluids by considering the impact of MHD.
  - To introduce Lie group transformation.
  - To apply the methods of shooting and finite difference and bvp4c function available in MATLAB for the numerical solution of the governing mathematical models.
  - To express the graphical presentation derived from numerical data with the help of the Tecplot 360.
  - To determine the effects of the flow control parameters on fluid velocity, temperature, and nanoparticle concentration distributions.
  - To analyse the numerical outcomes of the flow control parameters on fluid velocity, temperature, and nanoparticle concentration distributions.
  - To work out the dynamics of important physical quantities like the drag coefficient, heat transfer rate, mass transfer rates and density number for different physical scenarios.

### **1.3 Thesis Framework**

The title of the current thesis is “Study on Nonlinear Elastico-Viscous Pulsatile Nanofluid Slip Flow over Porous Channel Stretching Sheet”. Besides of introduction in Chapter 1 and the

literature review in Chapter 2, the major part of the thesis consists of six chapters, in which a precise problem is modelled and researched. Chapter 1 provides a brief analysis arranged from numerous research articles, journals, proceedings, and books concerning the current thesis materials.

In Chapter 2, the theoretical review is arranged to achieve knowledge of the basic concepts of nanofluid dynamics. It is an essential part of the study to better understand the behaviour of a particle in flow. This chapter covers definitions and a brief discussion of MHD and nanofluids, their important applications, heat transfer, Lie group analysis, and magnetic field. The solution techniques, the Finite difference method (FDM) and the shooting method have been described in detail. The boundary value problem solver `bvp4c` function technique in MATLAB is revised here. Obviously, this chapter provides a solid foundation for the next chapters to come.

Chapter 3 is titled “Magneto Hall Effect on Unsteady Elastico-Viscous Nanofluid Slip Flow in a Channel in Presence of Thermal Radiation and Heat Generation with Brownian motion”. In this chapter, the parametric behavior of magneto-hydrodynamic flow of elasto-viscous nanofluid in a channel with slip condition in the presence of dynamic effects of Hall current, thermal radiation, heat generation and Brownian motion is studied. In order to get primary and secondary velocities, temperatures, nanoparticle volume fraction, and concentration distributions within the boundary layer entering the issue, we solve the governing equations numerically using the implicit Finite Difference Method (FDM). [66]

Chapter 4 is titled “Numerical Study of the Effect of Variable Viscosity on Unsteady Pulsatile Nanofluid Flow through a Couette Channel of Stretching Wall with Convective Heat Transfer”. In this analysis, the nanofluid flow is motivated by the pressure gradient. The objective is to analyse the temperature-dependent viscosity effect on pulse-driven nanofluid flow’s heat and mass transfer characteristics. Solutions have been carried out employing the finite difference method (FDM), and the results have been displayed graphically and in tabular form with the significant agreement. [67]

Chapter 5 is titled “Analysis for Viscoelastic Nanofluid Flow in a Channel Integrating Ther-

mal Relaxation Time Using Two Parameters Lie Group Transformation”. The current research aims to explore the flow flux of the time-dependent Maxwell viscoelastic nanofluid pressed into two parallel walls with stretched porous surfaces by integrating the CCHF theory to describe the thermal temporal relaxation factor. The model equations combined with the boundary conditions are solved numerically using the collocation method developed by a MATLAB package known as *bvp4c*. [Submitted]

Chapter 6 is titled “Effect of Brownian diffusion on squeezing elastico-viscous Maxwell nanofluid flow with Cattaneo-Christov heat flux model in a channel in the presence of double slip effect”. The current work aims to analyze the effect of the thermal relaxation factor on the flow flux of time-dependent Maxwell viscoelastic nanofluid squeezed in rotating parallel plates with a porous stretched surface incorporating the Cattaneo-Christov heat flux model. Equations combined with the boundary conditions are solved numerically using finite difference code developed by a MATLAB boundary value problem solver known as *bvp4c*. [68]

The bibliography section arranges all the references cited throughout the thesis.

## CHAPTER 2

### RESEARCH BACKGROUND

The main content of this section is to review the terminologies concerned by the current thesis. A detailed review of MHD, nanofluid and viscoelastic fluid is quantitatively prepared. The governing principles of physical aspects, dimensional analysis and numerical techniques are precisely synthesized. The problem statement, goals and objectives, and methodology are also presented.

#### 2.1 Fluid Terminologies

##### 2.1.1 Fluids

In nature, matter exists in either of three states: solid, liquid, or gaseous states. Solids have a specific shape and a significant degree of rigidity. From the strength of materials, we know that sufficiently large forces may measurably deform solids. A liquid placed into a container will take the shape of that container except for the top surface. If gas is allowed to flow into an evacuated container, it will entirely fill the container. It takes a relatively large force to change the total volume of a liquid. Both gases and liquids are classified as fluids [69].

*A fluid will deform continuously under shearing (tangential) stresses, no matter how small the stress. The magnitude of the stress depends on the rate of angular deformation.*

It takes little more than a quick glance to realize that the fluid dynamics is one of the most vital areas of physical science: life, as it is known, would not exist without fluids and the behaviour that fluids exhibit. The air for breathing and the water for drinking (most of the human body mass) are fluids. Air movement makes it comfortable in a warm chamber, and air provides the oxygen needed to support life. It is crucial for human health that these fluids move freely throughout the body, all the way down to the cellular level.



It's obvious that engineers need some familiarity with fluid behaviour in order to perform thorough analyses of many, if not most, of the systems they'll encounter. In this introductory chapter, we will begin by further emphasising the significance of fluid dynamics by providing concrete examples from the pure sciences and from technology in which knowledge of this field is essential to comprehending the physical phenomena (and, thus, the beginnings of a predictive capability, e.g., the weather) and the capability of designing and controlling devices such as internal combustion engines. We then list and explain why we will be focusing on three distinct theoretical approaches to fluid dynamics: (i) theoretical, (ii) experimental, and (iii) computational. The purpose of these lecture notes is to help students gain a better grasp of fluid motion, including its applications, dangers, and analytical and predictive capabilities.

**Importance of Fluids** Fluids' general significance can be divided into two groups: (i) the physical and natural sciences and (ii) the technological sciences. However, in today's era of emphasis on interdisciplinary studies, the more scientific and mathematical aspects of fluid phenomena are becoming increasingly important, and the second is often of more interest to an engineering student.

**Fluids in the natural sciences:** This is by no means an exhaustive list, but it does include some examples of fluid phenomena studied by physicists, astronomers, biologists, and others who are not directly involved in device design and analysis. The figures in this section shed light on a few of these features.

- Atmospheric sciences: (a) global circulation, (b) mesoscale weather patterns:
- Oceanography: (a) ocean circulation patterns, (b) effects of pollution on living organisms
- Geophysics: (a) convection (thermally-driven fluid motion) in the earth's mantle, (b) convection in the earth's molten core
- Astrophysics: (a) galactic structure and clustering, (b) stellar evolution
- Biological sciences: (a) circulatory and respiratory systems in animals, (b) cellular processes

**Fluids in technology:** Since fluids are used in so many technological tools, it is obvious that compiling a comprehensive list of their uses would be extremely difficult. From an engineering perspective, the following examples are both fascinating and necessary.

- Internal combustion engines – all types of transportation systems
- Turbojet, scramjet, rocket engines – aerospace propulsion systems
- Waste disposal: (a) chemical treatment, (b) incineration, (c) sewage transport and treatment
- Spread of pollution – both in the air (as smog) and on land, water, and air
- Power plants that use steam, gas, or wind turbines, or hydroelectric facilities to produce electricity
- Pipelines: (a) transportation of crude oil and natural gas, (b) irrigation systems, and (c) plumbing in commercial and residential buildings and homes
- Fluid/structure interaction: (a) the design of high-rise buildings; (b) oil rigs on the continental shelf; (c) dams, bridges, etc.; and (d) aircraft and launch vehicle airframes and control systems
- Heating, ventilating and air-conditioning (HVAC) Systems
- High-density electronic device cooling systems: personal computers (PCs) to supercomputers (supercomputers) in the digital realm
- Solar heat and geothermal heat utilisation
- Artificial hearts, kidney dialysis machines, insulin pumps
- Automobile, truck, and other vehicle spray painting, container filling, operation of various hydraulic devices, chemical vapour deposition, drawing of synthetic fibres, wires, rods, etc., and many more are all examples of manufacturing processes.

As we can see from the preceding examples, fluids permeate virtually every facet of our daily lives. Therefore, engineers need to have the ability to foresee the behaviour of fluids. In particular, even though most engineers are not fluid dynamicists, they will still need to interact with those who are quite frequently on a technical basis, and having even a foundational understanding of fluid dynamics will make those interactions more fruitful.

### 2.1.2 Boundary Layer Concept

Historically, researchers may thank Ludwig Prandtl (1874-1953), a professor at the University of Göttingen, for developing the idea of a boundary layer in a fluid's movement across a surface. On 12th August 1904 at the third International Mathematical Congress in Heidelberg, Germany, Ludwig Prandtl presented a paper entitled 'Über Flüssigkeitsbewegung bei sehr kleiner Reibung' [70] (English) 'On fluid flow with very little friction', which formed the foundation for future work on skin friction, heat transfer, and flow separation from the surface of the body.

General fluid equations had been known for many years, but the solutions to the equations did not adequately describe observed flow effects (such as wing stalls). L. Prandtl was the first to realise that the relative magnitude of the forces of inertia and viscosity shifted from a layer very close to the surface to a region far from the surface. He first came up with the interactive coupled, two-layer solution, which properly models many flow problems. He subsequently made fundamental contributions to finite wing theory and compressibility effects.

Prandtl explained that fluid viscosity plays a vital role in a thin layer adjacent to the surface, which he called 'Übergangsschicht' or 'Grenzschicht'. The English terminology is boundary layer or shear layer. He also simplified the equations for fluid flow by dividing the flow field into two zones: one within the boundary layer, dominated by viscosity and creating most of the drag realised by the boundary surface; and one outer the boundary layer, where viscosity can be ignored without significant effect on the solution.

For fluids having relatively small viscosity, the effect of internal friction, Due to viscous shearing, in a fluid flow is experienced only in a narrow region surrounding the fluid boundary.

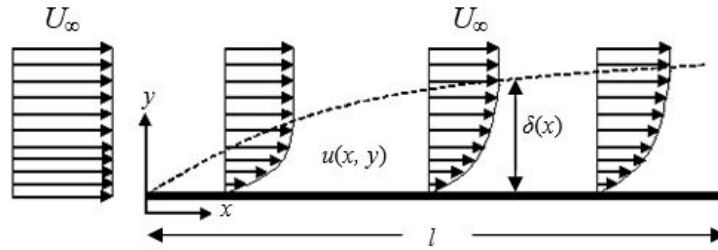


Figure 2.1: Boundary layer at a flat plate at zero incidences (schematic).

Hence, the liquid layer near the external surface becomes adhered to the surface, and the fluid velocity is zero in this region (that wets the body). The "no slip requirement" is mentioned in this context. This results in a sharp increase in speed when one moves from the edge into the flow. This velocity gradient in a fluid creates shear forces close to the border, slowing the flow rate to that of the boundary. Surface fluid layers are in motion. Thus, shearing occurs among the liquid's layers. Wall shear stress, represented by  $\tau_w$ , is the shear stress applied between the wall and the first moving layer adjacent to it. The boundary layer refers to the thin layer of fluid immediately adjacent to the surface of a solid barrier, such as a body or a hedge (or shear layer). The fluid's velocity,  $u$ , increases as a function of height,  $y$ . Distance from the surface to the height above the surface at which the velocity develops 99% of the free-stream velocity is the boundary layer thickness  $\delta$ . The Reynolds number describes the balance between inertial and viscous forces, and so determines the boundary layer thickness. The whole boundary layer is governed by viscous forces at low Reynolds numbers, and the flow is laminar. Nevertheless, inertial forces dominate the boundary layer for high Reynolds numbers, and the fluid develops turbulent.

Usually, hydrodynamic (velocity) and thermal are two types of boundary layers. When a fluid's velocity drops from its free-flow value to zero at a body's surface, that transition zone is called the hydrodynamic boundary layer. Heat is transferred by conduction, convection, or radiation when a fluid moves past a body that is either being heated or cooled. When a temperature difference exists between a body and the fluid next to it, heat energy will flow from the

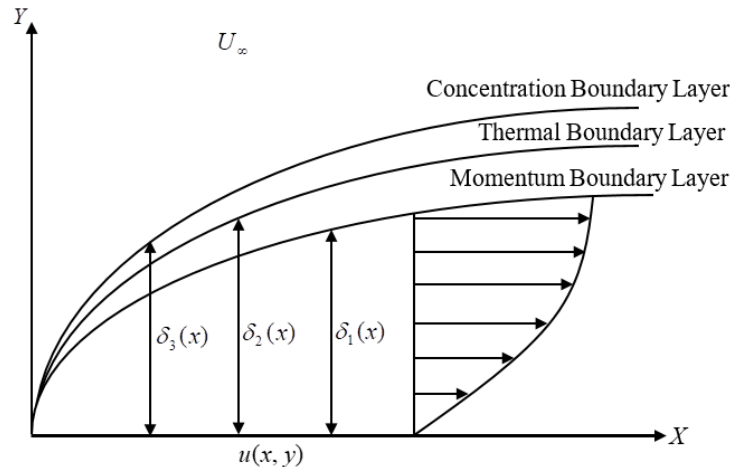


Figure 2.2: Boundary layer formulation.

body to the fluid; this is because, like the fluid's velocity, which rises from zero at the surface to the free stream, the temperature also rises from the boundary to the free stream. As a result, it is reasonable to assume that the temperature of the fluid next to the wall is the same as the temperature of the wall at the interface and hence, is also identical to the temperature of the bulk fluid at some point in the fluid. The term "thermal boundary layer" refers to the extremely thin layer of air just below the skin's surface. We can investigate a single or multiple boundary layers depending on the characteristics of the fluid flow.

**Velocity boundary layer ( $\delta_1$ ):** When in contact with a fixed surface, fluid particles have no tangential velocity. Particles in a fluid that come into contact with a moving surface will also move at the same rate. The term "no-slip condition" describes this phenomenon in the field of fluid dynamics. A fluid's flow results in shear stress due to the net transfer of momentum from regions of high to low velocity. The skin friction of a fluid is a key parameter that can be calculated using the velocity boundary layer.

**Thermal boundary layer ( $\delta_2$ ):** Temperature differences between the surface and the free stream zone cause the formation of the thermal boundary layer. The rate of heat transfer via convection is heavily dependent on the thermal boundary layer.

**Concentration boundary layer ( $\delta_3$ ):** The presence of concentration gradients between the sur-

face and the free stream leads to the formation of a concentration boundary layer in a fluid region. This boundary layer is crucial because it controls the speed of mass transfer via convection.

### **Methods of boundary layer control**

Several methods of controlling boundary layers have been developed experimentally and are also based on theoretical considerations. These can be classified as follows:

- The motion of the solid wall.
- Acceleration of the boundary layer (blowing).
- Suction.
- Injection of different gases (binary boundary layer).
- Prevention of transition to turbulent flow by the provision of suitable shapes.
- Cooling of the wall
- Variable viscosity

#### 2.1.3 Magnetohydrodynamics (MHD)

When discussing the motion of fluids that conduct electricity in a magnetic field, the term "magnetohydrodynamics" (MHD) is often used. The letters MHD stand for magneto, hydro, and dynamic, all of which refer to magnetic fields, fluids, and movement, respectively. Hydromagnetic and magnetohydrodynamic are both synonyms for MHD. Saltwater, liquid metals (such as mercury, gallium, and molten iron), and ionised gases or plasmas all fall under the category of "fluids" (such as the solar atmosphere). Swedish physicist Hannes Alfvén (1908-1995) founded the field of magnetohydrodynamics (MHD), for which he was awarded the Nobel Prize in Physics in 1970. MHD has since found fruitful applications in many areas of plasma physics[71].

MHD describes events in which the velocity field  $V$  and the magnetic field  $B$  are coupled in an electrically conducting fluid. In a conducting fluid subjected to a magnetic field, an electric

current with a density of  $J$  is produced (electromagnetism). The magnetic field is altered, and the induced current pushes the liquid. Each volume of watery materials exposed to a magnetic field  $B$  experiences a magnetohydrodynamic (MHD) force equal to  $J \times B$ , also known as the Lorentz force. Navier-Stokes equation of fluid dynamics and Maxwell's equation of electromagnetism are coupled to form the standard equations that describe MHD flows.

#### 2.1.4 Application of MHD

There are lots of natural phenomena and engineering problems amenable to MHD analysis. Electrically conductive fluids are abundant in nature, although their conductivities vary widely. As magnetic fields are everywhere, it follows that MHD processes must occur anytime conductive fluids are present in natural marvels. On the other hand, MHD is of particular technical importance due to its frequency in many industrial applications.

**MHD Pump:** The pumping system is a real-world application of the MHD force, as it directly converts electrical energy into mechanical force on the working liquid. There have been EM pumps for a long time, and several successful systems have been designed and industrialised. In 1907, a prototype magnetically driven (MHD) pump was created [72].

**MHD Generators:** Michael Faraday manufactured the first MHD generator in 1831. This generator converts a magnetic field and an electrically conductive fluid into usable electricity. It may convert mechanical or thermal energy into electrical power. Obtaining electrical conductivity using an MHD generator may be done in a few different ways. Since 1959, researchers all around the world have been working hard to perfect this method of increasing the efficiency of electric conversion, and reduce emissions from coal and gas plants [73, 74].

**MHD Flow Meters:** An electromagnetic flow measurement method exposes a flow to a magnetic field and measures the force acting on the magnetic field generating system. Another

standard MHD device is the EM flow meter. In 1832 Michael Faraday endeavoured to regulate the velocity of the Thames river [75]. The theory of inductive flowmeter has been developed and comprehensively summarised by [76]. MHD can also be used to build a flowmeter for blood, initiated by Kolin [77].

**Metallurgy:** More recently, MHD devices have been used to agitate, levitate, and control liquid metal flows for metallurgical processing [78]. High-level requirements for metallurgy production determine a transition to a tangibly advanced level of primary processing performance technology of semi-finished, poured and cast products. Therefore, the task of metal ingots and the quality of blanks must be solved comprehensively; that is, the quality of the alloy must be controlled at the preparation stage, intermediate processing and pouring.

**MHD Propulsion:** MHD is smart because it has no moving parts, so a good design can be quiet, reliable, efficient, and inexpensive. MHD propulsion is a method of propelling sea vessels using only electric and magnetic fields with no moving parts by means of MHD. The first ship to be powered was the Yamato, built by Mitsubishi in 1991.

#### 2.1.5 Heat Transfer

Heat transfer is one of the central mechanical processes. The inception of higher heat flow in automated processes has necessitated new equipment to develop heat transfer. Heat transfer must be managed efficiently in any industrial facility by adding, removing, or moving within/through the relevant sectors. For instance, microprocessors have frequently become smaller and more powerful, and heat flow necessities have progressively boosted over time, leading to new challenges in thermal management. Besides, there is growing attention to advancing the efficiency of existing heat transfer processes. An example is automotive systems, where improved heat transfer could lead to smaller heat exchangers for cooling, resulting in reduced vehicle weight.



Temperature differences between boundaries or between an edge and the ambient fluid can cause temperature differences within the fluid itself. Also contributing to temperature shifts are processes like radioactivity, the absorption of thermal radiation, and the release of latent heat as vaporised fluid condenses. To put it simply, heat transfer is the process by which thermal energy and heat are created, converted, and communicated between physical arrangements as a result of a temperature gradient. Heat transfer describes the exchange of thermal energy and often occurs in engineering systems and everyday life. *Conduction, convection* and *radiation* are three approaches to heat transfer.

### **Convection**

Convection states the heat transfer that occurs between a moving body and fluid having different temperatures. The fluid's random molecular and bulk mobility inside the boundary layer keeps the convection method of heat transfer active. The convective heat of a fluid is affected by the fluid's viscosity, thermal conductivity, specific heat, and density. The fluid's viscosity also modifies its velocity profile. There is a wide range of practical uses for heat transmission, from maximising it, as in heat exchangers, to minimising it, as in steam pipes. Today's technology makes extensive use of heat transfer in power plants, heat exchangers, and nuclear power plants.

There are many methods available to improve heat transfer in mechanical processes. The flow of heat can be estimated using Newton's Law of Cooling,

$$Q = -h A \Delta T$$

Here  $Q$  is the heat flow,  $h$  is the heat transfer coefficient,  $A$  is the heat transfer region, and  $\Delta T$  is the temperature variance [79]. We can see from this equation that increased heat transfer can be achieved by:

- increasing  $\Delta T$
- increasing  $A$

- increasing  $h$
1. Heat flow can be increased by creating a more significant temperature difference  $\Delta T$ ; however,  $\Delta T$  is often limited by the materials' properties or by mechanical processes. To avoid a meltdown and runaway reactions, a nuclear reactor's maximum temperature, for instance, must be kept below a particular value. As a result, increasing  $\Delta T$  requires decreasing the coolant temperature. Nuclear reaction rate and mechanical process efficiency would both suffer as a result.
  2. One common technique for enhancing heat transfer is to increase the area of contact, or  $A$ . Radiators and plate-and-frame heat exchangers are two examples of heat exchangers that aim to maximise this heat transfer area [80]. However, due to the inherent limitations of the region, this policy is inapplicable to microprocessors and microelectromechanical systems (MEMS). Increasing the size of the heat exchanger, which could result in unwelcome weight gains, is sometimes the only option for expanding the heat transfer area in aerospace and automotive technologies.
  3. Finally, improvements in heat transfer can be achieved by either (a) employing more efficient heat transfer methods or (b) enhancing the transport properties of the heat transfer material, both of which increase the heat transfer coefficient,  $h$ . Forcing a gas to circulate through a system increases the heat transfer coefficient compared to a system that uses natural convection alone. Heat transfer devices often make use of fluids as heat carriers or coolants.

Additives to liquid coolants improve the specific properties. For example, glycols are mixed with water to lower their freezing point and raise their boiling point. Otherwise, the heat transfer coefficient can be increased by enhancing the properties of the coolant for a given method of heat transfer.

Traditional heat transfer fluids have a low thermal conductivity, so despite extensive prior R & D on heat transfer enhancement, little progress has been made in cooling proficiencies.

During this era of intensifying global competition, industries must develop and implement heat transfer fluids with significantly higher thermal conductivities than those currently on the market [79]. It is common knowledge now that the thermal conductivity of a solid metal is many times higher than that of a liquid at room temperature. At room temperature, copper's (*Cu*) thermal conductivity is presumably 3000 times higher than motor oil's and 700 times higher than water's. Once again, metallic liquids have superior thermal conductivities compared to non-metallic liquids. Therefore, compared to standard heat transfer fluids, it is expected that fluids containing suspended solid metallic particles will have significantly higher thermal conductivity [80]. In the case of nano-sized particles, the resulting dispersion is identified as a nanofluid [25].

Thus, actual uses of heat transfer fluids include vehicular and avionics cooling systems in the transportation industry, hydraulic heating and cooling systems in buildings, petrochemical, textile, food, pulp, paper, and other industrial processing. For these manufacturing purposes, the thermal conductivity of fluids performs a dynamic role in improving energy-efficient heat transfer technologies.

#### 2.1.6 Nanofluids

In the early century, a common issue was the difficulty of combining conduction and convection. Because ingredients that conduct heat evenly (such as metals) do not flow perfectly, materials that flow uniformly (such as water and air) do not conduct heat ideally. Heating metals into liquid form was one option but was considered impractical due to the extensive energy required to reach the essential temperatures. In 1873 Maxwell [81] recommended a different mechanism by adding micron-sized particles of highly-conductive solids to the base fluid to enhance the thermal properties. For over a century, it was the only possible way to develop the thermal properties by adding these particles in diameters as small as millimetres and micrometres. Unfortunately, several adverse effects were also raised in the fluid. These concerns of rapid settling, erosion in their containers, blockage of tiny passages, and considerable pressure fall denied the heat transfer benefits of the liquid. These problems were highly undesirable in many practical applications.

If particles settle down rapidly like micro-particles, supplementary particles must mix to swap the steady particles, causing degradation in the heat transfer development. There is a solid motivation to develop innovative heat transfer fluids with significantly higher conductivities to enrich thermal characteristics to overwhelm the difficulty.

To address these issues, nanofluids were the first to successfully suspend nanometer-sized particles in fluids, rather than micrometre-sized particles. Nanoparticles have a much larger surface area than larger particles and can remain suspended for much longer. Nanoparticles can efficiently absorb and transfer heat because about 20% of their atoms are located near the surface. Conversely, micro-particles have most of their atoms deep within, making them incapable of conducting heat. Furthermore, the suspended particles increase the surface area of the fluid and its heat capacity. When compared to using larger particles, using smaller suspended particles (nanometer-sized particles) significantly improves effective thermal conductivity (micrometre-sized particles).

### **Synthesis of Nanofluids**

The *single-step method*, in which nanoparticles are vaporised directly into the base fluid, and the *two-step method*, in which nanoparticles are first equipped by either the inert gas-condensation technique or chemical vapour deposition method before being dispersed into the base fluid, are the two procedures used in the invention of nanofluids.

**Two-step method:** The most common approach to making nanofluids is a two-stage process. Dry powders of nanoparticles, nanotubes, nanofibers, or other nanomaterials are first created, usually by the condensation of an inert gas [82]. In a second processing stage, the nano-sized powder is disseminated in a fluid with the use of intensive magnetic force agitation, ultrasonic agitation, high-shear mixing, homogenising, and ball milling to reduce particle aggregation and enhance dispersion behaviour. Furthermore, carbon multi-walled nanotubes and other materials for nanofluids have been manufactured by chemical vapour deposition (CMWNT) [83]. Surface

surfactants are added to the fluids to enhance the stability of nanoparticles in fluids. Yet, high-temperature applications raise further concerns about the surfactants' performance.

The two-step method is the most economical method to produce nanofluids on a huge scale because nanopowder synthesis techniques have already been scaled to industrial production levels. In some cases, the two-step process works well, such as nanofluids consisting of oxide nanoparticles dispersed in deionised water [27]. Less success has been discovered when producing nanofluids containing heavier metal nanoparticles. A fundamental problem with two-step processes is that the nanoparticles are in an aggregated state after several hours of sonication. Due to the difficulty of preparing stable nanofluids by the two-step method, several advanced techniques have been industrialised to produce nanofluids, including the one-step method.

**One-Step Method:** The formulation of nanofluids using a single stage of physical vapour condensation was developed to lessen the buildup of nanoparticles. The particles are created in the same step that they are dispersed across the basic fluid. This preparation technique prevents nanoparticles from agglomerating throughout the drying, storage, transportation, and dispersal processes, hence increasing fluid stability [84]. Nanoparticles are produced in a single process and are suspended evenly and securely in the base fluid. Nevertheless, only low vapour pressure fluids are properly matched with the procedure, and the leftover reactants are left in the nanofluids after a one-step approach due to incomplete reaction or stabilisation.

In nanofluids, spherical particles are the norm. Nanoparticles of various shapes are eaten, including rods, tubes, cylinders, and discs. The heat transfer characteristics and transport properties of the base fluid are altered by the suspended metallic or non-metallic nanoparticles. Theoretically, at normal temperatures, it's easy to see that solid metals have greater thermal conductivity than liquids. Compared to non-metallic liquids, metallic liquids have exceptional heat conductivity. It follows that the thermal conductivities of fluids containing metallic nanoparticles should be dramatically improved. Experimental results show that the thermal conductivities of both the base fluid and the nanoparticles affect the thermal conductivities of the resulting

nanofluid. The advantages of well-organised nanofluids are expected to include

- higher heat conduction,
- more stability
- microchannel cooling without clogging
- reduced chances of erosion and
- reduction in pumping power [85].

### 2.1.7 Thermal Transport Properties of Nanofluids

The ground-breaking research with nanofluids showed that nanofluids have new thermal transport phenomena that demonstrates remarkable enhancement in thermal conductivity, viscosity, and convective heat transfer coefficients compared to those of traditional base fluids. Precise mathematical explanation of nanofluid properties are one of the enthusiastic trends.

#### **Thermal Conductivity of Nanofluids**

Since roughly the time of Maxwell, who was one of the first people to study conduction analytically through suspension particles, there has been a significant amount of theoretical interest in the investigation of the transport properties of heterogeneous mixtures. Maxwell [81] ignored the interactions between the particles in his hypothetical highly dilute suspension of spherical particles. The term "effective thermal conductivity" was coined by him denoted as  $\kappa_{eff}$  and given by

$$\kappa_{eff} = \kappa_f \frac{(\kappa_s + 2\kappa_f) - 2\varphi(\kappa_f - \kappa_s)}{(\kappa_s + 2\kappa_f) + \varphi(\kappa_f - \kappa_s)}$$

Eastman *et al.* [86] reported that the thermal conductivity of ethylene-glycol increased 40% with 0.3 vol % copper nanoparticles of 10nm diameters.

To account for non-spherical particles, Hamilton and Crosser [87] introduced a shape factor that can be determined experimentally for various materials, extending Maxwell's study of spherical particles.

Heterogeneous two-component systems have a value for thermal conductivity, according to Hamilton and Crosser, given by

$$\kappa_{eff} = \kappa_{bf} \frac{(\kappa_s + (n - 1)\kappa_f) - (n - 1)\varphi(\kappa_f - \kappa_s)}{(\kappa_s + (n - 1)\kappa_f) + \varphi(\kappa_f - \kappa_s)}$$

where the empirical shape factor,  $n$  is defined by  $n = 3/\Psi$  and  $\Psi$  (ratio surface area and volume) is the sphericity of the particle. The Hamilton-Crosser model yields the Maxwell model when  $\Psi = 1$ . This model is valid as long as the conductivity of the particles is larger than the conductivity of the continuous phase at least by a factor of 100.

**Thermal conductivity and particle volume fraction:** The thermal conductivity of a nanofluid has been demonstrated to be affected by the particle volume fraction or the volumetric concentration of the nanoparticle in the nanofluid. The thermal conductivity of nanofluids with low nanoparticle volume fractions was shown to be considerably higher in experiments than that of the base fluid. Das *et al.* [28] observed 10 – 25% thermal conductivity increases linearly in water with 1 – 4 vol % alumina nanoparticles. In their studies, Lee and Choi [27] showed that the thermal conductivity enhancement increases linearly with particle volume fraction.

**Thermal conductivity and particle material:** When the bulk temperature of the nanofluid increases,  $T$ , the molecules and nanoparticles inside it become more active due to improved Brownian motion, allowing for a greater rate of energy transfer between locations in a given amount of time. Das *et al.* [28] tested  $Al_2O_3$ -water nanofluids at temperatures ranging from 21 to 51°C. They found that the thermal conductivity enhancement rose from 2% at 21°C to 10.8% at 51°C for 1 vol. %  $Al_2O_3$ -water nanofluid, and from 9.4% at 21°C to 24.4% at 51°C for 4 vol %.

**Thermal conductivity and base fluid:** According to the Maxwell thermal conductivity model [81], as thermal conductivity of a mixture's base fluid decreases, the thermal conductivity ratio of nanofluid's thermal conductivity increases. Wang *et al.* [88] used  $Al_2O_3$  and  $CuO$  nanoparticles to prepare nanofluids with several base fluids; water, ethylene glycol, vacuum pump fluid, and

engine oil.  $Al_2O_3$ -EG nanofluid had the highest thermal conductivity ratio.

**Thermal conductivity and particle size:** The particle size/diameter is recognised to be an essential characteristic of the thermal conductivity of nanofluids, and a wide range of nanoparticles is created, from 5 to 100nm. Nanofluids containing various nanoparticles were used by Chopkar *et al.* [89] to investigate the impact of particle size on heat conductivity. The base fluids were distilled water and ethylene glycol (EG). The sizes of the nanoparticles ranged from 30 to 120nm. Enhancement in thermal conductivity was shown to increase with decreasing particle size for all four types of nanofluids.

**Thermal conductivity and particle shape:** Nanofluids' thermal conductivity can be affected by the form of their particles. The thermal conductivity of a SiC-water nanofluid was investigated by Xie *et al.* [90] utilising both spherical particles with an average diameter of 26nm and cylindrical particles with an average diameter of 600nm. Longer than they are wide, cylindrical particles are the norm. The thermal conductivity of water-based nanofluids with spherical particles was found to be increased by 15.8%, while that of nanofluids with cylindrical particles was found to be increased by 22.9% when both particle shapes were used. To sum up, spherical particles exhibit somewhat less improvement than nanorods.

### Viscosity of nanofluids

Atypical viscosity of nanofluids enhances relative to the base fluids. For nanoparticle concentrations not above 4%, Brinkman [91] formula is as follows:

$$\mu_{nf} = \frac{\mu_f}{(1 - \varphi)^{2.5}}$$

Pak and Cho [92] estimated that at 1 – 10 vol % of nanoparticles of alumina and titania in pure water, viscosity is much higher than that of regular water.

### Density of Nanofluids

Computation of the effective density of nanofluids is straightforward and can be valued by the physical principle of the mixture rule showing very good agreement with some experimental



data. Nanofluids as a mixture of consisting of a continuous base fluid and solid nanoparticles implies the correlation of density as

$$\rho_{nf} = (1 - \varphi) \rho_f + \varphi \rho_s$$

### **Specific Heat of Nanofluids**

The specific heat is the extent of heat per unit mass expected to increase the temperature by 1°C. The correlation between heat and temperature change is frequently expressed by the the specific heat CP. The specific heat of nanofluids can be defined as

$$(\rho c_p)_{nf} = (1 - \varphi)(\rho c_p)_f + \varphi(\rho c_p)_s$$

### **Electric Conductivity of Nanofluids:**

The Wiedemann-Franz law states that a metal's thermal conductivity follows the same metal's electrical conductivity very closely due to the free motion of valence electrons [93]. Maxwell's definition of static electric conductivity states that  $\sigma$  is proportional to the phase volumetric fraction  $\varphi$  as

$$\frac{\sigma_{nf}}{\sigma_f} = 1 + \frac{3(\sigma_s/\sigma_f - 1)\varphi}{(\sigma_s/\sigma_f + 2) - (\sigma_s/\sigma_f - 1)\varphi}$$

The electrical conductivity of the alumina nanoparticles in water was conducted by Ganguly *et al.* [94] and a linear dependence of electrical conductivity on volumetric concentration has been observed.

Table 2.1: Thermo-physical properties of base fluids and nanoparticles

Materials	$\rho$	$C_P$	$\kappa$	$\beta$	$\sigma$
Water	997.1	4179	0.613	21E-05	5.5E-06
Ethylene glycol	1115	2415-2430	0.253	57E-05	1.07E-06
Kerosene	780	2090	0.149	9.9E-04	5.0E-11
Engine Oil	884	1909	0.145	70E-05	1.00E-07
Mineral Oil	920	1670	0.138	64E-05	1.00E-07
Blood	1063	3594	0.492	0.18E-05	6.67E-01
Copper (Cu)	8933	385	401	1.67E-05	5.96E+07
Silver (Ag)	10500	235	429	1.89E-05	6.3E+07
Iron	7870	460	80	58E-05	1.00E+07
Aluminium	2701	902	237	2.31E-05	3.50E+07
Cobalt	8900	420	100	1.3E-05	1.7E+07
Alumina ( $Al_2O_3$ )	3970	765	40	0.85E-05	3.69E+07
Titanium Oxide ( $TiO_2$ )	4250	686.2	8.9538	0.90E-05	2.38E+06
CuO	6510	540	18	0.85E-05	5.96E+07
Fe3O4	5180	670	80.4	20.6E-05	1.12E+05
ZnO	5610	495.04	29	4.7E-05	7.261E-05

Table 2.2: Dynamical viscosity of base fluids

Base fluids	$\mu$
Water	0.001003
Ethylene glycol	0.0162
Kerosene	0.00164
Blood	0.00287

### 2.1.8 Application of Nanofluids

Increase in thermal conductivity at low nanoparticle concentrations; high temperature-dependent thermal conductivity; non-linear increase in thermal conductivity with nanoparticle concentration; and escalation in boiling critical heat flux are four characteristics sought in energy systems (fluid and thermal systems), and all four are present in nanofluids. Industrial coolants, smart fluids, nuclear reactor coolants, geothermal energy extraction, nanofluids in automotive fuels, brake fluids, coolants in car radiators, cooling of microelectronics, and the bio and pharmaceutical industry are all examples of areas where these unique properties could be put to use to improve heat transfer and energy efficiency [95, 96, 97].

#### **Heat Transfer Applications**

Several articles have emphasised the potential of nanofluids in heat transfer applications since the invention of nanofluids approximately two decades ago [98, 99]. The use of nuclear power plants and geothermal energy extraction are further examples.

**Industrial Cooling Application:** Routbort claims that switching to nanofluids for industrial cooling will dramatically cut energy consumption and pollution levels [100]. In tyre plants, for instance, the inability to efficiently cool the rubber during processing limits the productivity of many industrial processes, necessitating large quantities of heat transfer fluids. Tire manufacturers can increase their profit margins and decrease their production costs by switching to nanofluids based on water. Most often, industrial coolants are used in HVAC systems in buildings, as well as in the public utility sector, the oil and gas business, the food and beverage processing sector, the chemicals and plastics sector, the solar energy conversion sector, and the plastics sector. For the US industry, replacing cooling and heating water with nanofluids can conserve 1 trillion Btu of energy [100]. Polyalphaolefin nanofluids containing exfoliated graphite nanoparticle fibres were studied in a flow-loop experiment by Nelson *et al.* [101], who found that their specific heat was 50% greater, and their convective heat transfer was boosted by 10% compared

to those of the polyalphaolefin.

**Smart Fluid:** The proliferation of battery-powered electronics like cellphones and laptops during this age of energy conservation has highlighted the importance of careful technological management of power supplies. The properties of smart materials can be altered in significant ways; e.g., smart materials with variable viscosity may turn from a fluid which flows effortlessly to a solid. Nanofluids have been demonstrated to handle this role in some instances as smart fluids.

Heat transfer may be decreased or increased on demand by using nanofluids as a smart material functioning as a heat valve. Magneto-rheostatic (MR) materials, in particular, are nanofluids made of extremely small iron particles dispersed in oil. Car shocks, washing machine vibration damping, prosthetic limbs, workout equipment, and machine component cleaning are just some of the industrial applications being developed for MR fluids.

**Nuclear Reactors:** A nuclear reactor is a device for containing and managing nuclear chain reactions that can last for an extended period of time. Aside from producing electricity and medical isotopes for imaging and cancer treatment, reactors are also used to propel aircraft carriers and submarines.

Heavy atomic fuel is loaded into a reactor vessel where neutrons are produced. This generates a great deal of thermal energy. The coolants are heated up by the heat transfer and then sent to spin a turbine, which in turn spins a generator to create electricity. As a result, people are no longer trapped by their reliance on polluting fossil fuels, and can instead pursue a more sustainable lifestyle. Kim *et al.* [102], at MIT's Nuclear Science and Engineering Department, conducted feasibility studies on employing nanofluids in the nuclear energy business as an alternative to enhancing the water-cooled nuclear system's heat removal. PWRs can increase power and economic performance by using nanofluids as core reactor coolants. Nanofluids can also be utilised in PWR and boiling water reactor emergency core cooling systems (ECCs) to cool hot surfaces faster and increase power plant safety. If the nanofluid has a greater post-CHF heat

transfer rate, the ECC system accumulators and safety injection can enhance peak-cladding-temperature margins in the nominal-power core or maintain them in uprated cores.

Nanofluids might prevent serious incidents in which the core melts and sinks to the reactor vessel. In such incidents, eliminating decay heat via the vessel wall keeps the molten fuel within. Nanofluid can boost nuclear reactors' in-vessel retention by 40%, but CHF on the vessel's exterior surface limits this process [103].

**Geothermal Power Extraction:** Nanofluids can be highly specialised drilling fluids with superior performance in high-temperature drilling. Nanofluids can be used to cool the pipes used to extract energy from the earth's crust, which can be anywhere from 5 to 10 kilometres in length and 500 to 1000 degrees Celsius in temperature. It has been proposed that nanofluids, as a type of fluid superconductor, might be employed as a working fluid in a pressurised water reactor (PWR) power plant system to collect energy from the earth's core and convert it into useful work energy [104].

**Electronic Applications:** Microfluidic applications, such as those found in computers, rely on nanofluids for cooling the microchips that power the devices. Current electronic systems produce a great deal of heat because of the fast growth of modern technology, which hinders the performance of the devices and reduces their dependability [104].

**Cooling of Personal Computers and Microchips:** Heat dissipation limits smaller high-density microchips. High heat generation and limited heat removal surface area make thermal management difficult for advanced electronic equipment. Nanofluids can cool computer processors due to their excellent thermal conductivity and heat transfer coefficient. Jang and Choi [105] found that a microchannel heat sink using nanofluids might be the next-generation ultrahigh heat flux cooling technology.

Nanofluids using silver or titanium nanoparticles can efficiently cool high-energy-density

devices. Heat pipes with nanofluids containing gold nanoparticles have far lower thermal resistance than water at the same charge volume [106].

**Nanofluid-based optical filter optimisation for PV/T systems:** Specialised nanoparticle suspensions, such as nanofluid-based filters for hybrid solar photovoltaic/thermal (PV/T) applications, can be used to fabricate optical filters. Since nanofluids may function as both a volumetric solar absorber and a flowing heat transmission medium, they are well-suited for this specific application. Savings on both electrical and thermal energy costs may be substantial with well-designed PV/T systems for use in homes and businesses.

**Automotive Applications:** Coolants, gasoline additives, lubricants, shock absorbers, and refrigerants are just some of the ways that cars have incorporated nanofluids. Vehicle radiators and hybrid electric vehicle power electronics frequently employ nanofluids for cooling. Conventional vehicle thermal systems—including radiators, engines, heating, ventilation, and air conditioning (HVAC)—use synthetic high-temperature heat transfer fluids with poor heat transfer qualities, such as engine oils, automatic transmission fluids, coolants, lubricants, and more. Nanofluids' superior heat conductivity might be useful in such applications.

**Nanofluid Coolant:** Manufacturers need to decrease the amount of energy required to overcome wind resistance on the road in order to improve the aerodynamic designs of vehicles and, in turn, the fuel economy. Smaller and lighter parts in a nanofluid engine would reduce fuel use, which would save money for drivers and keep the environment safer. As a researcher at Argonne National Laboratory analysing the potential of nanofluids in transportation, Singh *et al.* [107] found that by adding high-thermal-conductive nanofluids to radiators, the radiator's frontal area can be reduced by as much as 10%. This new aerodynamic automotive design minimises the aerodynamic drag, leading to a fuel saving of up to 5% and reducing emissions. Nanofluid use also reduces friction and wear, reduces parasitic losses, and operates components such as pumps

and compressors, hence more than 6% fuel savings.

**Nanofluid in Fuel:** Due to pure aluminium's strong oxidation activity, plasma arc-produced aluminium nanoparticles are coated in thin coatings of aluminium oxide, which increases water interaction and hydrogen breakdown during burning. Alumina works as a catalyst, and aluminium nanoparticles break down water to produce hydrogen during burning. Exhaust emissions from a diesel engine using diesel fuel mixed with aqueous aluminium nanofluid were found to increase total combustion heat while decreasing smoke and nitrous oxide concentrations [85, 97].

**Brake and Other Vehicular Nanofluids:** There is a growing need for braking systems like brake nanofluid, which have enhanced heat dissipation mechanisms, and properties as vehicle aerodynamics are improved, and drag forces are reduced. Nanofluids will enhance heat transfer performance and eliminate safety concerns caused by brake oil's sensitivity to the heat generated during braking [104].

**Heating Buildings and Reducing Pollution:** In frigid climates, heat transfer fluids include ethylene or propylene glycol combined with water. Kulkarni *et al.* [24] found that nanofluids in heat exchangers reduced volumetric and mass flow rates, saving pumping power. Smaller heating units consume less electricity and produce less liquid and material waste, reducing environmental pollutants.

**Magnetic Drug Targeting:** Metabolism requires magnetism. Haemoglobin, an iron complex, is magnetic. Magnetite,  $Fe_3O_4$ , is one of the most widely utilised biomaterials for cell separation, drug administration, and hyperthermia [98]. Chemotherapy typically fails because of the inability to accurately administer and concentrate medications in damaged regions. Failing to focus locally increases harmful effects on neighbouring organs and tissues. Magnetic medicine delivery might target precisely. Biocompatible magnetic particles (ferrofluids) carry medicine

into circulation. An external magnetic field reduces blood flow in particular locations. Here, magnetic carriers gently release the medication.

In localised tumour treatment, magnetic fluids reduce adverse effects and improve efficacy [95]. Hence, magnetically targeted drugs can replace huge amounts of freely circulating medication. Drug concentrations in the targeted location will be much greater than with systemic distribution. Magnetic drug targeting has shown promise in advanced cancer and sarcoma patients [85]. MHD equations and Finite Element analysis study blood magnetic particle-external magnetic field interactions. Such therapies' effectiveness can be measured. Injectable magnetic fluids may be able to restore all retinal damage, prompting new uses. Due to the magnetic fluid's ability to drive towards hard-to-reach eye locations, the researchers believe a magnetised silicone fluid approach might improve tissue repairs and precision.

**Nano-drug Delivery:** Modern technology has led to the development of bio-micro electromechanical systems (MEMS), such as an electronically activated drug delivery microchip [99], a controlled delivery system via silicon and electroactive polymer technologies, a MEMS-based DNA sequence developed by Cepheid [108], and in-plane and out-of-plane hollow micro-needles for dermal/transdermal drug delivery [85]. Micro- or nano-drug administration allows target-cell responses to medicinal stimuli to be monitored and controlled, improving biological cell activity and medication development. Microdevices provide precise implanted and transdermal medication delivery. Nano-drug delivery (ND) methods release drugs slowly. Consequently, the therapeutic window will maintain medication concentration.

**Nanocryosurgery:** Nano-cryosurgery may improve tumour therapy. Cryosurgery freezes unwanted tissues. Due to its therapeutic benefits, cryosurgery is becoming a preferred cancer therapy choice. Yan and Liu's calculations showed that intentionally loading target tissues with high-thermal-conductivity nanoparticles can lower the ultimate temperature, increase the maximum freezing rate, and increase the ice volume [109]. Nanoparticle-enhanced freezing might



also allow traditional cryosurgery to manipulate ice ball size, shape, image, and direction. Due to their biocompatibility, magnetite ( $Fe_3O_4$ ) and diamond are the most common and effective freezing enhancers [96].

### 2.1.9 Mass Transfer

The mass transfer includes molecular diffusion and convective mass transport. A mixture's species concentration differential causes mass transfer. Like the temperature gradient, the species concentration gradient in a mixture drives mass transfer. Thermal diffusion can cause the mass transfer. Concentration gradients can also cause temperature gradients and heat transfer. These phenomena are connected.

Mass transfer activities in the industry include distillation columns, scrubbers, activated carbon beds, and liquid-liquid extraction. Industrial cooling towers combine mass transfer with other transport methods. Several technological applications combine heat and mass transport.

### 2.1.10 Newton's Law of Viscosity

Viscosity, the retardance to flow of a fluid, is a fluid property arising from collisions between neighbouring particles in a fluid that is moving at different velocities. Viscosity acts against the motion of any solid object through the fluid and against the fluid's movement past stationary obstacles. Viscosity also acts internally on the fluid between slower- and faster-moving adjacent layers. The fluid viscosity is the extent of its resistance to slow deformation by shear stress. For liquids, it corresponds to the colloquial term 'thickness'. For example, oil has a much higher viscosity than water.

Let an element of fluid experience stress exerted on it by other aspects of the fluid which surround it. The stress on the element surface is resolved into two components: normal and tangential to the surface, which are called 'pressure' and 'shear stress', respectively. Pressure is applied whether the fluid is moving or at rest, but shear stress occurs only in moving fluids.

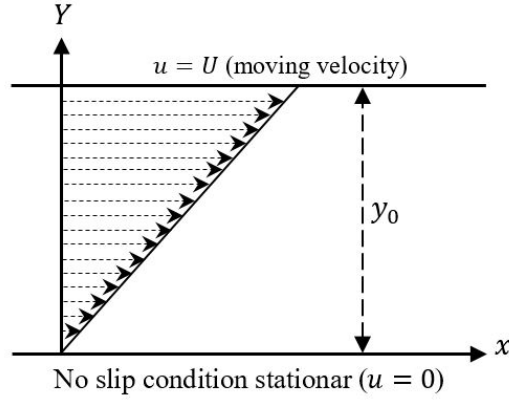


Figure 2.3: Geometrical configuration of viscosity

Consider two parallel plates placed at a distance  $y_0$  apart. The space between in is filled with fluid. The lower plate is stationary, and a force  $F$  is functional to the upper body, which is moving relative to the lower one with velocity  $U$ . Let  $A$  is the area of the upper plate. The ratio of the force per unit extent to the velocity decrease in the distance  $y_0$  is expressed as,

$$\frac{F}{A} \propto \frac{U}{y_0} \quad \Rightarrow \quad F = \mu \frac{AU}{y_0} \quad (2.1)$$

And the frictional or tangential, or shear stress  $\tau$  employed by the fluid at the upper plate is

$$\tau = \frac{F}{A} = \mu \frac{U}{y_0} \quad (2.2)$$

In the case of the differential unit,  $\frac{U}{y_0}$  is considered as the velocity gradient is vertical to the direction of shear or the rate of angular deformation,  $\frac{du}{dy}$ . Hence the shearing stress is

$$\tau = \mu \frac{du}{dy} \quad (2.3)$$

This relationship is known as Newton's Law of Viscosity. The proportionality constant  $\mu$  is the coefficient of dynamic molecular viscosity, simply the viscosity of the fluid. The CGS unit of  $\mu$  is poise, such that.  $1 - poise = (dyne - s)/(cm^2)$ ; i.e.  $[\mu] = [ML^{-1}T^{-1}]$

A fluid is viscous when normal stress and shearing stress exist. Syrup, honey, oil, etc., are regarded as viscous fluids. All fluids are composed of molecules discretely spaced and in continuous motion. For Mechanical analysis, a fluid is treated as a continuum.

If  $\tau = 0$ , then  $\mu = 0$ , and the fluid is ideal or perfect. Especially if the viscosity is constant and the fluid is incompressible through the liquid flow, the equation governing the shear stress in the Cartesian coordinate system is

$$\tau_{ij} = \mu \left( \frac{\partial u_i}{\partial x_j} + \frac{\partial u_j}{\partial x_i} \right) \quad (2.4)$$

**Kinematic viscosity  $\nu$ :** The ratio of the viscosity coefficient ( $\mu$ ) to the fluid density ( $\rho$ ) is called the kinematic viscosity and is denoted by  $\nu$ , which has a unit  $m^2/s$ . Thus

$$\nu = \frac{\mu}{\rho} \quad (2.5)$$

The CGS unit of  $\nu$  is stoke, such that  $1 - \text{stoke} = (cm^2)/sec$ ; i.e.  $[\nu] = [L^2T^{-1}]$

### 2.1.11 Newtonian Fluids

Sir Isaac Newton (1642 - 1726) first described the fluids' flow behaviour, expressing the relation between shearing stress and shear rate. According to his description, those fluids are called Newtonian if shear stress is directly proportional to the angular deformation rate starting with zero stress and zero deformation, *i.e.* the relation between the shear stress and the strain rate is linear in a Newtonian fluid. Newtonian fluids include air, water, honey, organic solvents, and mercury, whose viscosities depend only on pressure and temperature and are independent of the fluid's motion-time. In these cases, the constant of proportionality is defined as the absolute or dynamic viscosity directly related to molecular interactions. So, it is a thermodynamic property of a natural fluid in the macroscopic sense, which generates shear stress between two fluid elements.

### 2.1.12 Non-Newtonian Fluids

Non-Newtonian fluids assist in understanding the wide variety of fluids in the physical world. In comparison to Newtonian fluids, non-Newtonian fluids reveal either

- shear thinning or thickening (a non-linear correlation between shear stress and shear rate)
- or yield stress below which no flow occurs
- or deformation history (Rheopectic and Thixotropic), i.e., viscosity depends on the length of time of exposure to stress
- or a combination of elastic and viscous effects, i.e. viscoelastic effect
- or a combination of all of the above.

Non-Newtonian behaviour of fluids can be caused by several factors related to the structural reorganization of the fluid molecules due to flow.

*i)* A fluid is shear thickening (Dilatants) if the fluid viscosity improves as the shear rate increases. A typical example of shear-thickening fluids is a mixture of cornstarch and water. Fluids are shear thinning (Pseudo plastics) if the viscosity falls as the shear rate increases. Shear thinning fluids are universal in industrial and biological processes. Usual examples include ketchup, paints and blood. In polymer melts and solutions, the alignment of the highly anisotropic chains results in decreased viscosity. In colloids, the segregation of the different phases in the flow causes a shear-thinning behaviour.

*ii)* A Bingham plastic fluid like Casson fluid has yield stress (minimum stress to be applied before they flow) which must be outstripped before it will turn to flow like a liquid. As a result, the viscosity drops with increasing tension. These are precisely non-Newtonian fluids, but once the flow begins, they perform effectively as Newtonian fluids (i.e. shear stress is proportionate to shear rate). Toothpaste, mayonnaise and tomato ketchup are specimens of such products.

*iii)* Non-Newtonian fluids may depend on the length of time of exposure to stress. Rheopectic fluids or Anti-Thixotropic fluids oblige a steadily increasing shear stress to preserve a constant

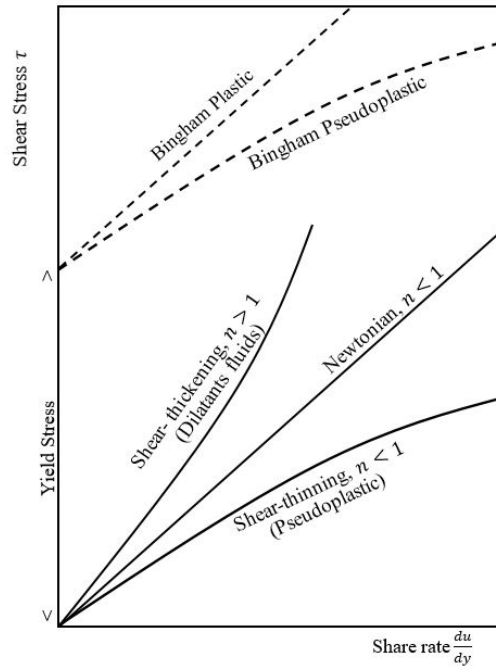


Figure 2.4: Newtonian and Non-Newtonian Fluid

strain rate, e.g., synovial fluid, printer ink, and gypsum paste. Thixotropic fluids exert dynamic viscosity decreased with the time for which the shearing forces are applied, e.g. jelly, yoghurt, peanut butter, and paints.

*iv)* Viscoelastic or elastico-viscous non-Newtonian fluids may exhibit elasticity and viscosity mechanical characteristics simultaneously. Examples of viscoelastic fluids are polymers, paints, latex, honey, ceramics and liquid metals.

**Power-law fluid model:** When the shear stress  $\tau$  of a Non-Newtonian fluid is a non-linear function of the rate of deformation is called power-law fluid (also called the Ostwald–de Waele relationship). The model, considering the power-law index  $n$ , is expressed as

$$\tau = \mu \left( \left| \frac{du}{dy} \right|^{n-1} \frac{du}{dy} \right) \quad (2.6)$$

The value on  $n$  determines the class of the fluid as

- $n < 1$  for Shear-thinning fluid (Pseudo plastics)
- $n = 1$  for Newtonian fluid
- $n > 1$  for Shear-thickening (Dilatants fluids)

For  $n < 1$  or  $n > 1$  represents the non-Newtonian fluid.

## 2.2 Governing Principles of Physical Aspects

From the basis of studying Magneto Fluid Dynamics (MFD) for a boundary layer, heat and mass transfer of the flow of an electrically conducting viscous nanofluid is approximately neutral with thermal diffusion, viscous dissipation, Brownian motion, and thermophoresis. Three fundamental principles govern the physical aspects of any fluid, i.e. conservation of (i) mass, (ii) momentum, and (iii) energy, with a combination of Brownian and thermophoresis diffusions.

**Equation of Continuity:** The mass conservation law is the basis for the continuity equation, also known as the mass conservation equation. Fluid mass entering a given section of the flow region is equal to fluid mass leaving that same section. In a way that prevents the addition or subtraction of any mass. The vector form of the continuity equation is derived for a turbulent flow of nanofluids, and it looks like this

$$\frac{\partial \rho}{\partial t} + \nabla \cdot (\rho V) = 0 \quad (2.7)$$

**Momentum equation:** According to the principle of conservation of momentum, the amount of momentum in a given region remains constant. According to Newton's laws of motion, the action of forces can only alter momentum; it cannot create or destroy any new momentum. According to Newton's second law of motion, the net sum of the forces acting on a body is equal to the rate of change of momentum of that body. The equation of momentum of nanofluid flow

becomes:

$$\rho \frac{dV}{dt} = F + \nabla \cdot \tau \quad (2.8)$$

**Energy equation:** Based on energy conservation, the equation states that energy is neither produced nor shattered but can be transformed from one form to another. It is derived from the first law of thermodynamics. Considering the Brownian motion and thermophoresis effects on nanofluid, the energy equation is

$$\rho C_P \frac{dT}{dt} = \nabla \cdot (\kappa \nabla T) + \mu \Phi - (C_P)_s J_s \cdot \nabla T \quad (2.9)$$

**Concentration Equation:** Based on the principle of mass conservation for all components of a fluid mixture, the concentration equation (also known as the diffusion equation) is established. The mass of a species entering a control volume, minus the mass of the same species leaving the volume, equals the mass stored in the volume at a constant rate in the absence of chemical reactions. In this case, the concentration equation having combined effects of Brownian motion and thermophoresis is given as

$$\frac{dC}{dt} = -\frac{1}{\rho_s} \nabla \cdot J_s \quad (2.10)$$

Here  $\frac{d}{dt} = \frac{\partial}{\partial t} + V \cdot \nabla$  is the material derivative;  $V = (u, v, w)$  is the three-dimensional velocity of the viscous fluid;  $\tau$  is the Cauchy stress tensor;  $\Phi$  is the viscous dissipation term that describes the conversion of mechanical energy to heat;  $J_s$  is the sum of Brownian and thermophoresis diffusions.

Buongiorno [5] disclosed the combination of Brownian and thermophoresis diffusions given by

$$J_s = -\rho_s D_B \nabla C - \rho_s D_T \frac{\nabla T}{T_a} \quad (2.11)$$

Here,  $D_B$  is the Brownian diffusion coefficient,  $D_T$  is the thermal diffusion coefficient, and  $T_a$  is the reference temperature.

### 2.2.1 Formation of the Model Equations

The unsteady laminar course of an incompressible fluid rotating with a uniform angular velocity  $\Omega$  is considered to establish the governing equations. A uniform magnetic field  $B$  is imposed. The MHD energy equation for a viscous incompressible electrically conducting nanofluid consists of mass diffusions and Joule heating. The MHD species equation represents the nanofluid volume fraction.

$$\begin{aligned}\nabla \cdot V &= 0 \\ \frac{\partial V}{\partial t} + (V \cdot \nabla)V + 2\Omega \times V &= \frac{1}{\rho} \nabla \cdot \tau + \frac{1}{\rho} (J \times B) \\ \frac{\partial V}{\partial t} + (V \cdot \nabla)T &= \frac{1}{\rho C_P} \nabla \cdot (\kappa \nabla T) + \frac{(\rho C_P)_s}{\rho C_P} \left( D_B \nabla C \cdot \nabla T + \frac{D_T}{T_a} \nabla T \cdot \nabla T \right) + \frac{J \cdot J}{\rho C_P} \\ \frac{\partial V}{\partial t} + (V \cdot \nabla)C &= \nabla \cdot \left( D_B \nabla C + \frac{D_T}{T_a} \nabla T \right)\end{aligned}$$

To arrange a 3D model corresponding to the coordinates  $(x, y, z)$ , let  $V = (u, v, z)$  is the velocity vector;  $F = (F_x, F_y, F_z)$  is the body force;  $J = (J_x, J_y, J_z)$  is the current density vector;  $B = (B_x, B_y, B_z)$  is the magnetic field vector;  $\Omega = (\Omega_x, \Omega_y, \Omega_z)$  is the angular vorticity vector; and  $\nabla = \hat{i} \frac{\partial}{\partial x} + \hat{j} \frac{\partial}{\partial y} + \hat{k} \frac{\partial}{\partial z}$  is a vector operator. And the viscous dissipation function is given by

$$\begin{aligned}\Phi &= 2 \left[ \left( \frac{\partial u}{\partial x} \right)^2 + \left( \frac{\partial v}{\partial y} \right)^2 + \left( \frac{\partial w}{\partial z} \right)^2 \right] + \left( \frac{\partial u}{\partial y} + \frac{\partial v}{\partial x} \right)^2 + \left( \frac{\partial v}{\partial z} + \frac{\partial w}{\partial y} \right)^2 \\ &\quad + \left( \frac{\partial w}{\partial x} + \frac{\partial u}{\partial z} \right)^2 - \frac{2}{3} \left( \frac{\partial u}{\partial x} + \frac{\partial v}{\partial y} + \frac{\partial w}{\partial z} \right)^2\end{aligned}$$



### 2.2.2 Magnetic Field Effect

A uniform magnetic field vector  $B = (B_x, B_y, B_z) = (0, B_0, 0)$  is imposed on the horizontal plate along the  $y$ -axis surrounded by an electrically non-conducting fluid. The equation of conservation of electric charge is

$$\nabla \cdot J = 0 \text{ or, } \frac{\partial J_x}{\partial x} + \frac{\partial J_y}{\partial y} + \frac{\partial J_z}{\partial z} = 0$$

$$\frac{\partial J_y}{\partial y} = 0$$

which implies that  $J_y = \text{constant}$ . Assume  $J_y = 0$  everywhere in the flow.

From the MHD generalized Ohm's law, it is obtained:

$$J = \sigma(E + V \times B)$$

$\sigma$  is the electric conductivity of the material. When an electric field is absent, the MHD generalized Ohm's law becomes:

$$J = \sigma(V \times B) = \sigma \begin{vmatrix} \hat{i} & \hat{j} & \hat{k} \\ u & 0 & 0 \\ 0 & B_0 & 0 \end{vmatrix} = \sigma B_0 u \hat{k}$$

Now

$$J \times B = \begin{vmatrix} \hat{i} & \hat{j} & \hat{k} \\ 0 & 0 & \sigma B_0 u \\ 0 & B_0 & 0 \end{vmatrix} = -\sigma B_0 u \hat{i}$$

$$\implies (J \times B)_x = -\sigma B_0 u$$

Again, there arises a magnetohydrodynamic effect, named the joule heating effect due to

MHD, in the thermal energy distribution of a nanofluid represented by the term  $\frac{J \cdot J}{\sigma}$ , where

$$J \cdot J = \sigma B_0 u \hat{k} \cdot \sigma B_0 u \hat{k} = \sigma^2 B_0^2 u^2.$$

**Magnetic field effect along the y-axis for 2D-Flow (u,w):**

$$J = \sigma(V \times B)$$

So

$$J = \sigma(V \times B) = \sigma \begin{vmatrix} \hat{i} & \hat{j} & \hat{k} \\ u & 0 & w \\ 0 & B_0 & 0 \end{vmatrix} = -\sigma B_0 w \hat{i} + \sigma B_0 u \hat{k}$$

Now

$$J \times B = \begin{vmatrix} \hat{i} & \hat{j} & \hat{k} \\ -\sigma B_0 w & 0 & \sigma B_0 u \\ 0 & B_0 & 0 \end{vmatrix} = -\sigma B_0^2 u \hat{i} - \sigma B_0^2 w \hat{k}$$

$$\implies J \times B = (-\sigma B_0^2 u, 0, -\sigma B_0^2 w) = (H_x, 0, H_z)$$

### 2.2.3 Hall Current Effect

The Hall current has an effect on an electrically conducting fluid in the presence of a magnetic field applied along the  $y$ -axis. The effect of magneto-Hall current gives rise to a force in the  $z$ -direction, which induces a cross-flow in the  $z$ -direction, and hence the flow becomes three-dimensional. Since Hall term is considered, the current density  $J$  is given by the generalized Ohm's law

$$J = \sigma[E + V \times B - \gamma(J \times B)]$$

Here,  $\gamma = \text{Hall factor} = 1/e n_e$ ;  $e = \text{charge electron}$ ;  $n_e = \text{mass of electron}$ ;  $E = \text{applied electric field}$ ;  $m = \sigma\gamma B_0 = \text{Hall parameter}$ ;  $B = (0, B_0, 0)$  is applied along  $y$ -axis.

If electric field is absent,

$$\begin{aligned}
 J &= \sigma(V \times B - \gamma(J \times B)) \implies J + \sigma\gamma(J \times B) = \sigma(V \times B) \\
 \implies \begin{vmatrix} J_x \\ 0 \\ J_z \end{vmatrix} + \sigma\gamma \begin{vmatrix} \hat{i} & \hat{j} & \hat{k} \\ J_x & 0 & J_z \\ 0 & B_0 & 0 \end{vmatrix} &= \sigma \begin{vmatrix} \hat{i} & \hat{j} & \hat{k} \\ u & 0 & w \\ 0 & B_0 & 0 \end{vmatrix} \\
 \implies [J_x \hat{i} \quad 0 \quad J_z \hat{k}] + \sigma\gamma[-\hat{i}J_z B_0 \quad 0 \quad \hat{k}J_x B_0] &= \sigma[-\hat{i}w B_0 \quad 0 \quad \hat{k}u B_0] \\
 \implies \begin{cases} J_x - \sigma\gamma J_z B_0 = -\sigma w B_0 \\ J_z + \sigma\gamma J_x B_0 = \sigma u B_0 \end{cases} \\
 \implies \begin{cases} J_x - m J_z = -\sigma B_0 w \\ J_z + m J_x = \sigma B_0 u \end{cases}
 \end{aligned}$$

Let  $m = \sigma\gamma B_0$ . Solving for  $J_x$  and  $J_z$ , we get

$$\begin{aligned}
 \begin{cases} J_x = \frac{\sigma B_0}{1+m^2}(mu - w) \\ J_z = \frac{\sigma B_0}{1+m^2}(u + mw) \end{cases} \\
 \implies J = [J_x \quad 0 \quad J_z] = \left[ \frac{\sigma B_0}{1+m^2}(mu - w) \quad 0 \quad \frac{\sigma B_0}{1+m^2}(u + mw) \right]
 \end{aligned}$$

The Lorentz force is given by

$$J \times B = \begin{vmatrix} \hat{i} & \hat{j} & \hat{k} \\ \frac{\sigma B_0}{1+m^2}(mu - w) & 0 & \frac{\sigma B_0}{1+m^2}(u + mw) \\ 0 & B_0 & 0 \end{vmatrix} = \hat{i} \frac{-\sigma B_0^2}{1+m^2}(u + mw) + \hat{k} \frac{-\sigma B_0^2}{1+m^2}(w - mu)$$

$$J \times B = \left( \frac{-\sigma B_0^2}{1+m^2}(u+mw), 0, \frac{-\sigma B_0^2}{1+m^2}(w-mu) \right) = (H_x, 0, H_z) \quad (2.12)$$

$$\frac{J \cdot J}{\sigma} = \frac{\sigma B_0^2}{(1+m^2)}(u^2+w^2) \quad (2.13)$$

Here,  $\frac{J \cdot J}{\sigma}$  is the expression for the Joule heating effect.

### 2.3 Viscoelastic Fluid Model

Some fluids have elastic properties, which allow them to spring back when shear stress is released, e.g. egg white. These fluids cannot be described satisfactorily by the theory of elasticity or viscosity, but a combination of viscosity-elasticity fluid models can design viscoelastic fluids. Some of the features that are commonly observed in viscoelastic fluids are:

- the shear rate dependence; the viscosity decreases with increasing shear rate;
- the normal stress effects, unequal normal stresses in different directions;
- the high elasticity recovery in shear.

Because of the diversity in the physical structure of non-Newtonian fluids, it is impossible to describe their mechanical behaviour by a single constitutive equation. For this reason, many constitutive equations have been proposed.

#### 2.3.1 Second-Grade Fluid Model:

The Rivlin-Ericksen model [110] and Noll's simple fluid model [111] are among those that have received considerable attention from both experimentalists and theorists. Coleman and Noll [112] proposed the constitutive equation of the second-grade fluid in 1961, where the stress tensor is the totality of all tensors. It can be moulded from the velocity field with up to two derivatives. So that an incompressible second-order fluid has a constitutive equation based on

the postulate given:

$$\tau = -PI + \mu A_1 + \alpha_1 A_2 + \alpha_2 A_1^2$$

Here,  $I$  is the identity tensor;  $\mu$  is the zero shear viscosity;  $A_1, A_2$  are the Rivlin-Ericksen tensors;  $\alpha_1, \alpha_2$  are the material contents; the symmetric fragment of the velocity gradient tensor is  $\nabla V$ . Second-grade rheological model is to be thermodynamically compatible; the Clasius-Duhem inequality should hold together with the Helmholtz free energy being at its minimum whenever the fluid is locally at rest. Thermodynamically constraints put some restrictions on the sign and magnitude of the material moduli:  $\mu \geq 0, \alpha_1 \geq 0; \alpha_1 + \alpha_2 = 0$ .

The symmetric portion of the velocity gradient tensor  $\nabla V$  is given by

$$A_1 = \nabla V + (\nabla V)^{\text{tr}}$$

And  $A_2$  is expressed as

$$A_2 = \frac{\partial A_1}{\partial t} + (V \cdot \nabla)A_1 + A_1 \cdot \nabla V + (\nabla V)^{\text{tr}} \cdot A_1$$

The material contents  $\alpha_1$  and  $\alpha_2$  are related to the first and second normal stress coefficients  $\Psi_1$  and  $\Psi_2$ , and  $\nabla V$  is the velocity gradient tensor written as

$$\nabla V = \begin{bmatrix} \frac{\partial u}{\partial x} & \frac{\partial u}{\partial y} & \frac{\partial u}{\partial z} \\ \frac{\partial v}{\partial x} & \frac{\partial v}{\partial y} & \frac{\partial v}{\partial z} \\ \frac{\partial w}{\partial x} & \frac{\partial w}{\partial y} & \frac{\partial w}{\partial z} \end{bmatrix}$$

Following all the relations mentioned above, the stress tensor can be expressed as

$$\tau = -PI + \mu A_1 + \alpha_1 \left( \frac{\partial A_1}{\partial t} + (V \cdot \nabla)A_1 + A_1 \cdot \nabla V + (\nabla V)^{\text{tr}} \cdot A_1 - A_1^2 \right)$$

Hence, the stress tensor  $\tau$  along the x- and y-direction can be written as

$$\begin{aligned}\tau_{xx} &= -P + 2\mu \frac{\partial u}{\partial x} + \alpha_1 \left( 2 \frac{\partial^2 u}{\partial t \partial x} + 2u \frac{\partial^2 u}{\partial x^2} + 2v \frac{\partial^2 u}{\partial x \partial y} - \left( \frac{\partial u}{\partial y} \right)^2 + \left( \frac{\partial v}{\partial x} \right)^2 \right) \\ \tau_{xy} = \tau_{yx} &= \mu \left( \frac{\partial u}{\partial y} + \frac{\partial v}{\partial x} \right) + \alpha_1 \left( \frac{\partial^2 u}{\partial t \partial y} + \frac{\partial^2 v}{\partial t \partial x} + v \frac{\partial^2 u}{\partial y^2} + u \frac{\partial^2 v}{\partial x^2} \right. \\ &\quad \left. + \frac{\partial u}{\partial x} \frac{\partial u}{\partial y} + \frac{\partial v}{\partial x} \frac{\partial v}{\partial y} + u \frac{\partial^2 u}{\partial x \partial y} + v \frac{\partial^2 v}{\partial x \partial y} - \frac{\partial u}{\partial x} \frac{\partial v}{\partial x} - \frac{\partial u}{\partial y} \frac{\partial v}{\partial y} \right) \\ \tau_{yy} &= -P + 2\mu \frac{\partial v}{\partial y} + \alpha_1 \left( 2 \frac{\partial^2 v}{\partial t \partial y} + 2v \frac{\partial^2 v}{\partial y^2} + 2u \frac{\partial^2 v}{\partial x \partial y} + \left( \frac{\partial u}{\partial y} \right)^2 - \left( \frac{\partial v}{\partial x} \right)^2 \right)\end{aligned}$$

Finally,

$$\operatorname{div} \tau = \nabla \cdot \tau = \begin{bmatrix} \frac{\partial}{\partial x} & \frac{\partial}{\partial y} \end{bmatrix} \cdot \begin{bmatrix} \tau_{xx} & \tau_{xy} \\ \tau_{yx} & \tau_{yy} \end{bmatrix} = \begin{bmatrix} \frac{\partial \tau_{xx}}{\partial x} + \frac{\partial \tau_{xy}}{\partial y} & \frac{\partial \tau_{yx}}{\partial x} + \frac{\partial \tau_{yy}}{\partial y} \end{bmatrix}$$

yields  $\operatorname{div} \tau$  along the x-axis:

$$\begin{aligned}\operatorname{div} \tau|_x &= \frac{\partial \tau_{xx}}{\partial x} + \frac{\partial \tau_{xy}}{\partial y} = -\frac{\partial P}{\partial x} + 2\mu \frac{\partial u^2}{\partial x^2} + \mu \frac{\partial u^2}{\partial y^2} + \mu \frac{\partial^2 v}{\partial x \partial y} \\ &\quad + \alpha_1 \left( \frac{\partial^3 u}{\partial t \partial y^2} + 2 \frac{\partial^3 u}{\partial t \partial x^2} + \frac{\partial^3 v}{\partial t \partial x \partial y} + v \frac{\partial^3 u}{\partial y^3} + 2u \frac{\partial^3 u}{\partial x^3} + u \frac{\partial^3 v}{\partial x \partial y^2} \right. \\ &\quad \left. + u \frac{\partial^3 v}{\partial x^2 \partial y} + v \frac{\partial^3 v}{\partial x \partial y^2} + 2v \frac{\partial^3 u}{\partial x^2 \partial y} + 2 \frac{\partial v}{\partial x} \frac{\partial^2 v}{\partial x^2} + 2 \frac{\partial v}{\partial y} \frac{\partial^2 v}{\partial x \partial y} + 2 \frac{\partial u}{\partial x} \frac{\partial^2 u}{\partial x^2} \right. \\ &\quad \left. + \frac{\partial u}{\partial y} \frac{\partial^2 v}{\partial x^2} + \frac{\partial v}{\partial x} \frac{\partial^2 v}{\partial y^2} + \frac{\partial u}{\partial x} \frac{\partial^2 u}{\partial y^2} + \frac{\partial v}{\partial x} \frac{\partial^2 u}{\partial x \partial y} - \frac{\partial u}{\partial x} \frac{\partial^2 v}{\partial x \partial y} - \frac{\partial u}{\partial y} \frac{\partial^2 v}{\partial y^2} \right)\end{aligned}$$

and  $\operatorname{div} \tau$  along the y-axis:

$$\begin{aligned}\operatorname{div} \tau|_y &= \frac{\partial \tau_{yx}}{\partial x} + \frac{\partial \tau_{yy}}{\partial y} = -\frac{\partial P}{\partial y} + \mu \frac{\partial v^2}{\partial x^2} + 2\mu \frac{\partial v^2}{\partial y^2} + \mu \frac{\partial^2 u}{\partial x \partial y} \\ &\quad + \alpha_1 \left( \frac{\partial^3 v}{\partial t \partial x^2} + 2 \frac{\partial^3 v}{\partial t \partial y^2} + \frac{\partial^3 u}{\partial t \partial x \partial y} + u \frac{\partial^3 v}{\partial x^3} + 2v \frac{\partial^3 v}{\partial y^3} + v \frac{\partial^3 v}{\partial x^2 \partial y} \right. \\ &\quad \left. + v \frac{\partial^3 u}{\partial x \partial y^2} + u \frac{\partial^3 u}{\partial x^2 \partial y} + 2u \frac{\partial^3 v}{\partial x \partial y^2} + 2 \frac{\partial u}{\partial y} \frac{\partial^2 u}{\partial y^2} + 2 \frac{\partial u}{\partial x} \frac{\partial^2 u}{\partial x \partial y} + 2 \frac{\partial v}{\partial y} \frac{\partial^2 v}{\partial y^2} \right. \\ &\quad \left. + \frac{\partial v}{\partial x} \frac{\partial^2 u}{\partial y^2} + \frac{\partial u}{\partial y} \frac{\partial^2 u}{\partial x^2} + \frac{\partial v}{\partial y} \frac{\partial^2 v}{\partial x^2} + \frac{\partial u}{\partial y} \frac{\partial^2 v}{\partial x \partial y} - \frac{\partial v}{\partial y} \frac{\partial^2 u}{\partial x \partial y} - \frac{\partial v}{\partial x} \frac{\partial^2 u}{\partial x^2} \right)\end{aligned}$$

### 2.3.2 Upper Convected Maxwell (UCM) Fluid Model

The elasto-viscous behaviour will be realized if elastic stress is applied to the fluid, and the resulting strain will be time-dependent and characterized by relaxation time [1]. The constitutive equation considering time-dependent stress relaxation is

$$\rho \mathbf{a} = \rho \frac{d\mathbf{V}}{Dt} = \mathbf{F} + \nabla \cdot \boldsymbol{\tau} + (\mathbf{J} \times \mathbf{B}) \quad (2.14)$$

$\mathbf{a}$  is the acceleration vector;  $\boldsymbol{\tau}$  is the Cauchy stress tensor for UCM fluid given by

$$\boldsymbol{\tau} = -PI + \mathbf{S} \quad (2.15)$$

The extra stress tensor  $\mathbf{S}$  is defined by

$$\mathbf{S} + \lambda_s \frac{d\mathbf{S}}{dt} = \mu \mathbf{A}_1 \quad (2.16)$$

Here  $\lambda_s > 0$  is the stress relaxation time factor where  $\lambda_s = 0$  describes the Newtonian fluids, and  $\mathbf{A}_1$  is the Rivlin-Ericksen tensor. In addition, when the magnetic field is present, four more laws are considered as follows:

$$\nabla \cdot \mathbf{E} = \frac{\rho_c}{\epsilon_p} \quad (\text{Gauss's Law})$$

$$\nabla \times \mathbf{E} = -\frac{\partial \mathbf{B}}{\partial t} \quad (\text{Faraday's Law})$$

$$\nabla \times \mathbf{B} = \mu_0 \mathbf{J} + \mu_0 \epsilon_p \frac{\partial \mathbf{E}}{\partial t} \quad (\text{Ampere's Law with Maxwell's correction})$$

$$\nabla \cdot B = 0 \quad (\text{Gauss's Law for magnetism})$$

Here,  $J = \sigma(E + V \times B)$  is the current density;  $\epsilon_p$  is the permittivity of free space,  $\mu_0$  is the magnetic permeability;  $\sigma$  is the fluid electrical conductivity;  $E$  is the electric field;  $B(0, B_0, 0)$  is the magnetic flux;  $B_0$  is the applied magnetic field strength along the  $y$ -axis.

The following equations are used for the two-rank tensor  $S$ , a vector  $b$  and a scalar function  $\psi$ , respectively.

$$\frac{dS}{dt} = \frac{\partial S}{\partial t} + (V \cdot \nabla)S - LS - SL^{\text{tr}}$$

$$\frac{db}{dt} = \frac{\partial b}{\partial t} + (V \cdot \nabla)b - Lb$$

$$\frac{d\psi}{dt} = \frac{\partial \psi}{\partial t} + (V \cdot \nabla)\psi$$

Combining 2.14 and 2.15, the momentum equation for UCM fluid model takes the form

$$\rho a = -\nabla P + \nabla \cdot S + J \times B \quad (2.17)$$

The electromagnetic body force ignoring induced magnetic field takes the form

$$J \times B = \sigma[(V \times B) \times B]$$

To eliminate  $S$ , apply the operator  $(1 + \lambda_S \frac{d}{dt})$  onto eqn. 2.14 to get

$$\rho(1 + \lambda_S \frac{d}{dt})a = -(1 + \lambda_S \frac{d}{dt})\nabla P + (1 + \lambda_S \frac{d}{dt})\nabla \cdot S + (1 + \lambda_S \frac{d}{dt})J \times B \quad (2.18)$$



Eqn. 2.18 in view of the result  $\frac{d}{dt}\nabla\cdot = \nabla\cdot\frac{d}{dt}$  given by Harris [49] is

$$\rho\left(\mathbf{a} + \lambda_S \frac{d\mathbf{a}}{dt}\right) = -\left(1 + \lambda_S \frac{d}{dt}\right)\nabla P + \nabla\cdot\left(1 + \lambda_S \frac{d}{dt}\right)\mathbf{S} + \left(1 + \lambda_S \frac{d}{dt}\right)\mathbf{J} \times \mathbf{B}$$

Eqn. 2.16 gives

$$\rho\left(\mathbf{a} + \lambda_S \frac{d\mathbf{a}}{dt}\right) = -\left(1 + \lambda_S \frac{d}{dt}\right)\nabla P + \mu\nabla\cdot\mathbf{A}_1 + \left(1 + \lambda_S \frac{d}{dt}\right)\mathbf{J} \times \mathbf{B} \quad (2.19)$$

The first Rivlin-Ericksen tensor is given by

$$\mathbf{A}_1 = \begin{bmatrix} 2\frac{\partial u}{\partial x} & \frac{\partial u}{\partial y} + \frac{\partial v}{\partial x} \\ \frac{\partial u}{\partial y} + \frac{\partial v}{\partial x} & 2\frac{\partial v}{\partial y} \end{bmatrix}$$

And the vector  $\mathbf{a}$  is given by

$$\frac{d\mathbf{a}}{dt} = \frac{\partial\mathbf{a}}{\partial t} + (\mathbf{V}\cdot\nabla)\mathbf{a} - L\mathbf{a}$$

along with

$$\mathbf{a} = \left( \left( \frac{\partial u}{\partial t} + u\frac{\partial u}{\partial x} + v\frac{\partial u}{\partial y} \right), \left( \frac{\partial v}{\partial t} + u\frac{\partial v}{\partial x} + v\frac{\partial v}{\partial y} \right), 0 \right) = (a_x, a_y, 0)$$

Now,

$$\frac{\partial a_x}{\partial t} = \frac{\partial}{\partial t} \left( \frac{\partial u}{\partial t} + u\frac{\partial u}{\partial x} + v\frac{\partial u}{\partial y} \right) = \frac{\partial^2 u}{\partial t^2} + u\frac{\partial^2 u}{\partial t\partial x} + \frac{\partial u}{\partial t}\frac{\partial u}{\partial x} + v\frac{\partial^2 u}{\partial t\partial y} + \frac{\partial v}{\partial t}\frac{\partial u}{\partial y}$$

And

$$\begin{aligned} (\mathbf{V}\cdot\nabla)a_x &= \left( u\frac{\partial}{\partial x} + v\frac{\partial}{\partial y} \right) \left( \frac{\partial u}{\partial t} + u\frac{\partial u}{\partial x} + v\frac{\partial u}{\partial y} \right) \\ &= u\frac{\partial^2 u}{\partial t\partial x} + u\left(\frac{\partial u}{\partial x}\right)^2 + u^2\frac{\partial^2 u}{\partial x^2} + 2uv\frac{\partial^2 u}{\partial x\partial y} + u\frac{\partial v}{\partial x}\frac{\partial u}{\partial y} + v\frac{\partial^2 u}{\partial t\partial y} + v\frac{\partial u}{\partial x}\frac{\partial u}{\partial y} + v^2\frac{\partial^2 u}{\partial y^2} + v\frac{\partial u}{\partial y}\frac{\partial v}{\partial y} \end{aligned}$$

$$\begin{aligned}
La &= \begin{bmatrix} \frac{\partial u}{\partial x} & \frac{\partial u}{\partial y} \\ \frac{\partial v}{\partial x} & \frac{\partial v}{\partial y} \end{bmatrix} \left( \frac{\partial u}{\partial t} + u \frac{\partial u}{\partial x} + v \frac{\partial u}{\partial y}, \frac{\partial v}{\partial t} + u \frac{\partial v}{\partial x} + v \frac{\partial v}{\partial y} \right) \\
&= \left( \frac{\partial u}{\partial t} \frac{\partial u}{\partial x} + u \left( \frac{\partial u}{\partial x} \right)^2 + v \frac{\partial u}{\partial x} \frac{\partial u}{\partial y} + \frac{\partial u}{\partial y} \frac{\partial v}{\partial t} + u \frac{\partial u}{\partial y} \frac{\partial v}{\partial x} + v \frac{\partial u}{\partial y} \frac{\partial v}{\partial y}, \right. \\
&\quad \left. \frac{\partial u}{\partial t} \frac{\partial v}{\partial x} + u \frac{\partial u}{\partial x} \frac{\partial v}{\partial x} + v \frac{\partial u}{\partial y} \frac{\partial v}{\partial x} + \frac{\partial v}{\partial t} \frac{\partial v}{\partial y} + u \frac{\partial v}{\partial x} \frac{\partial v}{\partial y} + v \left( \frac{\partial v}{\partial y} \right)^2 \right)
\end{aligned}$$

And

$$La|_x = \frac{\partial u}{\partial t} \frac{\partial u}{\partial x} + u \left( \frac{\partial u}{\partial x} \right)^2 + v \frac{\partial u}{\partial x} \frac{\partial u}{\partial y} + \frac{\partial u}{\partial y} \frac{\partial v}{\partial t} + u \frac{\partial u}{\partial y} \frac{\partial v}{\partial x} + v \frac{\partial u}{\partial y} \frac{\partial v}{\partial y}$$

Therefore,  $\frac{da}{dt}$  along the  $x$ -axis is defined as

$$\begin{aligned}
\frac{da_x}{dt} &= \frac{\partial a_x}{\partial t} + (V \cdot \nabla) a_x - La|_x \\
&= \frac{\partial^2 u}{\partial t^2} + u \frac{\partial^2 u}{\partial t \partial x} + \frac{\partial u}{\partial t} \frac{\partial u}{\partial x} + v \frac{\partial^2 u}{\partial t \partial y} + \frac{\partial v}{\partial t} \frac{\partial u}{\partial y} \\
&+ u \frac{\partial^2 u}{\partial t \partial x} + u \left( \frac{\partial u}{\partial x} \right)^2 + u^2 \frac{\partial^2 u}{\partial x^2} + 2uv \frac{\partial^2 u}{\partial x \partial y} + u \frac{\partial v}{\partial x} \frac{\partial u}{\partial y} + v \frac{\partial^2 u}{\partial t \partial y} + v \frac{\partial u}{\partial x} \frac{\partial u}{\partial y} + v^2 \frac{\partial^2 u}{\partial y^2} + v \frac{\partial u}{\partial y} \frac{\partial v}{\partial y} \\
&\quad - \left( \frac{\partial u}{\partial t} \frac{\partial u}{\partial x} + u \left( \frac{\partial u}{\partial x} \right)^2 + v \frac{\partial u}{\partial x} \frac{\partial u}{\partial y} + \frac{\partial u}{\partial y} \frac{\partial v}{\partial t} + u \frac{\partial u}{\partial y} \frac{\partial v}{\partial x} + v \frac{\partial u}{\partial y} \frac{\partial v}{\partial y} \right)
\end{aligned}$$

So,

$$\frac{da_x}{dt} = \frac{\partial^2 u}{\partial t^2} + 2u \frac{\partial^2 u}{\partial t \partial x} + 2v \frac{\partial^2 u}{\partial t \partial y} + 2uv \frac{\partial^2 u}{\partial x \partial y} + u^2 \frac{\partial^2 u}{\partial x^2} + v^2 \frac{\partial^2 u}{\partial y^2} \quad (2.20)$$

Also, the divergence of a tensor

$$\nabla \cdot A_1 = \begin{bmatrix} \frac{\partial}{\partial x} & \frac{\partial}{\partial y} \end{bmatrix} \cdot \begin{bmatrix} 2 \frac{\partial u}{\partial x} & \frac{\partial u}{\partial y} + \frac{\partial v}{\partial x} \\ \frac{\partial u}{\partial y} + \frac{\partial v}{\partial x} & 2 \frac{\partial v}{\partial y} \end{bmatrix} = \begin{bmatrix} 2 \frac{\partial^2 u}{\partial x^2} + \frac{\partial^2 u}{\partial y^2} + \frac{\partial^2 v}{\partial x \partial y} & 2 \frac{\partial^2 v}{\partial y^2} + \frac{\partial^2 v}{\partial x^2} + \frac{\partial^2 u}{\partial x \partial y} \end{bmatrix}$$

Hence,

$$\nabla \cdot A_1|_x = 2 \frac{\partial^2 u}{\partial x^2} + \frac{\partial^2 u}{\partial y^2} + \frac{\partial^2 v}{\partial x \partial y} \quad (2.21)$$

**Hall current effect due to the magnetic field along  $y$ -axis:** Since Hall term is considered and the current density is  $J$  then

$$J \times B = \left( \frac{-\sigma B_0^2}{1+m^2}(u+mw), 0, \frac{-\sigma B_0^2}{1+m^2}(w-mu) \right) = (H_x, 0, H_z)$$

Now

$$\begin{aligned} (1 + \lambda_S \frac{d}{dt}) J \times B &= (J \times B) + \lambda_S \frac{d}{dt} (J \times B) \\ &= (J \times B) + \lambda_S \left( \frac{\partial}{\partial t} + (V \cdot \nabla) - L \right) (J \times B) \\ &= (H_x, 0, H_z) + \lambda_S \left( \frac{\partial}{\partial t} (H_x, 0, H_z) + (V \cdot \nabla) (H_x, 0, H_z) - L (H_x, 0, H_z) \right) \\ &= (H_x, 0, H_z) + \lambda_S \left( \left( \frac{\partial H_x}{\partial t}, 0, \frac{\partial H_z}{\partial t} \right) + \left( u \frac{\partial}{\partial x} + v \frac{\partial}{\partial y} \right) (H_x, 0, H_z) - \left( H_x \frac{\partial u}{\partial x}, 0, H_x \frac{\partial w}{\partial x} \right) \right) \end{aligned}$$

Then along the  $x$ -axis,

$$\begin{aligned} (1 + \lambda_S \frac{d}{dt}) J \times B|_x &= H_x + \lambda_S \left( \frac{\partial H_x}{\partial t} + u \frac{\partial H_x}{\partial x} + v \frac{\partial H_x}{\partial y} - H_x \frac{\partial u}{\partial x} \right) \\ &= \frac{-\sigma B_0^2}{(1+m^2)} \left( u + mw + \lambda_S \left( \frac{\partial u}{\partial t} + v \frac{\partial u}{\partial y} + m \left( \frac{\partial w}{\partial t} + u \frac{\partial w}{\partial x} + v \frac{\partial w}{\partial y} - w \frac{\partial u}{\partial x} \right) \right) \right) \end{aligned} \quad (2.22)$$

Similarly, along the  $z$ -axis,

$$\begin{aligned} (1 + \lambda_S \frac{d}{dt}) J \times B|_z &= \\ \frac{\sigma B_0^2}{(1+m^2)} &\left( mu - w + \lambda_S \left( m \left( \frac{\partial u}{\partial t} + u \frac{\partial u}{\partial x} + v \frac{\partial u}{\partial y} + w \frac{\partial w}{\partial x} \right) - \frac{\partial w}{\partial t} - v \frac{\partial w}{\partial y} \right) \right) \end{aligned} \quad (2.23)$$

Finally, the required UCM model under the Hall effect is expressed as

$$\begin{aligned} & \rho \left( \frac{\partial u}{\partial t} + u \frac{\partial u}{\partial x} + v \frac{\partial u}{\partial y} + \lambda_s \left( \frac{\partial^2 u}{\partial t^2} + 2u \frac{\partial^2 u}{\partial t \partial x} + 2v \frac{\partial^2 u}{\partial t \partial y} + 2uv \frac{\partial^2 u}{\partial x \partial y} + u^2 \frac{\partial^2 u}{\partial x^2} + v^2 \frac{\partial^2 u}{\partial y^2} \right) \right) \\ &= -\frac{\partial P}{\partial x} + \mu \frac{\partial^2 u}{\partial y^2} - \frac{\sigma B_0^2}{(1+m^2)} \left( u + mw + \lambda_s \left( \frac{\partial u}{\partial t} + v \frac{\partial u}{\partial y} + m \left( \frac{\partial w}{\partial t} + u \frac{\partial w}{\partial x} + v \frac{\partial w}{\partial y} - w \frac{\partial u}{\partial x} \right) \right) \right) \end{aligned} \quad (2.24)$$

$$\begin{aligned} & \rho \left( \frac{\partial w}{\partial t} + u \frac{\partial w}{\partial x} + v \frac{\partial w}{\partial y} + \lambda_s \left( \frac{\partial^2 w}{\partial t^2} + 2u \frac{\partial^2 w}{\partial t \partial x} + 2v \frac{\partial^2 w}{\partial t \partial y} + 2uv \frac{\partial^2 w}{\partial x \partial y} + u^2 \frac{\partial^2 w}{\partial x^2} + v^2 \frac{\partial^2 w}{\partial y^2} \right) \right) \\ &= \mu \frac{\partial^2 w}{\partial y^2} + \frac{\sigma B_0^2}{(1+m^2)} \left( mu - w + \lambda_s \left( m \left( \frac{\partial u}{\partial t} + u \frac{\partial u}{\partial x} + v \frac{\partial u}{\partial y} + w \frac{\partial w}{\partial x} \right) - \frac{\partial w}{\partial t} - v \frac{\partial w}{\partial y} \right) \right) \end{aligned} \quad (2.25)$$

**Cattaneo–Christov Model:** Cattaneo–Christov model is proposed by adding thermal relaxation time in Fourier’s Law, also called the modified Fourier heat conduction law, presented by

$$\mathbf{q} + \lambda_T \left( \frac{\partial \mathbf{q}}{\partial t} + \mathbf{V} \cdot \nabla \mathbf{q} - \mathbf{q} \cdot \nabla \mathbf{V} + (\nabla \cdot \mathbf{V}) \mathbf{q} \right) = -\kappa \nabla T$$

Here,  $\kappa$  is the thermal conductivity and  $\lambda_T > 0$  is the thermal relaxation time parameter for the heat flux where  $\lambda_T = 0$  simplifies the expression (7) to classical Fourier’s law.

### 2.3.3 Couette Parallel Flow

Two parallel plates of very long dimensions in the  $x$  and  $z$  directions. Top plate moves at a velocity  $U$  and is at temperature  $T$ . Bottom plate is stationary i.e. velocity = 0. Distance between plates =  $L$ .

## 2.4 Dimensional Analysis

Dimensional analysis is unique in mathematics and the physical sciences for ambiguity surrounding a well-used term’s meaning. This analysis is a mathematical technique commonly

used to determine the relationships between several physical variables that influence the flow in fluid mechanics, heat transfer in thermodynamics, and so forth. Dimensional analysis mentions the fundamental technique of relating finite characteristics within a system or between systems using the fact that the value of a unit of measurement stays unaffected regardless of the quantity or the method for which it is used. In detail, scientific perception in fluid mechanics is quantitatively based on concepts of physical phenomena, each of which is a unit of measurement that has been assigned. The quantities in SI or MKS units are adopted to obtain a numerical solution. It is appropriate to adopt a dependable dimensional scheme composed of the smallest number of dimensions in terms of which all the physical entities may be expressed. The fundamental dimensions of the procedure are length  $[L]$ , time  $[T]$ , mass  $[M]$ , and force  $[F]$ , related by Newton's second law of motion,  $F = ma$ . Dimensionally, the law may also be written as,

$$[F] = \left[ \frac{ML}{T^2} \right] \quad \Rightarrow \quad \left[ \frac{FT^2}{ML} \right] = 1$$

Clearly, when three of the dimensions are well-known, the fourth can be stated in terms of the other three. Consequently, three autonomous dimensions are adequate for any physical phenomenon found in Newtonian technicalities. They are usually chosen as  $[MLT]$  (mass, length, time) or  $[FLT]$  (force, length, time). For example, the specific mass ( $\rho$ ) may be expressed either as  $[ML^{-3}]$  or as  $[FT^2L^{-4}]$ , and fluid pressure ( $P$ ), which is commonly described as force per unit area  $[FL^{-2}]$ , may also be expressed as  $[MLT^{-2}]$  using the (mass, length, time) system. A summary of some of the entities frequently used in fluid mechanics, together with their dimensions in both systems, is given in Table 2.3.

### **Practicality of Dimensional Analysis**

Dimensional analysis is a potent tool in many disciplines, not just in fluid mechanics. It provides a technique to plan and carry out experiments and enables one to scale up results from the model to the prototype. Purpose:

- To verify an equation complies with the principle of homogeneity of dimensions.

Table 2.3: Entities commonly used in fluid mechanics and their dimensions

Entity	MLT System
Mass ( $m$ )	M
Length ( $L$ )	L
Time ( $t$ )	T
Area ( $A$ )	L <sup>2</sup>
Volume ( $V$ )	L <sup>3</sup>
Velocity ( $v$ )	LT <sup>-1</sup>
Acceleration ( $a$ )	LT <sup>-2</sup>
Force ( $F$ ) and Weight ( $W$ )	MLT <sup>-2</sup>
Specific weight ( $\gamma = F/V$ )	ML <sup>-2</sup> T <sup>-2</sup>
Pressure ( $P = F/A$ ) and stress ( $\tau$ )	ML <sup>-1</sup> T <sup>-2</sup>
Energy ( $E$ ) and work ( $w$ )	ML <sup>2</sup> T <sup>-2</sup>
Momentum ( $mv$ )	MLT <sup>-1</sup>
Specific mass/ density ( $\rho$ )	ML <sup>-3</sup>
Dynamic viscosity ( $\mu$ )	ML <sup>-1</sup> T <sup>-1</sup>
Kinematic viscosity ( $\nu$ )	L <sup>2</sup> T <sup>-1</sup>

- To renovate from one system of units to another.
- To determine or derive a relationship between two physical characteristics.
- To determine or derive a relationship between two quantities.
- To express one attribute in terms of another.

Usefulness:

- Offering and interpreting experimental data.
- Tackling problems not amenable to a direct theoretical solution.
- Examination of equations.
- Establishing the relative importance of particular physical phenomena.
- Physical modelling.

Methods for dimensional analysis: *i*) Rayleigh Method *ii*) Buckingham II Theorem:

## 2.5 Boundary–Layer Approximation

With the concept of the MHD boundary layer phenomena, let  $\delta$  be the non-dimensional boundary layer thickness which is considered to be very small everywhere, where

$$\delta = \frac{\text{Original boundary layer thickness}}{L}$$

Now it is assumed that  $\delta \ll 1$  be the order of magnitude of  $\delta$ , i.e.  $O(\delta) = \varepsilon$ . Then it can be written in the order of magnitude of  $y$ ,  $v$  and  $B_0$  are equal to  $\varepsilon$ , i.e.  $O(y) = \varepsilon$ ,  $O(v) = \varepsilon$  and  $O(B_0) = \varepsilon$ . Also, it is considered that the order of magnitude of  $\nu$ , i.e. order of  $\frac{\mu}{\rho}$  is  $\varepsilon^2$ , which implies that  $O(\nu) = O(\mu/\rho) = \varepsilon^2$ .

Now determine the order of magnitude of each term in considering the order of  $u$ ,  $x$  and  $t$  are equal to one, i.e.  $O(u) = 1$ ,  $O(x) = 1$  and  $O(t) = 1$ . Hence  $O(\frac{\partial u}{\partial x}) = 1$  and  $O(\frac{\partial^2 u}{\partial x^2}) = 1$ ;  $O(\frac{\partial u}{\partial t}) = 1$ ;  $O(\frac{\partial u}{\partial y}) = \frac{1}{\varepsilon}$ ;  $O(\frac{\partial^2 u}{\partial y^2}) = \frac{1}{\varepsilon^2}$ ;  $O(\frac{\partial v}{\partial t}) = \varepsilon$ ;  $O(\frac{\partial v}{\partial x}) = \varepsilon$ ;  $O(\frac{\partial v}{\partial y}) = 1$ ;  $O(\frac{\partial^2 v}{\partial x^2}) = \varepsilon$ ;  $O(\frac{\partial^2 v}{\partial y^2}) = \frac{1}{\varepsilon}$  within the boundary layer.

The viscous forces in the boundary layer can become of the same order of magnitude as the inertia forces only if the Reynolds number is of the order of  $1/\varepsilon^2$  i.e.  $O(\text{Re}) = \frac{1}{\varepsilon^2}$

## 2.6 Dynamic Similarity Analysis

The theory of dynamic similarity can be stated as follows:

When the model and prototype are geometrically similar (that is, the model is a perfect scale duplicate of the prototype), and if each independent dimensionless factor for the scheme is equal to the corresponding separate dimensionless parameter for the prototype, then the conditional dimensionless parameter for the prototype will be similar to the analogous dependent dimensionless parameter for the model. In fluid mechanics, dynamic similarity is when two geometrically similar vessels (same shape, different sizes) with the same boundary conditions (e.g., no-slip, centre-line velocity) and the same Reynolds and Womersley numbers, the fluid flows will be identical. It can be seen from inspection of the underlying Navier-Stokes equation, with geo-

metrically similar bodies, equal Reynolds and Womersley Numbers, the functions of velocity  $(u', v', w')$  and pressure  $(P')$  for any variation of flow.

### 2.6.1 Lie Symmetry Analysis

Some basics of Lie symmetry methods for solving differential equations are discussed below, Olver (1986) [113]; Ovsiannikov (1982) [114]; Bluman *et al.* (1988) [115].

**Symmetry transformations of differential equations:** A symmetry transformation of a differential equation is one in which the equation does not undergo any changes.

Consider a  $k$ th-order  $k \geq 1$  system of differential equations

$$F^\alpha(x, u, u_{(1)}, \dots, u_{(k)}) = 0; \quad \alpha = 1, \dots, m \quad (2.26)$$

where  $u = (u^1, \dots, u^m)$  is the dependent variable, function of the independent variable  $x = (x^1, \dots, x^n)$ ; and  $u_{(1)}, \dots, u_{(k)}$  are the collection of all first, second up to  $k$ th-order derivatives of  $u$ .

A transformation of the variables  $x$  and  $u$ , viz.

$$\bar{x}^i = f^i(x, u), \quad \bar{u}^\alpha = g^\alpha(x, u); \quad i = 1, \dots, n; \quad \alpha = 1, \dots, m \quad (2.27)$$

is called a symmetry transformation of the system (2.26) if it is invariant with the new variables  $\bar{x}$  and  $\bar{u}$ , that is

$$F^\alpha(\bar{x}, \bar{u}, \bar{u}_{(1)}, \dots, \bar{u}_{(k)}) = 0; \quad \alpha = 1, \dots, m \quad (2.28)$$

**Lie symmetry method for partial differential equations:** In this article, the classical Lie symmetry approach to solving a system of partial differential equations is discussed. Let us consider a  $p$ th-order system of partial differential equations in  $n$  independent variables  $x =$



$(x^1, \dots, x^n)$ ; and  $m$  dependent variables  $u = u^1, \dots, u^m$ , viz.

$$E(x, u, u_{(1)}, \dots, u_{(p)}) = 0 \quad (2.29)$$

where  $u_{(k)}$ ;  $1 \leq k \leq p$  denotes the set of all  $k$ th-order derivatives of  $u$  with respect to the independent variables defined by

$$u_{(k)}^\alpha = \frac{\partial^k u}{\partial x_{i_1} \dots \partial x_{i_k}} \quad (2.30)$$

With  $1 \leq i_1 \leq \dots \leq i_k \leq n$ .

For finding the symmetries of Eq. (2.30), we first construct the group of invertible transformations depending on the actual parameter  $a$ ; which leaves Eq. (2.30) invariant, namely

$$\bar{x}_1 = f^1(x, u, a), \dots, \bar{x}_n = f^n(x, u, a), \bar{u}^\alpha = g^\alpha(x, u, a) \quad (2.31)$$

The initial set of transformations is said to form a one-parameter group because it possesses the closure property, is associative, and allows for inverses and identity transformation. Given that  $a$  is a negligibly small parameter, the expansion of the transformations (2.31) can be written as

$$\bar{x}_1 = \bar{x} + a\xi_1(x, u) + O(a^2), \dots, \bar{x}_n = \bar{x} + a\xi_n(x, u) + O(a^2) \quad (2.32)$$

$$\bar{u}_1 = \bar{u} + a\xi_1(x, u) + O(a^2), \dots, \bar{u}_n = \bar{u} + a\xi_n(x, u) + O(a^2) \quad (2.33)$$

The transformations (2.33) are the infinitesimal transformations and the finite transformations are found by solving the Lie equations

$$\xi_1(\bar{x}, \bar{u}) = \frac{d\bar{x}_1}{da}, \dots, \xi_n(\bar{x}, \bar{u}) = \frac{d\bar{x}_n}{da}, \eta(\bar{x}, \bar{u}) = \frac{d\bar{u}}{da} \quad (2.34)$$

with the initial conditions

$$\bar{x}_1(\bar{x}, \bar{u}, a)|_{a=0} = x_1, \dots, \bar{x}_n(\bar{x}, \bar{u}, a)|_{a=0} = x_n \quad (2.35)$$

$$\bar{u}_1(\bar{x}, \bar{u}, a)|_{a=0} = u_1, \dots, \bar{u}_n(\bar{x}, \bar{u}, a)|_{a=0} = u_n \quad (2.36)$$

where  $\bar{x} = (\bar{x}^1, \dots, \bar{x}^n)$  and  $\bar{u} = (\bar{u}^1, \dots, \bar{u}^n)$ .

## 2.7 Dimensionless Parameters

### Reynolds Number (Re)

The ratio of the force of inertia to viscous forces is generally known as the Reynolds number. It is named after Osborne Reynolds. This is arguably the most significant dimensionless number in fluid dynamics. The mathematical formulation is as follows

$$\text{Re} = \frac{\text{Inertia force}}{\text{Viscous force}} = \frac{\rho U_0^2 l^2}{\mu U_0 l} = \frac{U_0 l}{\nu}$$

If the viscous forces are dominant, then the Reynolds number is low. For example, heavy oils, grease, blood etc. On the other hand, if the inertial forces are dominant, this gives large Reynolds number values. Air and water are prominent examples. In making the flow equations non-dimensional, the Reynolds number appears in the equation. The flow types depend on the Reynolds number to a large extent. At the low Reynolds number, the flow remains laminar. As the Reynolds number increases, the stability of the flow starts to decrease, and, at a very high Reynolds number, the flow becomes turbulent. Typical values of Re are:

- $\text{Re} < 2000$  for laminar flow
- $2000 \leq \text{Re} \leq 4000$  for tangential flow
- $\text{Re} > 4000$  for turbulent flow

## Prandtl Number (Pr)

The Prandtl number Pr is a non-dimension quantity approaching the ratio of momentum diffusivity (kinematic viscosity) and thermal diffusivity. Prandtl number is reliant only on the fluid-fluid state. It is defined as

$$\text{Pr} = \frac{\text{viscous diffusion rate}}{\text{thermal diffusion rate}} = \frac{\nu}{\alpha} = \frac{\mu c_p}{\kappa}$$

The values of  $\nu = \frac{\mu}{\rho}$  demonstrate the effects of the viscosity of the fluid. The value of  $\alpha = \frac{\kappa}{\rho C_p}$  shows the thermal diffusivity due to heat conduction. Thus the Prandtl number shows the relative importance of heat conduction and viscosity of a fluid.  $\text{Pr} = \frac{\nu}{\alpha} = \text{viscous diffusion rate/thermal diffusion rate}$ .

Typical values of Pr are:

- Around 0.16-0.7 for mixtures of noble gases
- 0.63 for oxygen
- 0.71 for air at 20°C
- 1.38 for gaseous ammonia
- Around 7 for water (at 20°C )
- Around 11.47 for water (at 4°C )
- Between 100 and 40,000 for engine oil
- Around  $1 \times 10^{25}$  for Earth's mantle

Pr is roughly constant for most gases at various temperatures and pressures. Hence, it may adjust gas thermal conductivity at high temperatures, which is difficult to quantify experimentally due to convection currents.

Small Pr means heat diffusion is faster than momentum diffusion (velocity). Thermal boundary layers are substantially thicker than velocity boundary layers. The Prandtl number Pr assesses momentum and heat diffusion efficiency in velocity and thermal boundary layers. Gases

have a near-unity Prandtl number. Hence diffusion transfers energy and momentum. Energy and momentum diffusion rates are much higher in liquid metals. Hence, liquid metals have a significantly thicker thermal boundary layer than the velocity boundary layer. Oils for  $Pr \gg 1$  are the opposite. From this understanding,  $Pr$  greatly impacts the relative development of the velocity and thermal boundary layers.

### **Grashof Number ( $Gr$ )**

The Grashof number  $Gr$  is dimensionless in fluid dynamics and heat transfer which approximates the buoyancy ratio to the viscous force acting on a watery material. It is defined as,

$$Gr = \frac{g\beta L^3 \Delta T}{\nu^2}$$

This number is of great importance for natural convection flow, and is similar to the Reynolds number. A critical value of  $Gr$  is used to indicate transition from laminar to turbulent flow in free convection.

The Modified Grashof number due to the solutal state of the fluid is defined as,

$$Gm = \frac{g\beta^* L^3 \Delta C}{\nu^2}$$

### **Magnetic parameter ( $M$ )**

The Magnetic parameter is obtained from the ratio of the magnetic force to the inertia force and is defined as,

$$M = \frac{\text{Magnetic force}}{\text{Inertia force}} = \frac{\sigma B_0^2 \nu}{\rho U_0^2}$$

### **Eckert Number ( $Ec$ )**

The Eckert number  $Ec$  is a dimensionless number which provides a measure of the kinetic energy of the flow relative to the enthalpy difference across the thermal boundary layer. It plays a vital role in high-speed flows for which viscous dissipation is significant. It is defined as:

$$Ec = \frac{\text{kinetic energy}}{\text{enthalpy}} = \frac{U_0^2}{C_p \Delta T}$$

### **Suction Parameter ( $fw$ )**

The Suction parameter is defined as,

$$fw = \frac{v_0}{U_0}$$

### **Thermal radiation Parameter ( $R$ )**

The thermal Radiation parameter is defined as,

$$R = \frac{16\sigma_1 T_\infty^3}{3\kappa_1 \kappa}$$

Thermal radiation is sometimes an essential mechanism of heat transfer. The rate at which a perfect emitter, called a blackbody since it absorbs all incident thermal radiation, emits energy by the mechanism of thermal radiation. Examples of processes in which radiative transport plays a significant role are heat transfer from spacecraft, in the fireboxes of boilers of central electrical generating plants, and warming of solar collectors by the sun.

### **Schmidt Number**

The Schmidt number, named after the German engineer Ernst Heinrich Wilhelm Schmidt, is a

dimensionless quantity. The Schmidt number is expressed as the ratio of the momentum diffusivity (kinematic viscosity) and the mass diffusivity. It may characterize the fluid flows in which there are simultaneous diffusion convection processes of the momentum and mass. The Schmidt number labels mass momentum transfer given below:

$$Sc = \frac{\text{momentum diffusivity}}{\text{molecular diffusivity}} = \frac{\nu}{D_T} = \frac{\mu}{\rho D_T}$$

Typical values of  $Sc$  are:

- 0.22 correspond to hydrogen at temperature 25°C and pressure 1 atm.
- 0.6 correspond to water vapour at temperature 25°C and pressure 1 atm.
- Around 1.0 for methanol (at 25°C)
- The heat transfer along the Schmidt number is the Prandtl number.

Schmidt number  $Sc$  measures the relative effectiveness of momentum and mass transport by diffusion in the velocity and concentration boundary layers, respectively.

### **Soret number ( $Sc$ )**

Thermodiffusion (thermophoresis/thermomigration/Soret effect) is a fact perceived in mixtures of moving particles where different types of particles reveal dissimilar responses to the force of a temperature gradient. Thermophoresis is most often applied to aerosol mixtures but can also refer to the singularity in all phases of matter. The Soret effect is usually applied to liquid mixtures, which behave by different and less well-known mechanisms than gas mixtures. Thermophoresis may not apply to term migration in solids, especially in multiphase alloys. The Soret number is defined as,

$$Sc = \frac{D_T \Delta T}{\nu \Delta C}$$

The Soret effect is the diffusion of substance in an asymmetrically heated mixture of gases or a solution caused by a temperature gradient in the arrangement. The Swiss scientist J. Soret was

the first to discover thermo-diffusion (1879).

### **Dufour effect ( $Du$ )**

The Dufour effect refers to the energy flux connecting to the mass concentration gradient arising as a coupled effect of irreversible processes. It is the common phenomenon of the Soret effect. The concentration gradient results in a temperature change. The Dufour effect is usually considered negligible for binary liquid mixtures, whereas the effect can be significant in binary gas mixtures. A Swiss physicist first observed the result. The Dufour number is defined as,

$$Du = \frac{D_T \Delta C}{\nu \Delta T}$$

### **Nusselt Number ( $Nu$ )**

The proportion of convective to conductive heat transfer across the boundary within a fluid is called the Nusselt number ( $Nu$ ). The conductive module is assessed under similar conditions as the heat convection but with a (hypothetically) stationary fluid. The Nusselt number is defined as

$$Nu = \frac{q''_w \text{ convection}}{q''_w \text{ conduction}} = \frac{hL}{\kappa}$$

where  $L$  is the characteristic length,  $\kappa$  is the thermal conductivity of the fluid and  $h$  is the convection heat transfer coefficient.

A Nusselt number close to unity, namely convection and conduction of similar magnitude, is characteristic of laminar flow. A larger Nusselt number relates to more dynamic convection, with the turbulent flow usually in the 100-1000 range.

### **Sherwood Number ( $Sh$ )**

The Sherwood number, usually written as  $Sh$ , is a dimensionless number operated in the mass-

transfer operation. It signifies the ratio of convective mass transport to diffusive mass transport between the wall and bulk fluid. It is defined as

$$Sh = \frac{h^* L}{D_T}$$

$h^*$  is the convective mass transfer coefficient and  $D_T$  is the mass diffusivity coefficient.

## 2.8 Numerical Technique

The world is distinguished by arrangement in space and time, and it is forever fluctuating in complex ways that cannot be exactly resolved. Therefore, the numerical solutions of PDEs lead to some of the most imperative and computationally intensive tasks in all of the numerical analyses. When formulated into mathematical models, many physical phenomena in applied science and engineering fall into a category of systems known as non-linear coupled partial differential equations. Most of these problems can be formulated as second-order partial differential equations. A system of non-linear coupled partial differential equations with boundary conditions is complicated to solve analytically. Advanced numerical methods have been employed to obtain the solution to such problems. Hence two numerical procedures have been adopted to obtain solutions. The usual transformation transforms the governing equations into a non-dimensional system of non-linear coupled partial differential equations with initial and boundary conditions. Hence the solution to our problem would be based on advanced numerical methods.

The Finite Difference Method, Nachtsheim-Swigert shooting method and boundary value problem solver *bvp4c* package in MATLAB are the numerical approaches used to solve the coupled governing model equations.

### 2.8.1 Finite Difference Method (FDM)

The finite difference method is used to solve the boundary value problem by discretizing the continuous solution domain, approximating the exact derivatives by finite difference approximation,



and substituting it into the boundary value problem to obtain the finite difference equation.

The approximations developed by Strikwerda that make it possible to replace differential equations with finite difference equations are the foundation upon which the finite difference techniques are built in 1989 [116, 117]. Algebraic forms are used in their finite difference approximations, and the solutions are connected to grid nodes. Hence, there are three stages to a finite difference solution:

1. Organizing the answer using grids of nodes.
2. Finite difference equivalency, which maps solutions to grid points, is used to generate approximations to the given differential equation.
3. Fixing the boundary and/or starting conditions and solving the difference equations is the item.

Let us consider a two-dimensional region to solve the governing partial differential equations by the finite difference method, as shown in Fig.2.5. A rectangular grid with a grid spacing  $\Delta x$  and  $\Delta y$  in  $x$  and  $y$  directions covers it. Mesh points, lattice points, or nodal points are where parallel lines connect to calculate dependent variable values. Discretizing the governing partial differential equations over the region of interest yields essentially similar algebraic equations. The discretization replaces each derivative of the partial differential equation at a mesh location with a finite difference approximation based on the dependent variable values at the mesh point and its near neighbours and boundary points. Algebraic equations result.

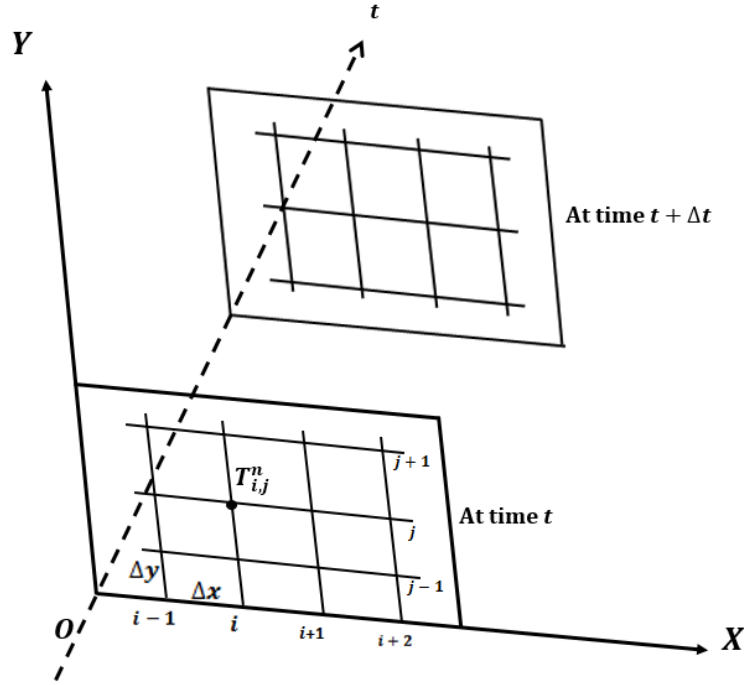


Figure 2.5: Space-Time index notation

To construct standard finite difference approximations to common partial derivatives, suppose that  $U$  is a function of two spatial coordinates,  $x$  and  $y$ , and time  $t$ . Let the subscripts  $i$  and  $j$  represent  $x$  and  $y$  coordinates, respectively, and superscript  $n$  represents time. Let the mesh spacing in  $x$  and  $y$  directions be denoted by  $\Delta x$  and  $\Delta y$ , respectively, the time step by  $\Delta t$ . The partial derivatives of  $U$  will be approximated with respect to  $x$ . As  $t$  and  $y$  are held constant  $U$  is effectively a function of the single variable  $x$ , Taylor's formula can be used, where the ordinary derivative terms are partial derivatives, and the arguments are  $(t, x, y)$  instead of  $x$ . Finally, the step size  $h$  will be replaced by  $\Delta x$  to indicate the change of  $x$  so that,

$$\begin{aligned}
 U(t, x_0 + \Delta x, y_0) &= U(t, x_0, y_0) + \Delta x U_x(t, x_0, y_0) + \frac{\Delta x^2}{2!} U_{xx}(t, x_0, y_0) + \\
 &\dots + \frac{\Delta x^{n-1}}{(n-1)!} U_{(n-1)}(t, x_0, y_0) + O(\Delta x^n)
 \end{aligned}$$

Now with truncating error of order  $O(\Delta x^2)$  and higher then, we have

$$U(t, x_0 + \Delta x, y_0) = U(t, x_0, y_0) + \Delta x U_x(t, x_0, y_0) + O(\Delta x^2) \quad (2.37)$$

Rearranging the above equation, we get

$$\begin{aligned} U_x(t, x_0, y_0) &= \frac{U(t, x_0 + \Delta x, y_0) - U(t, x_0, y_0)}{\Delta x} - \frac{O(\Delta x^2)}{\Delta x} \\ U_x(t, x_0, y_0) &= \frac{U(t, x_0 + \Delta x, y_0) - U(t, x_0, y_0)}{\Delta x} - O(\Delta x) \end{aligned}$$

Above equation holds at any point  $(t, x_0, y_0)$ . In numerical schemes for solving PDEs there are restrictions to a grid of discrete  $x$  values  $x_1, x_2, \dots, x_N$  and discrete  $t$  levels  $t_1, t_2, \dots, t_N$ . Assume a constant grid spacing  $\Delta x$  in  $x$  so that  $x_{i+1} = x_i + \Delta x$ . Evaluating for a point  $(t_n, x_i, y_i)$  on the grid gives

$$U_x(t_n, x_i, y_j) = \frac{U(t_n, x_{i+1}, y_j) - U(t_n, x_i, y_j)}{\Delta x} - O(\Delta x)$$

Using common subscript/superscript notation,

$$U_{i,j}^n = U(t_n, x_i, y_j)$$

So dropping the term  $O(\Delta x)$ , the first-order forward difference approximation to  $U_x(t_n, x_i, y_j)$  becomes,

$$U_x(t_n, x_i, y_j) = \frac{U_{i+1,j}^n - U_{i,j}^n}{\Delta x} \quad (2.38)$$

Replacing  $\Delta x$  by  $-\Delta x$  in Eqn. (2.37),

$$U(t, x_0 - \Delta x, y_0) = U(t, x_0, y_0) - \Delta x U_x(t, x_0, y_0) + O(\Delta x^2)$$

Evaluation of the above equation at  $(t_n, x_i, y_j)$  and rearrangement like previous manners gives the first-order backward difference approximation to  $U_x(t_n, x_i, y_j)$ ,

$$U_x(t_n, x_i, y_j) = \frac{U_{i,j}^n - U_{i-1,j}^n}{\Delta x} \quad (2.39)$$

Subtraction of the expression (2.39) from (2.40) evaluated at  $(t_n, x_i, y_j)$  gives the first-order central difference approximation  $U_x(t_n, x_i, y_j)$

$$U_x(t_n, x_i, y_j) = \frac{U_{i+1,j}^n - U_{i-1,j}^n}{2\Delta x} \quad (2.40)$$

For second-order or higher-order partial derivatives, Eqn. (2.40) needs to derive higher approximations,

$$U(t, x_0 + \Delta x, y_0) = U(t, x_0, y_0) + \Delta x U_x(t, x_0, y_0) + \frac{\Delta x^2}{2!} U_{xx}(t, x_0, y_0) \quad (2.41)$$

$$+ \frac{\Delta x^3}{3!} U_{xxx}(t, x_0, y_0) + O(\Delta x^4) \quad (2.42)$$

Replace  $\Delta x$  by  $-\Delta x$  in (2.42) to get

$$U(t, x_0 - \Delta x, y_0) = U(t, x_0, y_0) - \Delta x U_x(t, x_0, y_0) + \frac{\Delta x^2}{2!} U_{xx}(t, x_0, y_0) \quad (2.43)$$

$$- \frac{\Delta x^3}{3!} U_{xxx}(t, x_0, y_0) + O(\Delta x^4) \quad (2.44)$$

Adding (2.42) and (2.44) gives

$$U(t, x_0 + \Delta x, y_0) + U(t, x_0 - \Delta x, y_0) = 2U(t, x_0, y_0) + \Delta x^2 U_{xx}(t, x_0, y_0) + O(\Delta x^4) \quad (2.45)$$

Using the discrete notation at the point  $(t, x_0, y_0)$  and dropping the term  $O(\Delta x^4)$  yields the second-order central difference approximation to  $U_{xx}(t, x_0, y_0)$ ,

$$U_{xx}(t, x_0, y_0) = \frac{U_{i+1,j}^n - 2U_{i,j}^n + U_{i-1,j}^n}{\Delta x^2} \quad (2.46)$$

The expressions for mixed derivatives can be obtained by differentiating for each variable, in turn. Thus, for example,

$$U_{xy}(t, x_0, y_0) = \frac{U_{i+1,j+1}^n - U_{i+1,j-1}^n - U_{i-1,j+1}^n + U_{i-1,j-1}^n}{4\Delta x\Delta y} \quad (2.47)$$

Higher-order derivatives can be discretised by proceeding with a similar technique. Time-independent finite difference approximation can also be conducted.

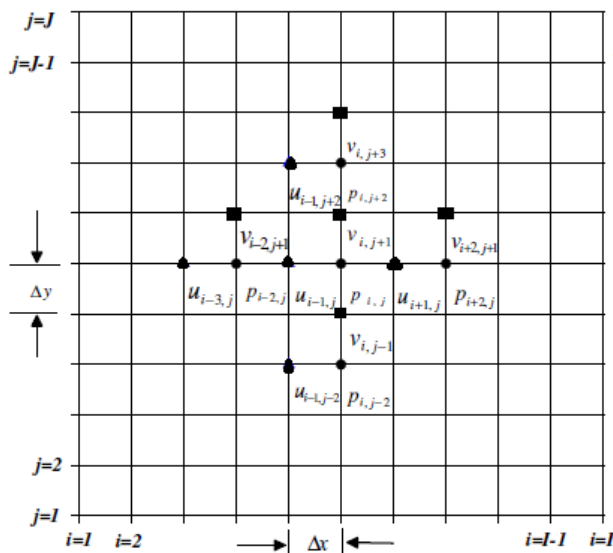


Figure 2.6: Finite difference space grid

## 2.8.2 Boundary Value Problem Solver *bvp4c* in MATLAB

Boundary value difficulties associated with the model are solved using a computer method (BVPs). The approach yields precise solutions to boundary layer equations, and it is well-described in the literature. The equations of the BVP are solved by the *bvp4c* package by applying the appropriate algorithm. The entire computation procedure is executed using a program which uses the symbolic and computational computer language MATLAB. The system of non-linear ordinary differential equations (ODEs) has been solved numerically using the boundary value problem solver, *bvp4c* function technique in MATLAB by Shampine and Thompson [118]. The equations are incorporated numerically as an IVP to a given terminal point. All these simplifications are done using the MATLAB package. The numerical procedure of *bvp4c* followed is:

- Nonlinear PDEs are reduced to 1st order ODEs
- Associated boundary conditions and initial guesses for these functions
- *bvp4c* returns the solution as a structure called *sol*
- Mesh selection is generated and returned in the field *sol.x*
- Solution can be fetched from array *sol.y* corresponding to *sol.x*
- let  $y(a)$  be the left boundary,  $y(b)$  be the right boundary
- Integrate the solution to get the required results

Consider a dummy system of non-linear coupled governing equations:

$$f'''(\eta) + c_1 f''(\eta) f(\eta) + c_2 f'(\eta) + c_3 f(\eta)^3 - c_4 \theta(\eta) = g_c \quad (2.48)$$

$$\theta''(\eta) + d_1 \theta'(\eta) + d_2 \theta(\eta) = h_d \quad (2.49)$$

Boundary conditions are:

$$f = a_1; \quad f' = a_2; \quad \theta = c_3 \quad \text{at } \eta = l_a \quad (2.50)$$

$$f' = b_2; \quad \theta = b_3 \quad \text{at } \eta = l_b \quad (2.51)$$

The transformed governing equations of third and second order must be reduced to a system of first-order differential equations. The equations now define new variables

$$f = y_1; \quad f' = y'_1 = y_2; \quad f'' = y'_2 = y_3; \quad \theta = y_4; \quad \theta' = y'_4 = y_5 \quad (2.52)$$

Thus, the two coupled higher-order differential equations and the corresponding boundary conditions can be transformed into five equivalent first ODEs subject to related boundary conditions. The system of first-order ODEs is as follows:

$$f' = y'_1 = y_2 \quad (2.53)$$

$$f'' = y'_2 = y_3 \quad (2.54)$$

$$f''' = -c_1 f''(\eta) f(\eta) - c_2 f'(\eta) - c_3 f(\eta)^3 + c_4 \theta(\eta) + g_c \quad (2.55)$$

$$\theta' = y'_4 = y_5 \quad (2.56)$$

$$\theta'' = -d_1 \theta'(\eta) - d_2 \theta(\eta) + h_d \quad (2.57)$$

And the boundary conditions are given by

$$y_1(l_a) = a_1; \quad y_2(l_a) = a_2; \quad y_3(l_a) = R_a; \quad y_4(l_a) = c_3; \quad y_5(l_a) = S_a; \quad (2.58)$$

The Classical Newton shooting method is applied for the refinement of initial guesses  $R_a$  and  $S_a$  subjected to the given tolerance to solve the initial value problem.

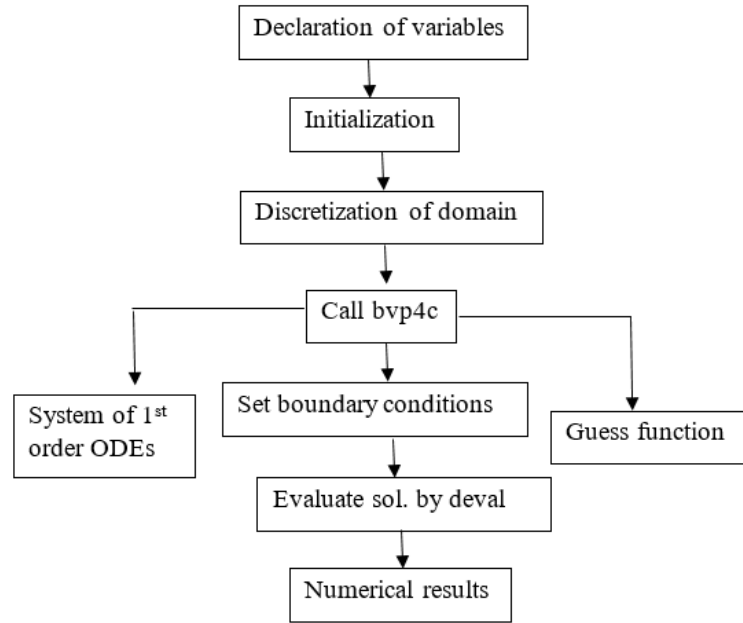


Figure 2.7: Finite difference space grid

### 2.8.3 Nachtsheim-Swigert Shooting Method

Boundary value difficulties are an inevitable consequence of many important physical problems (BVPs). When it comes to solving boundary value problems (BVPs) for ordinary differential equations, the shooting technique is among the most popular and powerful numerical algorithms. Due to its many benefits, including its generalizability, small storage footprint, and amenability to automation, we opted to use the shooting approach to tackle the boundary value problem in our research. The shooting technique is an iterative procedure that reframes the original boundary value issue as a set of linked initial value problems (IVPs) with suitable initial conditions. To solve the new issue, the IVP must be applied using initial conditions that are chosen arbitrarily but are close approximations to the boundary conditions at the ends. The operation is repeated with a new set of initial conditions until the desired precision is attained or a limit to the iteration is reached if the boundary conditions are not satisfied with the required accuracy. The resulting IVP is numerically solved using a method suitable for linear, ordinary differential equations. A convergence between the IVP and BVP solutions is expected. The 4th-order Runge-Kutta



method is used here because of the precision it offers. The Maple programming language is used to implement the aforementioned procedure's algorithm. Graphical representations of the calculated results are provided.

The differential equation is integrated numerically as an IVPs from the beginning of the interval (where the initial conditions are not specified) to the end. This is known as a shooting method. The validity of the assumed missing initial condition is then evaluated by contrasting the expected and observed values of the dependent variable at the endpoint. If there's a discrepancy, it'll be necessary to assume yet another value for the missing starting condition, and the process will be iterative. This procedure is repeated until there is an acceptable degree of agreement between the calculated and specified conditions at the terminal point. For such an iterative approach, one may wonder if there is a standardised means of determining the missing starting condition's next (assumed) value.

The asymptotic class of the boundary conditions for non-linear ODEs has two points. Values of the dependent variable are given for two values of the independent variable in two-point boundary conditions. The dependent variable's first derivative (and higher derivatives of the boundary layer equation, if it exists) will tend towards zero when the outer stated value of the independent variable is approached if an asymptotic boundary condition is specified. So, it's important to talk in-depth about the Nachtsheim-Swigert iteration method.

To get over these problems, Nachtsheim and Swigert [119] came up with an iterative approach. The system of equations and the boundary conditions can be easily treated by extending the Nachtsheim-Swigert iteration approach. In governing equations, there are three asymptotic boundary conditions

$$f''(0), g'(0), \theta'(0)$$

within the context of the initial-value method and Nachtsheim-Swigert iteration technique the

outer boundary conditions may be functionally represented as

$$f'(\eta_{max}) = f'(f''(0), g'(0), \theta'(0)) = \delta_1 \quad (2.59)$$

$$g(\eta_{max}) = g(f''(0), g'(0), \theta'(0)) = \delta_2 \quad (2.60)$$

$$\theta(\eta_{max}) = \theta(f''(0), g'(0), \theta'(0)) = \delta_3 \quad (2.61)$$

with the asymptotic convergence criteria given by

$$f''(\eta_{max}) = f''(f''(0), g'(0), \theta'(0)) = \delta_4 \quad (2.62)$$

$$g'(\eta_{max}) = g'(f''(0), g'(0), \theta'(0)) = \delta_5 \quad (2.63)$$

$$\theta'(\eta_{max}) = \theta'(f''(0), g'(0), \theta'(0)) = \delta_6 \quad (2.64)$$

choosing  $f''(0) = g_1$ ,  $g'(0) = g_2$ ,  $\theta'(0) = g_3$  and expanding in a first order Taylor's series,

$$f'(\eta_{max}) = f'_{cal}(\eta_{max}) + \frac{\partial f'}{\partial g_1} \Delta g_1 + \frac{\partial f'}{\partial g_2} \Delta g_2 + \frac{\partial f'}{\partial g_3} \Delta g_3 = \delta_1 \quad (2.65)$$

$$g(\eta_{max}) = g_{cal}(\eta_{max}) + \frac{\partial g}{\partial g_1} \Delta g_1 + \frac{\partial g}{\partial g_2} \Delta g_2 + \frac{\partial g}{\partial g_3} \Delta g_3 = \delta_2 \quad (2.66)$$

$$\theta(\eta_{max}) = \theta_{cal}(\eta_{max}) + \frac{\partial \theta}{\partial g_1} \Delta g_1 + \frac{\partial \theta}{\partial g_2} \Delta g_2 + \frac{\partial \theta}{\partial g_3} \Delta g_3 = \delta_3 \quad (2.67)$$

$$f''(\eta_{max}) = f''_{cal}(\eta_{max}) + \frac{\partial f''}{\partial g_1} \Delta g_1 + \frac{\partial f''}{\partial g_2} \Delta g_2 + \frac{\partial f''}{\partial g_3} \Delta g_3 = \delta_4 \quad (2.68)$$

$$g'(\eta_{max}) = g'_{cal}(\eta_{max}) + \frac{\partial g'}{\partial g_1} \Delta g_1 + \frac{\partial g'}{\partial g_2} \Delta g_2 + \frac{\partial g'}{\partial g_3} \Delta g_3 = \delta_5 \quad (2.69)$$

$$\theta'(\eta_{max}) = \theta'_{cal}(\eta_{max}) + \frac{\partial \theta'}{\partial g_1} \Delta g_1 + \frac{\partial \theta'}{\partial g_2} \Delta g_2 + \frac{\partial \theta'}{\partial g_3} \Delta g_3 = \delta_6 \quad (2.70)$$

The subscript *cal* indicates the value of the function at  $\eta_{max}$  determined from the trial integration.

Solution of these equations in a least-squares sense required determining the minimum value of

$$E = \delta_1^2 + \delta_2^2 + \delta_3^2 + \delta_4^2 + \delta_5^2 + \delta_6^2 \quad (2.71)$$

Now differentiating  $E$  with respect to  $g_1$  yields,

$$\delta_1 \frac{\partial \delta_1}{\partial g_1} + \delta_2 \frac{\partial \delta_2}{\partial g_1} + \delta_3 \frac{\partial \delta_3}{\partial g_1} + \delta_4 \frac{\partial \delta_4}{\partial g_1} + \delta_5 \frac{\partial \delta_5}{\partial g_1} + \delta_6 \frac{\partial \delta_6}{\partial g_1} = 0$$

Using the relations 2.65 to 2.70 we get,

$$\begin{aligned} & \left( f'_{cal} + \frac{\partial f'}{\partial g_1} \Delta g_1 + \frac{\partial f'}{\partial g_2} \Delta g_2 + \frac{\partial f'}{\partial g_3} \Delta g_3 \right) \frac{\partial f'}{\partial g_1} + \left( g_{cal} + \frac{\partial g}{\partial g_1} \Delta g_1 + \frac{\partial g}{\partial g_2} \Delta g_2 + \frac{\partial g}{\partial g_3} \Delta g_3 \right) \\ & \frac{\partial g}{\partial g_1} + \left( \theta_{cal} + \frac{\partial \theta}{\partial g_1} \Delta g_1 + \frac{\partial \theta}{\partial g_2} \Delta g_2 + \frac{\partial \theta}{\partial g_3} \Delta g_3 \right) \frac{\partial \theta}{\partial g_1} + \left( f''_{cal} + \frac{\partial f''}{\partial g_1} \Delta g_1 + \frac{\partial f''}{\partial g_2} \Delta g_2 + \right. \\ & \left. \frac{\partial f''}{\partial g_3} \Delta g_3 \right) \frac{\partial f''}{\partial g_1} + \left( g'_{cal} + \frac{\partial g'}{\partial g_1} \Delta g_1 + \frac{\partial g'}{\partial g_2} \Delta g_2 + \frac{\partial g'}{\partial g_3} \Delta g_3 \right) \frac{\partial g'}{\partial g_1} + \left( \theta'_{cal} + \frac{\partial \theta'}{\partial g_1} \Delta g_1 + \right. \\ & \left. \frac{\partial \theta'}{\partial g_2} \Delta g_2 + \frac{\partial \theta'}{\partial g_3} \Delta g_3 \right) \frac{\partial \theta'}{\partial g_1} = 0 \end{aligned}$$

After some rearrangement to get

$$\begin{aligned} & \left[ \left( \frac{\partial f'}{\partial g_1} \right)^2 + \left( \frac{\partial g}{\partial g_1} \right)^2 + \left( \frac{\partial \theta}{\partial g_1} \right)^2 + \left( \frac{\partial f''}{\partial g_1} \right)^2 + \left( \frac{\partial g'}{\partial g_1} \right)^2 + \left( \frac{\partial \theta'}{\partial g_1} \right)^2 \right] \Delta g_1 + \\ & \left( \frac{\partial f'}{\partial g_1} \frac{\partial f'}{\partial g_2} + \frac{\partial g}{\partial g_1} \frac{\partial g}{\partial g_2} + \frac{\partial \theta}{\partial g_1} \frac{\partial \theta}{\partial g_2} + \frac{\partial f''}{\partial g_1} \frac{\partial f''}{\partial g_2} + \frac{\partial g'}{\partial g_1} \frac{\partial g'}{\partial g_2} + \frac{\partial \theta'}{\partial g_1} \frac{\partial \theta'}{\partial g_2} \right) \Delta g_2 + \\ & \left( \frac{\partial f'}{\partial g_1} \frac{\partial f'}{\partial g_3} + \frac{\partial g}{\partial g_1} \frac{\partial g}{\partial g_3} + \frac{\partial \theta}{\partial g_1} \frac{\partial \theta}{\partial g_3} + \frac{\partial f''}{\partial g_1} \frac{\partial f''}{\partial g_3} + \frac{\partial g'}{\partial g_1} \frac{\partial g'}{\partial g_3} + \frac{\partial \theta'}{\partial g_1} \frac{\partial \theta'}{\partial g_3} \right) \Delta g_3 = \\ & - \left[ f'_{cal} \frac{\partial f'}{\partial g_1} + g_{cal} \frac{\partial g}{\partial g_1} + \theta_{cal} \frac{\partial \theta}{\partial g_1} + f''_{cal} \frac{\partial f''}{\partial g_1} + g'_{cal} \frac{\partial g'}{\partial g_1} + \theta'_{cal} \frac{\partial \theta'}{\partial g_1} \right] \end{aligned} \quad (2.72)$$

Again differentiating  $E$  with respect to  $g_2$  and rearranging we obtain,

$$\begin{aligned}
& \left( \frac{\partial f'}{\partial g_1} \frac{\partial f'}{\partial g_2} + \frac{\partial g}{\partial g_1} \frac{\partial g}{\partial g_2} + \frac{\partial \theta}{\partial g_1} \frac{\partial \theta}{\partial g_2} + \frac{\partial f''}{\partial g_1} \frac{\partial f''}{\partial g_2} + \frac{\partial g'}{\partial g_1} \frac{\partial g'}{\partial g_2} + \frac{\partial \theta'}{\partial g_1} \frac{\partial \theta'}{\partial g_2} \right) \Delta g_1 + \\
& \left[ \left( \frac{\partial f'}{\partial g_2} \right)^2 + \left( \frac{\partial g}{\partial g_2} \right)^2 + \left( \frac{\partial \theta}{\partial g_2} \right)^2 + \left( \frac{\partial f''}{\partial g_2} \right)^2 + \left( \frac{\partial g'}{\partial g_2} \right)^2 + \left( \frac{\partial \theta'}{\partial g_2} \right)^2 \right] \Delta g_2 + \\
& \left( \frac{\partial f'}{\partial g_2} \frac{\partial f'}{\partial g_3} + \frac{\partial g}{\partial g_2} \frac{\partial g}{\partial g_3} + \frac{\partial \theta}{\partial g_2} \frac{\partial \theta}{\partial g_3} + \frac{\partial f''}{\partial g_2} \frac{\partial f''}{\partial g_3} + \frac{\partial g'}{\partial g_2} \frac{\partial g'}{\partial g_3} + \frac{\partial \theta'}{\partial g_2} \frac{\partial \theta'}{\partial g_3} \right) \Delta g_3 = \\
& - \left[ f'_{cal} \frac{\partial f'}{\partial g_2} + g_{cal} \frac{\partial g}{\partial g_2} + \theta_{cal} \frac{\partial \theta}{\partial g_2} + f''_{cal} \frac{\partial f''}{\partial g_2} + g'_{cal} \frac{\partial g'}{\partial g_2} + \theta'_{cal} \frac{\partial \theta'}{\partial g_2} \right]
\end{aligned} \tag{2.73}$$

Finally differentiating  $E$  with respect to  $g_3$  and rearranging we obtain,

$$\begin{aligned}
& \left( \frac{\partial f'}{\partial g_1} \frac{\partial f'}{\partial g_3} + \frac{\partial g}{\partial g_1} \frac{\partial g}{\partial g_3} + \frac{\partial \theta}{\partial g_1} \frac{\partial \theta}{\partial g_3} + \frac{\partial f''}{\partial g_1} \frac{\partial f''}{\partial g_3} + \frac{\partial g'}{\partial g_1} \frac{\partial g'}{\partial g_3} + \frac{\partial \theta'}{\partial g_1} \frac{\partial \theta'}{\partial g_3} \right) \Delta g_1 + \\
& \left( \frac{\partial f'}{\partial g_2} \frac{\partial f'}{\partial g_3} + \frac{\partial g}{\partial g_2} \frac{\partial g}{\partial g_3} + \frac{\partial \theta}{\partial g_2} \frac{\partial \theta}{\partial g_3} + \frac{\partial f''}{\partial g_2} \frac{\partial f''}{\partial g_3} + \frac{\partial g'}{\partial g_2} \frac{\partial g'}{\partial g_3} + \frac{\partial \theta'}{\partial g_2} \frac{\partial \theta'}{\partial g_3} \right) \Delta g_2 + \\
& \left[ \left( \frac{\partial f'}{\partial g_3} \right)^2 + \left( \frac{\partial g}{\partial g_3} \right)^2 + \left( \frac{\partial \theta}{\partial g_3} \right)^2 + \left( \frac{\partial f''}{\partial g_3} \right)^2 + \left( \frac{\partial g'}{\partial g_3} \right)^2 + \left( \frac{\partial \theta'}{\partial g_3} \right)^2 \right] \Delta g_3 = \\
& - \left[ f'_{cal} \frac{\partial f'}{\partial g_3} + g_{cal} \frac{\partial g}{\partial g_3} + \theta_{cal} \frac{\partial \theta}{\partial g_3} + f''_{cal} \frac{\partial f''}{\partial g_3} + g'_{cal} \frac{\partial g'}{\partial g_3} + \theta'_{cal} \frac{\partial \theta'}{\partial g_3} \right]
\end{aligned} \tag{2.74}$$

We can write equations 2.72–2.74 in a system of linear equations as follows:

$$\begin{aligned}
a_{11} \Delta g_1 + a_{12} \Delta g_2 + a_{13} \Delta g_3 &= b_1 \\
a_{21} \Delta g_1 + a_{22} \Delta g_2 + a_{23} \Delta g_3 &= b_2 \\
a_{31} \Delta g_1 + a_{32} \Delta g_2 + a_{33} \Delta g_3 &= b_3
\end{aligned} \tag{2.75}$$

Where,

$$\begin{aligned}
a_{11} &= \left( \frac{\partial f'}{\partial g_1} \right)^2 + \left( \frac{\partial g}{\partial g_1} \right)^2 + \left( \frac{\partial \theta}{\partial g_1} \right)^2 + \left( \frac{\partial f''}{\partial g_1} \right)^2 + \left( \frac{\partial g'}{\partial g_1} \right)^2 + \left( \frac{\partial \theta'}{\partial g_1} \right)^2 \\
a_{12} &= \left( \frac{\partial f'}{\partial g_1} \frac{\partial f'}{\partial g_2} + \frac{\partial g}{\partial g_1} \frac{\partial g}{\partial g_2} + \frac{\partial \theta}{\partial g_1} \frac{\partial \theta}{\partial g_2} + \frac{\partial f''}{\partial g_1} \frac{\partial f''}{\partial g_2} + \frac{\partial g'}{\partial g_1} \frac{\partial g'}{\partial g_2} + \frac{\partial \theta'}{\partial g_1} \frac{\partial \theta'}{\partial g_2} \right)
\end{aligned}$$

$$a_{13} \left( \frac{\partial f'}{\partial g_1} \frac{\partial f'}{\partial g_3} + \frac{\partial g}{\partial g_1} \frac{\partial g}{\partial g_3} + \frac{\partial \theta}{\partial g_1} \frac{\partial \theta}{\partial g_3} + \frac{\partial f''}{\partial g_1} \frac{\partial f''}{\partial g_3} + \frac{\partial g'}{\partial g_1} \frac{\partial g'}{\partial g_3} + \frac{\partial \theta'}{\partial g_1} \frac{\partial \theta'}{\partial g_3} \right)$$

$$b_1 = - \left[ f'_{cal} \frac{\partial f'}{\partial g_1} + g_{cal} \frac{\partial g}{\partial g_1} + \theta_{cal} \frac{\partial \theta}{\partial g_1} + f''_{cal} \frac{\partial f''}{\partial g_1} + g'_{cal} \frac{\partial g'}{\partial g_1} + \theta'_{cal} \frac{\partial \theta'}{\partial g_1} \right]$$

$$a_{21} = a_{12}$$

$$a_{22} = \left( \frac{\partial f'}{\partial g_2} \right)^2 + \left( \frac{\partial g}{\partial g_2} \right)^2 + \left( \frac{\partial \theta}{\partial g_2} \right)^2 + \left( \frac{\partial f''}{\partial g_2} \right)^2 + \left( \frac{\partial g'}{\partial g_2} \right)^2 + \left( \frac{\partial \theta'}{\partial g_2} \right)^2$$

$$a_{23} = \left( \frac{\partial f'}{\partial g_2} \frac{\partial f'}{\partial g_3} + \frac{\partial g}{\partial g_2} \frac{\partial g}{\partial g_3} + \frac{\partial \theta}{\partial g_2} \frac{\partial \theta}{\partial g_3} + \frac{\partial f''}{\partial g_2} \frac{\partial f''}{\partial g_3} + \frac{\partial g'}{\partial g_2} \frac{\partial g'}{\partial g_3} + \frac{\partial \theta'}{\partial g_2} \frac{\partial \theta'}{\partial g_3} \right)$$

$$b_2 = - \left[ f'_{cal} \frac{\partial f'}{\partial g_2} + g_{cal} \frac{\partial g}{\partial g_2} + \theta_{cal} \frac{\partial \theta}{\partial g_2} + f''_{cal} \frac{\partial f''}{\partial g_2} + g'_{cal} \frac{\partial g'}{\partial g_2} + \theta'_{cal} \frac{\partial \theta'}{\partial g_2} \right]$$

$$a_{31} = a_{13}$$

$$a_{32} = a_{23}$$

$$a_{33} = \left( \frac{\partial f'}{\partial g_3} \right)^2 + \left( \frac{\partial g}{\partial g_3} \right)^2 + \left( \frac{\partial \theta}{\partial g_3} \right)^2 + \left( \frac{\partial f''}{\partial g_3} \right)^2 + \left( \frac{\partial g'}{\partial g_3} \right)^2 + \left( \frac{\partial \theta'}{\partial g_3} \right)^2$$

$$b_3 = - \left[ f'_{cal} \frac{\partial f'}{\partial g_3} + g_{cal} \frac{\partial g}{\partial g_3} + \theta_{cal} \frac{\partial \theta}{\partial g_3} + f''_{cal} \frac{\partial f''}{\partial g_3} + g'_{cal} \frac{\partial g'}{\partial g_3} + \theta'_{cal} \frac{\partial \theta'}{\partial g_3} \right]$$

By using *Cramer's rule* we can solve the system of equations (2.75) as follows

$$\Delta g_1 = \frac{\det A_1}{D}; \quad \Delta g_2 = \frac{\det A_2}{D}; \quad \Delta g_3 = \frac{\det A_3}{D}$$

where

$$D = \det A = \begin{bmatrix} a_{11} & a_{12} & a_{13} \\ a_{21} & a_{22} & a_{23} \\ a_{31} & a_{32} & a_{33} \end{bmatrix} \quad \det A_1 = \begin{bmatrix} b_1 & a_{12} & a_{13} \\ b_2 & a_{22} & a_{23} \\ b_3 & a_{32} & a_{33} \end{bmatrix}$$

$$\det A_2 = \begin{bmatrix} a_{11} & b_1 & a_{13} \\ a_{21} & b_2 & a_{23} \\ a_{31} & b_3 & a_{33} \end{bmatrix} \quad \det A_3 = \begin{bmatrix} a_{11} & a_{12} & b_1 \\ a_{21} & a_{22} & b_2 \\ a_{31} & a_{32} & b_3 \end{bmatrix}$$

Then we obtain the missing (unspecified) values  $g_1$ ,  $g_2$  and  $g_3$  from equations (2.72) – (2.74) are as follows:

$$\begin{aligned} g_1 &\cong g_1 + \Delta g_1 \\ g_2 &\cong g_2 + \Delta g_2 \\ g_3 &\cong g_3 + \Delta g_3 \end{aligned} \tag{2.76}$$

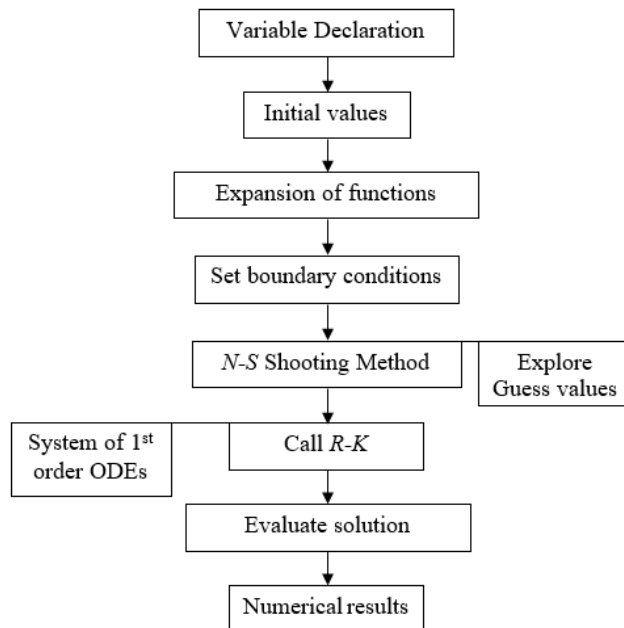


Figure 2.8: Algorithm of Nachtshiem-Swigert shooting method

## CHAPTER 3

### MAGNETO HALL EFFECT ON UNSTEADY ELASTICO-VISCOUS NANOFLUID SLIP FLOW IN A CHANNEL IN PRESENCE OF THERMAL RADIATION AND HEAT GENERATION WITH BROWNIAN MOTION

**Abstract.** The present note investigates the magneto hall effect on the unsteady flow of an elastico-viscous nanofluid in a channel with a slip boundary, considering the presence of thermal radiation and heat generation with Brownian motion. Numerical results are achieved by solving the governing equations by the implicit Finite Difference Method (FDM), obtaining primary and secondary velocities, temperature, nanoparticle volume fraction and concentration distributions within the boundary layer entering the problem. The influences of several interesting parameters, such as elastico-viscous parameter, magnetic field, hall parameter, heat generation, thermal radiation and Brownian motion parameters on velocity, heat and mass transfer characteristics of the fluid flow, are discussed with the help of graphs. Also, the effects of the pertinent parameters, which are of physical and engineering interest, such as the Skin friction parameter, Nusselt number and Sherwood number, are sorted out. It is found that these parameters significantly influence the flow field and other quantities of physical concern.

#### 3.1 Introduction

Most common fluids such as water, ethylene-glycol (EG), toluene or oil generally have poor heat transfer characteristics owing to their low thermal conductivity. A recent technique introduced by Choi [25] to improve the thermal conductivity of these fluids is to suspend nano-sized (diameter less than 100 nm) metallic particles such as aluminum, titanium, gold, copper, iron or their oxides in the fluid to enhance its thermal properties. In recent times, the flow analysis of nanofluids has been the topic of extensive research due to its characteristic in increasing ther-

mal conductivity in heat transfer process. Undoubtedly, the nanofluids are advantageous in the sense that they are more stable and have an acceptable viscosity and better wetting, spreading and dispersion properties on a solid surface (Buongiorno [41]; Khan and Pop [120]; Kuznetsov and Nield [121]; Gorla *et al.* [122]). Nanofluids are potential heat transfer fluids with enhanced thermo-physical properties and heat transfer performance can be applied in many devices and engineering applications such as microelectronics, micro-fluidics, transportation, biomedical, solid-state lighting and manufacturing for better performances. Matin *et al.* [123] considered the entropy generation minimization of the flow of air based nanofluid with  $Al_2O_3$ ,  $Cu$  and  $Ti$  nanoparticles with different volume fraction in MHD channel formed by two parallel isothermal plates and found Hartman and Peclet numbers. Haroun *et al.* [124] investigated heat and mass transfer in an unsteady MHD nanofluid boundary layer and Rahman *et al.* [125] numerically solved the problem of steady boundary layer flow of a nanofluid past a permeable exponentially shrinking surface using the Buongiorno's mathematical nanofluid model. Moreover, the current trend for the application of magneto-hydrodynamics is towards a strong magnetic field; so that the influence of electromagnetic force is noticeable, Sutton and Sherman [126]; Ali *et al.* [127] and many other researchers show that the Hall current has a marked effect on the magnetic force term. Now these days, elastico-viscous nanofluid has industrial importance since base fluids in realistic process exhibit dual properties. Some examples of elastico-viscous nanofluids include  $Al_2O_3$ -EG,  $CuO$ -EG and  $ZnO$ -EG. Recently, several authors [128, 129, 130, 131] are analyzing the natural convection flow considering elastico-viscous nanofluids due to its important industrial applications [132].

In this paper, the parametric behavior of magneto-hydrodynamic flow of elastico-viscous nanofluid in a channel with slip condition in the presence of dynamic effects of Hall current, thermal radiation, heat generation and Brownian motion is studied.



### 3.2 Mathematical Formulation

We consider flow of elastico-viscous incompressible and electrically conducting nanofluid with a velocity  $U_0$  between two insulating infinite permeable plates separated by a distance  $h$ . The  $x$ -axis is taken along the plates and  $y$ -axis is taken normal to the plates setting the lower stretching plate at  $y = 0$  with partial slip and the upper at  $y = h$ . The Hall current has an effect on an electrically conducting fluid in the presence of a magnetic field applied along the  $y$ -axis. The effect of magneto-Hall current gives rise to a force in the  $z$ -direction, which induces a cross-flow in the  $z$ -direction and hence the flow becomes three dimensional. The plates are assumed to be infinite in  $x$ - and  $z$ -directions which make the physical quantities not to change in these directions. Because of this, the conservation of mass takes the form, i.e.,  $div \bar{v}_{velocity}(t, y) = 0$  and due to the uniform suction the velocity component  $\bar{v}_{velocity}(t, y) = 0$  is assumed to have a constant value  $v_0$  in the  $y$ -direction.

The constitutive equation for the incompressible second order fluid is

$$\mathbf{S} = -p\mathbf{I} + \mu_1 A_1 + \mu_2 A_2 + \mu_3 (A_1)^2 \quad (3.1)$$

Here  $\mathbf{S}$  is the stress tensor,  $p$  is the hydrostatic pressure,  $A_n$ ,  $n = 1, 2$  are the kinematic Rivlin-Ericksen tensors,  $\mu_1$ ,  $\mu_2$ ,  $\mu_3$  are the material coefficients describing the viscosity, elastico- viscosity and cross-viscosity respectively, where  $\mu_1$  and  $\mu_3$  are positive and  $\mu_2$  is negative (Coleman and Noll [133]; Markovitz and Coleman [134]).

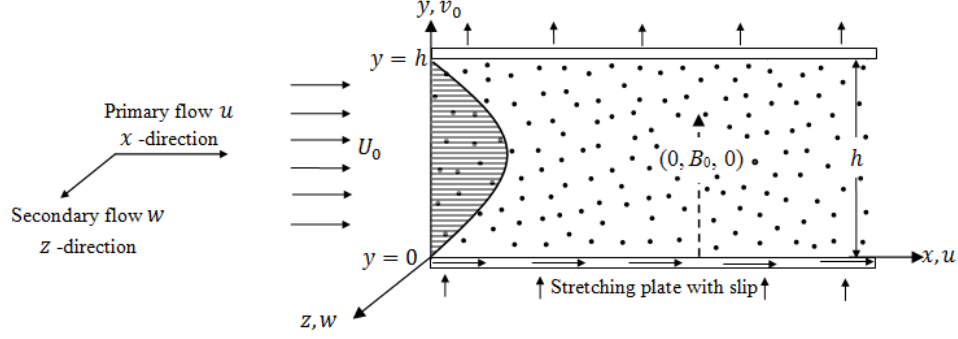


Figure 3.1: Physical model

Using the Buongiorno [41] nanofluid model, the governing equations for momentum, energy, nanoparticle volume fraction and nanoparticle concentration distributions are represented by

$$\begin{aligned} \frac{\partial u}{\partial t} + v_0 \frac{\partial u}{\partial y} &= \nu_f \frac{\partial^2 u}{\partial y^2} + \frac{\mu_2}{\rho_f} \left( \frac{\partial^3 u}{\partial t \partial y^2} + v_0 \frac{\partial^3 u}{\partial y^3} \right) - \frac{B_0}{\rho_f} J_z \\ &+ \frac{g_0}{\rho_f} (\rho_f (1 - \phi_h) (\beta_T (T - T_h) + \beta_C (C - C_h)) - (\rho_{nf} - \rho_f) (\phi - \phi_h)) \end{aligned} \quad (3.2)$$

$$\frac{\partial w}{\partial t} + v_0 \frac{\partial w}{\partial y} = \nu_f \frac{\partial^2 w}{\partial y^2} + \frac{\mu_2}{\rho_f} \left( \frac{\partial^3 w}{\partial t \partial y^2} + v_0 \frac{\partial^3 w}{\partial y^3} \right) + \frac{B_0}{\rho_f} J_x \quad (3.3)$$

$$\begin{aligned} \frac{\partial T}{\partial t} + v_0 \frac{\partial T}{\partial y} &= \alpha_f \frac{\partial^2 T}{\partial y^2} + \tau_{nf} \left( D_B \left( \frac{\partial T}{\partial y} \frac{\partial \phi}{\partial y} \right) + \frac{D_T}{T_m} \left( \frac{\partial T}{\partial y} \right)^2 \right) + \frac{\sigma \mu_e B_0^2 \lambda}{(\rho C_P)_f (1 + m^2 \lambda^2)} (u^2 + w^2) \\ &+ \frac{Q^*}{(\rho C_P)_f} (T - T_h) - \frac{1}{(\rho C_P)_f} \frac{\partial q_r}{\partial y} \end{aligned} \quad (3.4)$$

$$\frac{\partial \phi}{\partial t} + v_0 \frac{\partial \phi}{\partial y} = D_B \frac{\partial^2 \phi}{\partial y^2} + \frac{D_T}{T_m} \frac{\partial^2 T}{\partial y^2} \quad (3.5)$$

$$\frac{\partial C}{\partial t} + v_0 \frac{\partial C}{\partial y} = D_S \frac{\partial^2 C}{\partial y^2} + D_{CT} \frac{\partial^2 T}{\partial y^2} \quad (3.6)$$

Here  $(u, v, w)$  are the fluid velocity components in the  $x$ ,  $y$  and  $z$ -directions, respectively.  $T$ ,  $\phi$  and  $C$  are the Temperature, nanoparticle volume fraction and concentration within the boundary layer, respectively. Subscripts  $nf$  and  $f$  denote nanoparticle and the base fluid properties respectively. Here  $\nu$  is the kinematic viscosity;  $\rho$  is the density;  $\mu_2$  is the elasto-viscous parameter;  $B_0$  is the uniform magnetic field strength;  $J_x = \frac{\sigma\mu_e B_0 \lambda}{1+m^2\lambda^2}(m\lambda u - w)$  and  $J_z = \frac{\sigma\mu_e B_0 \lambda}{1+m^2\lambda^2}(u + m\lambda w)$  are the currents only to  $x$ - and  $z$ -axes, respectively, where  $\sigma$  is the electric conductivity;  $\mu_e$  is the viscosity of fluid;  $B_0$  is the uniform magnetic field strength;  $m$  is the hall parameter;  $\lambda = \text{Cos}\alpha_e$  where  $\alpha_e$  is the angle between the direction of the strong uniform magnetic field  $B_0$  and the plane transverse to the plates which are assumed to be electrically non-conducting;  $g_0$  is the acceleration due to gravity;  $\beta_T$ ,  $\beta_C$  are the volumetric coefficients of thermal and concentration expansions, respectively;  $\alpha_f$  is the thermal diffusivity;  $\tau_{nf} = \frac{(\rho C_p)_{nf}}{(\rho C_p)_f}$  is the ratio of effective heat capacity of nanoparticles and that of the base fluid;  $C_p$  is the specific heat at constant pressure;  $D_B$  is the Brownian diffusion coefficient;  $D_T$  is the thermophoretic diffusion coefficient;  $T_m$  is the mean temperature;  $Q^*$  is the volumetric rate of heat generation/absorption;  $q_r$  is the radiative heat flux;  $D_S$  is the solutal diffusivity of concentration and  $D_{CT}$  is the Soret diffusivity. Finally subscript  $h$  is for the parameters at the upper plate at  $y = h$ .

Rosseland diffusion approximation [9] yields  $q_r = -\frac{4\sigma_1}{3\kappa_1} \frac{\partial T^4}{\partial y}$  for thermal radiation, where  $\sigma_1$  is the Stefan-Boltzmann constant and  $\kappa_1$  is the mean absorption coefficient. Expanding  $T^4$  in a Taylor series about  $T_\infty$  and neglecting higher-order terms, we get  $\frac{\partial q}{\partial y} = -\frac{16\sigma_1 T_\infty^3}{3\kappa_1} \frac{\partial^2 T}{\partial y^2}$ . Thus the energy equation takes the form

$$\begin{aligned} \frac{\partial T}{\partial t} + v_0 \frac{\partial T}{\partial y} = & \alpha_f \frac{\partial^2 T}{\partial y^2} + \tau_{nf} \left( D_B \left( \frac{\partial T}{\partial y} \frac{\partial \phi}{\partial y} \right) + \frac{D_T}{T_m} \left( \frac{\partial T}{\partial y} \right)^2 \right) + \frac{\sigma\mu_e B_0^2 \lambda}{(\rho C_p)_f (1 + m^2 \lambda^2)} (u^2 + w^2) \\ & + \frac{Q^*}{(\rho C_p)_f} (T - T_h) + \frac{1}{(\rho C_p)_f} \frac{16\sigma_1 T_\infty^3}{3\kappa_1} \frac{\partial^2 T}{\partial y^2} \end{aligned} \quad (3.7)$$

For  $t \geq 0$ , boundary conditions (Chen and Zhu [135]; Srinivas [136]) are

$$\left. \begin{aligned} u &= \delta U_0 + \frac{\sqrt{k} \partial u}{\varepsilon}, \quad v = v_0, \quad w = 0, \quad T = T_0; \quad \phi = \phi_0, \quad C = C_0 \quad \text{at } y = 0 \\ u &= 0, \quad w = 0, \quad T = T_h, \quad \phi = \phi_h, \quad C = C_h \quad \text{at } y = h \end{aligned} \right\} \quad (3.8)$$

Here  $\delta$  is the stretching parameter,  $k$  is the permeability of the porous walls,  $\varepsilon$  is slip coefficient at the surface of the porous walls. We introduce the dimensionless variables as follows:

$$\begin{aligned} Y &= \frac{y}{h}; \quad U = \frac{u}{U_0}; \quad V = \frac{v_0}{U_0}; \quad W = \frac{w}{U_0}; \quad \tau = \frac{tU_0}{h}; \\ \theta &= \frac{T - T_h}{T_0 - T_h}; \quad F = \frac{\phi - \phi_h}{\phi_0 - \phi_h}; \quad \psi = \frac{C - C_h}{C_0 - C_h} \end{aligned} \quad (3.9)$$

And the parameters, Reynolds number  $Re = \frac{U_0 h}{\nu_f} = \frac{\rho_f U_0 h}{\mu}$ , elasto-viscous parameter  $K = \frac{-\mu_2 U_0}{\mu h}$ , magnetic field parameter  $M = \frac{\sigma \mu_e B_0^2 h}{\rho_f U_0}$ , mixed convection parameter  $\gamma = \frac{g_0(1-\phi_h)\beta_T h(T_0-T_h)}{U_0^2}$ , buoyancy ratio  $N_C = \frac{\beta_C(C_0-C_h)}{\beta_T(T_0-T_h)}$ , nanofluid buoyancy ratio  $N_R = \frac{(\rho_{nf}-\rho_f)(\phi_0-\phi_h)}{\rho_f(1-\phi_h)\beta_T(T_0-T_h)}$ , Prandtl number  $Pr = \frac{\nu}{\alpha} = \frac{\mu C_p}{\kappa}$ , Brownian motion parameter  $N_B = \frac{\tau_{nf} D_B(\phi_0-\phi_h)}{\nu h}$ , thermophoresis parameter  $N_T = \frac{\tau_{nf} D_T(T_0-T_h)}{\nu_f T_m h}$ , heat generation parameter  $Q = \frac{Q^* h}{U_0(\rho C_p)_f}$ , thermal radiation parameter  $R = \frac{\kappa_1 \kappa}{4\sigma_1 T_\infty^3}$ , Eckert number  $Ec = \frac{U_0^2}{C_p(T_0-T_h)}$ , nanofluid Lewis number  $Le = \frac{\nu_f}{D_B}$ , Schmidt number  $Sc = \frac{\nu}{D_S}$ , and Soret number  $Sr = \frac{D_{CT}(T_0-T_h)\nu}{(C_0-C_h)}$ .

The dimensionless governing equations can be written as follows:

$$\begin{aligned} \frac{\partial U}{\partial \tau} + V \frac{\partial U}{\partial Y} &= \frac{1}{Re} \frac{\partial^2 U}{\partial Y^2} - \frac{K}{Re} \left( \frac{\partial^3 U}{\partial \tau \partial Y^2} + V \frac{\partial^3 U}{\partial Y^3} \right) - \frac{M\lambda}{(1+m^2\lambda^2)} (U + m\lambda W) \\ &\quad + \gamma(\theta + N_C \psi - N_R F) \end{aligned} \quad (3.10)$$

$$\frac{\partial W}{\partial \tau} + V \frac{\partial W}{\partial Y} = \frac{1}{Re} \frac{\partial^2 W}{\partial Y^2} - K \left( \frac{\partial^3 W}{\partial \tau \partial Y^2} + V \frac{\partial^3 W}{\partial Y^3} \right) + \frac{M\lambda}{(1+m^2\lambda^2)} (m\lambda U - W) \quad (3.11)$$

$$\begin{aligned} \frac{\partial \theta}{\partial \tau} + V \frac{\partial \theta}{\partial Y} = & \left(1 + \frac{4}{3R}\right) \frac{1}{\text{Pr Re}} \frac{\partial^2 \theta}{\partial Y^2} + N_B \left(\frac{\partial \theta}{\partial Y} \frac{\partial F}{\partial Y}\right) + N_T \left(\frac{\partial \theta}{\partial Y}\right)^2 \\ & + \frac{M Ec \lambda}{(1 + m^2 \lambda^2)} (U^2 + W^2) + Q\theta \end{aligned} \quad (3.12)$$

$$\frac{\partial F}{\partial \tau} + V \frac{\partial F}{\partial Y} = \frac{1}{Le Re} \frac{\partial^2 F}{\partial Y^2} + \frac{N_T}{Le Re N_B} \frac{\partial^2 \theta}{\partial Y^2} \quad (3.13)$$

$$\frac{\partial \psi}{\partial \tau} + V \frac{\partial \psi}{\partial Y} = \frac{1}{Sc Re} \frac{\partial^2 \psi}{\partial Y^2} + \frac{Sr}{Re} \frac{\partial^2 \theta}{\partial Y^2} \quad (3.14)$$

together with the appropriate boundary conditions

$$\left. \begin{aligned} U = \delta U_0 + \gamma \frac{\partial U}{\partial Y}, \quad V = f_w, \quad W = 0, \quad \theta = 1; \quad F = 1, \quad \psi = 1 \quad \text{at } Y = 0 \\ U = 0, \quad W = 0, \quad \theta = 0, \quad F = 0, \quad \psi = 0 \quad \text{at } Y = 1 \end{aligned} \right\} \quad (3.15)$$

where  $\gamma = \frac{\sqrt{k}}{\varepsilon h}$  is the first order slip at the wall  $Y = 0$ . Then the quantities of practical interest in this study are the skin friction coefficients  $C_{fx}$ ,  $C_{fz}$ , the local Nusselt number  $Nu$  and Sherwood number  $Sh$  which are defined as

$$C_{fx} \propto \frac{\partial U}{\partial Y} \Big|_{Y=0}; \quad C_{fz} \propto \frac{\partial W}{\partial Y} \Big|_{Y=0}; \quad Nu \propto -\frac{\partial \theta}{\partial Y} \Big|_{Y=0}; \quad Sh \propto -\frac{\partial \psi}{\partial Y} \Big|_{Y=0} \quad (3.16)$$

### 3.3 Results and Discussion

Grid-independence studies show that the computational domain  $0 < \tau < \infty$  and  $0 < Y < 1$  can be divided into intervals with step sizes  $\Delta\tau = 0.0001$  and  $\Delta Y = 0.015$  for time and space, respectively. Convergence of the scheme is assumed when the values of every one of the unknowns  $U$ ,  $W$ ,  $\theta$ ,  $F$ ,  $\psi$  and their gradients differ by less than  $10^{-5}$  for the last two time steps for all values of  $Y$ .

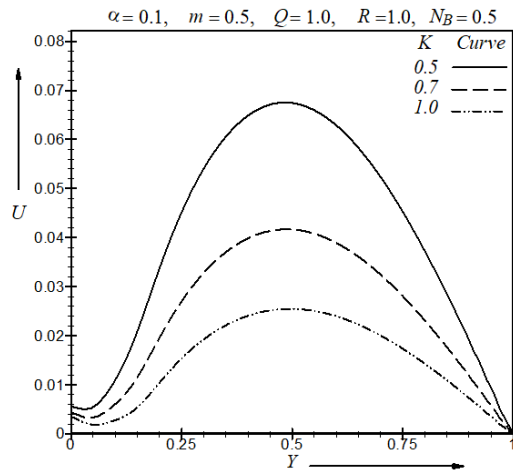


Figure 3.2: Primary velocity profile for  $K$

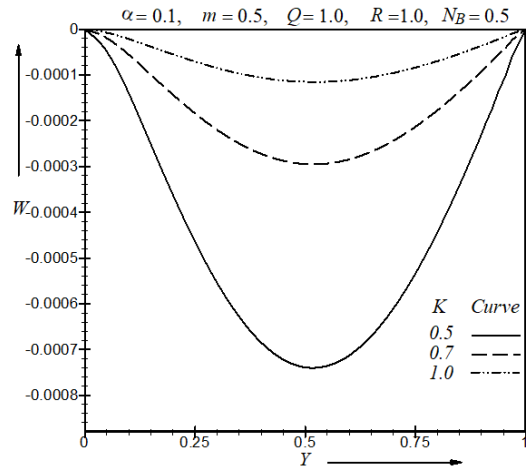


Figure 3.3: Secondary velocity profile for  $K$

As demonstrated in the above model, the angle between the direction of the strong uniform magnetic field and the plane transverse to the plate is zero i.e.,  $\alpha_e = 0^\circ$ , hence the value of the parameter  $\lambda$  is set at 1. The value of buoyancy ratio parameter  $\gamma = 3.0$  is taken to be positive to represent cooling of the plates. The Prandtl number  $Pr = 5.784$  is chosen arbitrarily corresponding to water-copper nanofluid;  $Sc = 0.94$  is taken for Carbon-Dioxide and  $f_w = 1$  is taken positive for uniform suction. In addition, numerical computations have been carried out considering  $\delta = 0.001$ ,  $Re = M = Ec = 1$ ,  $N_R = 3.0$ ,  $N_C = 0.1$ ,  $N_T = 0.5$ ,  $Le = 2$  and  $Sr = 1.0$ . The effect of several variables such as elasto-viscous parameter  $K$ , Hall current parameter  $m$ , radiation parameter  $R$ , heat source parameter  $Q$ , slip parameter  $\alpha$  and Brownian motion parameter  $N_B$  on the primary velocity, secondary velocity, temperature, nanoparticle volume fraction and concentration profiles are displayed in Fig. 3.2 – 3.13 while rest of the parametric effects are not substantial.

Figures 3.2 and 3.3 show the effect of elasto-viscous parameter  $K$  on the evolution of fluid motion and subsequent on the primary and secondary velocity profiles across the plates as time evolve, respectively. From these plots it is evident that increasing values of  $K$  opposes the motion of the fluid. It is observed from Fig. 3.4, the temperature field increases with the increase of heat source parameter  $Q$ . The heat source parameter has negative effect on nanoparticle

volume fraction shown in Fig. 3.5. Figure 3.6 depicts the primary velocity distribution for different values of the slip parameter  $\alpha$  and for the no-slip parameter  $\alpha = 0$ . It can be observed that the velocity decreases slightly with an increase of  $\alpha$  and the maximum is at the center of the channel. Figure 3.7 shows the significant effect of the Hall current parameter  $m$  on the secondary velocity distribution which is shaped reversely with the increase of  $m$ .

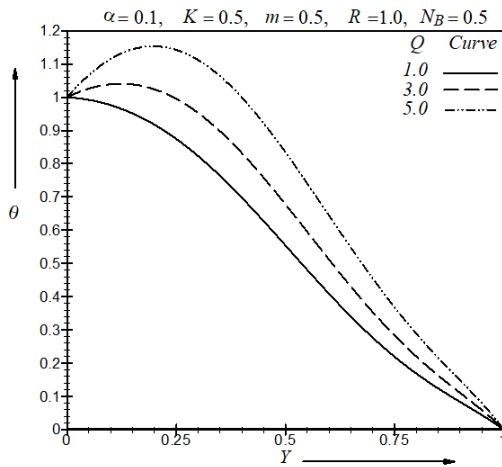


Figure 3.4: Temperature profile for  $Q$

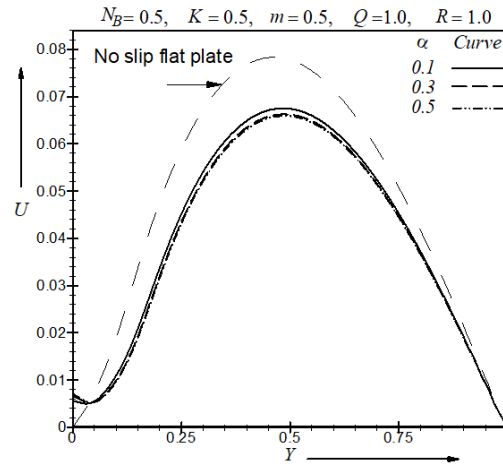


Figure 3.6: Primary velocity profile for  $\alpha$

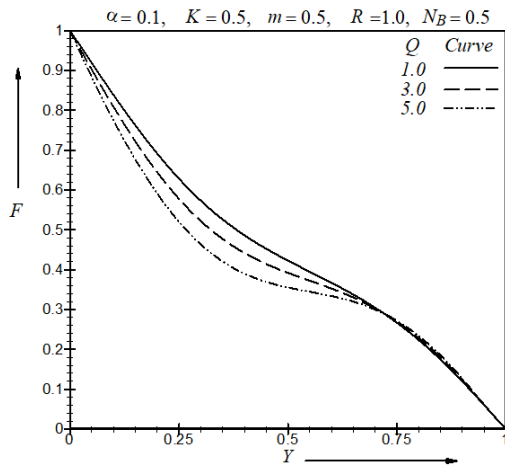


Figure 3.5: Volume fraction profile for  $Q$

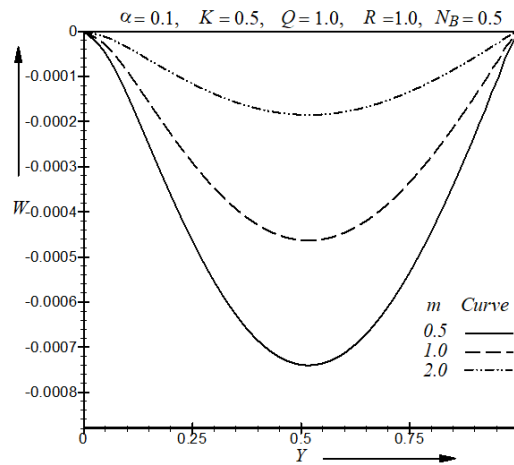


Figure 3.7: Secondary velocity profile for  $m$

From Fig. 3.8 it is seen that radiation  $R$  has increasing effect on the temperature field with the increase of  $R$ . The effect of  $R$  on the concentration profile is downbeat with the increase of  $R$  shown in Fig. 3.9. An increase in the Brownian motion of the nanoparticles leads to a decrease in the primary velocity at a large extent, shown in Fig. 3.10. It is examined from Fig. 3.11, the Brownian motion of the nanoparticles increases thermal transport which is an important mechanism for the enhancement of thermal conductivity of nanofluids.

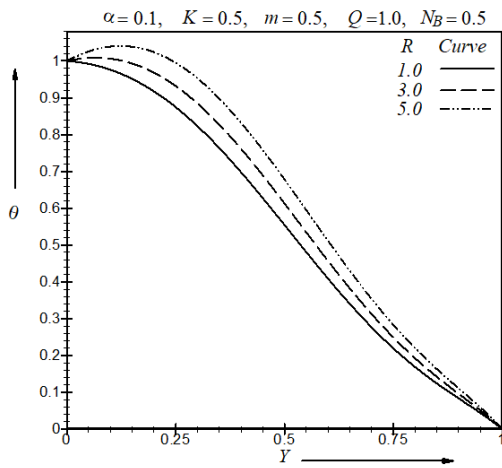


Figure 3.8: Temperature profile for  $R$

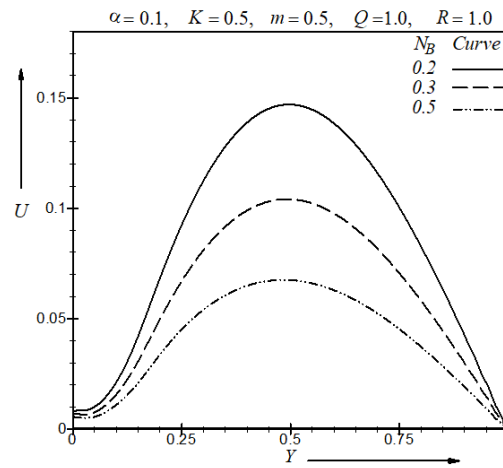


Figure 3.10: Primary velocity profile for  $N_B$

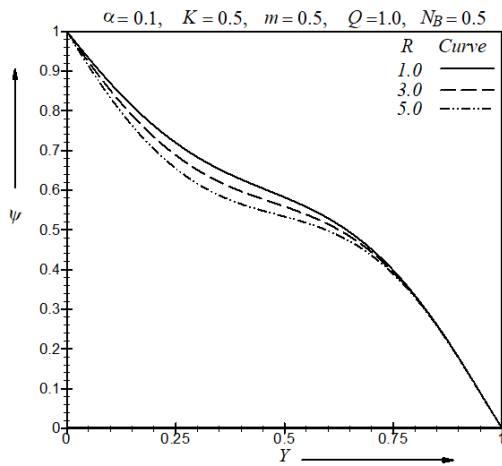


Figure 3.9: Volume fraction profile for  $R$

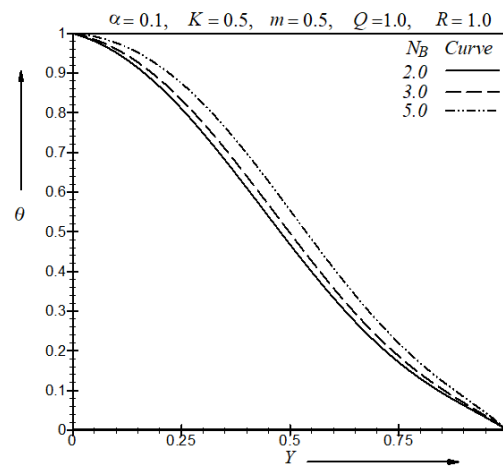


Figure 3.11: Temperature profile for  $N_B$



Figures 3.12 and 3.13 demonstrate that the raising Brownian motion parameter  $N_B$  reduces the mass volume fraction of nanoparticle and the concentration of fluid considerably.

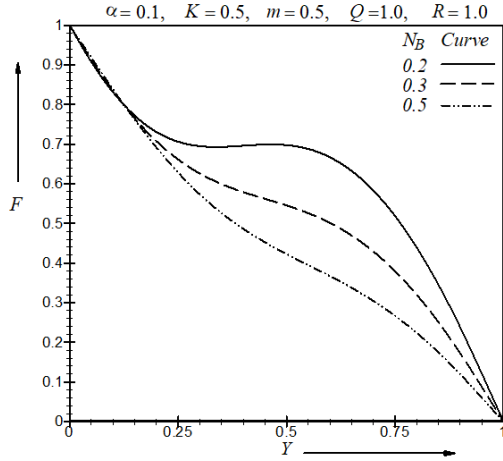


Figure 3.12: Volume fraction profile for  $N_B$

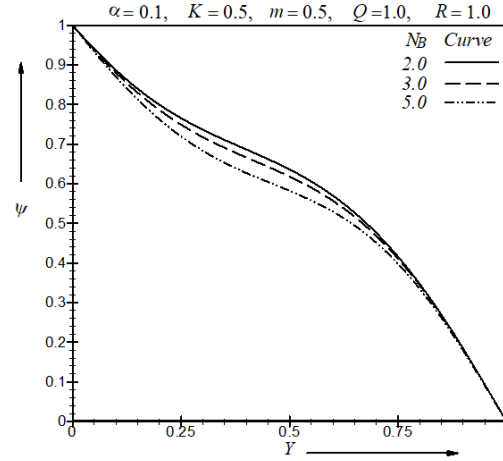


Figure 3.13: Concentration profile for  $N_B$

Table 3.1: Skin friction coefficients  $C_{fx}$ ,  $C_{fz}$ , the local Nusselt number  $Nu$  and Sherwood number  $Sh$  for several parameters.

$\alpha$	$K$	$m$	$Q$	$R$	$N_B$	$C_{fx}$	$C_{fz}$	$Nu$	$Sh$
0.1	0.5	0.5	1	1	0.5	0.039713	-0.00163	0.105346	1.386077
					0.3	0.093062	-0.00159	0.105350	1.386081
					0.7	0.064333	-0.00065	0.105393	1.386132
					1	0.039645	-0.00102	0.105370	1.386108
					3	0.048306	-0.00148	-0.60894	1.813578
					2	0.043865	-0.00156	-0.23700	1.593531
					0.3	0.014683	-0.00254	0.243965	1.300188

### **3.4 Conclusions**

The effect of magneto-Hall current in a elastico-viscous nanofluid layer in a channel with a slip plate is studied using finite difference method (FDM) employing a model that incorporates the effects of elastico-viscosity, Hall current, radiation, heat source, slip condition and Brownian motion. From this study, significant effect of the elastico-viscous parameter, heat source and Brownian motion is found.

## CHAPTER 4

### NUMERICAL STUDY OF THE EFFECT OF VARIABLE VISCOSITY ON UNSTEADY PULSATILE NANOFLUID FLOW THROUGH A COUETTE CHANNEL OF STRETCHING WALL WITH CONVECTIVE HEAT TRANSFER

**Abstract.** The current article desires to discover the pulse-driven Couette flow of Ag-water-based nanofluid restrained between two parallel plates with convective heat exchange with the ambient surrounding at the upper wall beneath the combined effects of thermophoresis, Brownian motion and temperature-dependent viscosity. The Buongiorno model is considered to illustrate the current flow analysis effectively. In this analysis, water as the base fluid and silver (Ag) as nanoparticles are exercised. The governing flow equations are generalised with the help of boundary layer approximations. Momentum, energy, and nanoparticle concentration equations are generated numerically using the finite difference method. The findings of non-dimensional parameters like Brownian motion parameter, Biot number, viscosity variation parameter, stretching velocity parameter, steady pressure gradient, phase angle, and amplitude are conferred graphically. As a final point, skin friction and Nusselt number are anticipated in numeric form with an excellent agreement. The achieved outcomes show that the velocity is directly proportional to the pulsatile pressure gradient.

#### 4.1 Introduction

Ultrahigh-performance cooling in engineering and industrial technologies is a vital part of the imperative issues in research today. With the mounting demand for resourceful cooling systems, more effective coolants are essential to maintaining the temperature of heat-generating engines and engineering devices such as electronic machinery below protected limits. Choi [25] first established the concept of nanofluids which are engineered by stably suspending and uniformly

dispersing a small amount of nanometer-sized (between 1 and 100 nm in diameter) ultrafine metallic, nonmetallic or ceramic particles in ordinary heat transfer fluids to generate fluids with enhanced transport properties and higher heat transfer performance.

Nanofluids encompassing extraordinary characteristics of providing unique physical and chemical properties, dominate enormous potential of applications to improve heat transfer, enhance efficiency, save energy and reduce emissions in several areas of engineering and industry, including vehicular cooling in transportation, power generation, defence, nuclear, space, micro-electronics equipment, Wong and Leon [96]; Sridhara and Satapathy [137]. Moreover, nanotechnology has offered the possibility of imaging cancer and delivering drugs on specific cells using nanoparticles, Farokhzad and Langer [138]; Uddin *et al.* [139]. Consequently, nanofluids are attracting significant interest from many scientists and researchers due to their enormous applications. Recent explorers Kuznetsov and Nield [121] discussed the study of the nanofluid flow passing stretching sheet. Following the Buongiorno nanofluid model [41], Karim *et al.* [66] described unsteady nanofluid slip flow in a channel Brownian motion. Wang [140] and Bestman [141] conferred the velocity distribution and shear stresses in an infinite channel. At present days, researchers are paying attention to investigating the nanofluid flow taking the effects of temperature-dependent viscosity into account (Ali and Makinde [142]; Mkwizu and Makinde [143]).

In this analysis, the nanofluid flow is motivated by the pressure gradient. The objective is to analyse the temperature-dependent viscosity effect on pulse-driven nanofluid flow's heat and mass transfer characteristics. Here a comparison study is prepared to take the fluid flow driven by a pulsatile and steady pressure gradient. In this study, Silver (*Ag*) nanoparticles are hosted in water-based nanofluids. Solutions have been carried out employing the finite difference method, and the results have been displayed graphically and in tabular form with the significant agreement.

## 4.2 Mathematical Model

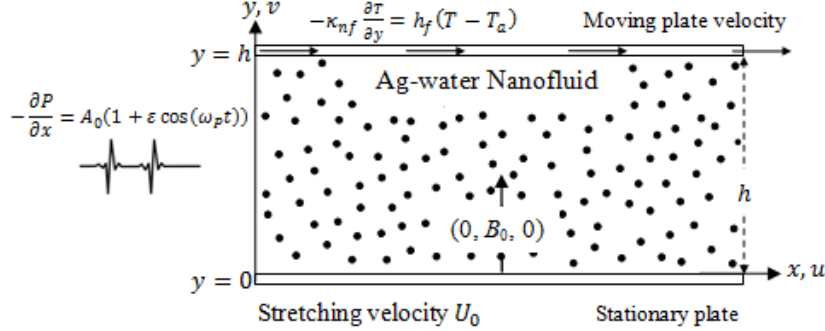


Figure 4.1: Physical configuration and coordinate system

An Unsteady, laminar, incompressible flow of nanofluid is retained in two parallel plates, which are considered a channel in the current work following Buongiorno Model [41]. In this analysis, the physical properties of water as the base fluid and silver (*Ag*) as nanoparticles are implemented. The fluid's viscosity is considered temperature-dependent, and a magnetic field is present in an upward direction that is normal to the lower plate. To arrange the model geometry, the  $x$ -axis is taken along the plate, and the  $y$ -axis is taken normal to the plates. The lower plate having stretching velocity  $U_0$  is at  $y = 0$ , and the upper plate with convective cooling at  $y = h$  is moving at velocity  $U_h$ . The depth of the channel ( $h$ ) is assumed small compared with the channel length ( $L$ ), so that  $d = h/L \ll 1$  [141]. As a result, the flow is considered fully developed, which makes the physical quantities not change in the flow direction. Because of this, the conservation of mass takes form, i.e.  $div \bar{q}_{velocity}(t, x) = 0$ , hence  $\partial u / \partial x = 0$ . And the upper wall of the channel exchanges heats with the ambient surroundings. And this flow is driven by a pulsatile pressure gradient applied across the ends of the channel given by [140, 141]

$$-\frac{\partial P}{\partial x} = A_0 + A_1 \text{Cos}(\omega_p t) = A_0(1 + \varepsilon \text{Cos}(\omega_p t)) \quad 0 \leq x \leq L \quad (4.1)$$

Here  $A_0$  is the steady component of pressure gradient,  $A_1$  is the amplitude of pulsatile component of pressure gradient,  $\omega_p = 2\pi f_p$  is the angular frequency, and  $\varepsilon = A_1/A_0$  is the non-dimensional amplitude of the pulse. Following the Buongiorno [41] mathematical model for a fully developed flow of nanofluids in the presence of the Brownian diffusion and thermophoresis diffusion, the governing equations for continuity, momentum, energy and nanoparticle concentration are given by the following equations:

$$\rho_{nf} \frac{\partial u}{\partial t} = -\frac{\partial P}{\partial x} + \frac{\partial}{\partial y} \left( \mu_{nf}(T) \frac{\partial u}{\partial y} \right) - \sigma B_0^2 u \quad (4.2)$$

$$\frac{\partial T}{\partial t} = \alpha_{nf} \frac{\partial^2 T}{\partial y^2} + \frac{\alpha_{nf} \mu_{nf}(T)}{\kappa_{nf}} \left( \frac{\partial u}{\partial y} \right)^2 + \tau_{nf} \left[ D_B \left( \frac{\partial T}{\partial y} \frac{\partial C}{\partial y} \right) + \frac{D_T}{T_a} \left( \frac{\partial T}{\partial y} \right)^2 \right] \quad (4.3)$$

$$\frac{\partial C}{\partial t} = D_B \frac{\partial^2 C}{\partial y^2} + \frac{D_B}{T_a} \frac{\partial^2 T}{\partial y^2} \quad (4.4)$$

The dynamic viscosity is assumed to be an exponentially decreasing function of temperature given by [142, 143]

$$\mu_f(T) = \mu_0 e^{-m(T-T_0)} \quad (4.5)$$

Assuming the upper wall of the channel exchanges heat with the ambient surroundings following Newton's law of cooling [143] and having no mass flux, the boundary conditions are preferred as

$$\left. \begin{aligned} u = U_0; \quad T = T_0; \quad C = C_0 \quad \text{at } y = 0 \\ u = U_h; \quad -\kappa_{nf} \frac{\partial T}{\partial y} = h_f(T - T_a); \quad D_B \frac{\partial C}{\partial y} = -\frac{D_T}{T_a} \frac{\partial T}{\partial y} \quad \text{at } y = h \end{aligned} \right\} \quad (4.6)$$

Here  $U_0$  is the stretching velocity of the lower plate,  $U_h$  is the velocity of the upper plate,  $T_a$  is the

ambient temperature,  $P$  is the nanofluid pressure,  $C_0$  is the nanoparticles' initial concentration,  $D_B$  is the Brownian diffusion,  $D_T$  is the thermophoretic diffusion,  $\mu_0$  is the nanofluid dynamic viscosity at the initial temperature  $T_0$  and  $m$  is the viscosity variation parameter,  $h_f$  is the heat transfer coefficient that describes the heat transferred from the heat plate to the surrounding nanofluids. Here the nanoparticle volume fraction is represented by  $\varphi$ . Also,  $\rho$ ,  $\kappa$ ,  $\alpha$  and  $C_p$  are the density, thermal conductivity, thermal diffusivity and, heat capacitance, respectively. And the suffices  $f$ ,  $s$  and  $nf$  represent the base fluid, solid nanoparticles and nanofluid, respectively. Relations among the physical properties of nanofluids are given by [144, 145]

$$\begin{aligned}\mu_{nf} &= \frac{\mu_f}{(1-\varphi)^{2.5}}, \quad \alpha_{nf} = \frac{\kappa_{nf}}{(\rho c_p)_{nf}}, \quad (\rho c_p)_{nf} = (1-\varphi)(\rho c_p)_f + \varphi(\rho c_p)_s \\ \frac{\kappa_{nf}}{\kappa_f} &= \frac{(\kappa_s + 2\kappa_f) - 2\varphi(\kappa_f - \kappa_s)}{(\kappa_s + 2\kappa_f) + \varphi(\kappa_f - \kappa_s)}, \quad \rho_{nf} = (1-\varphi)\rho_f + \varphi\rho_s,\end{aligned}\quad (4.7)$$

Table 4.1: Thermophysical properties of water as the base fluid and silver as the nanoparticles

Materials	$\rho$	$C_p$	$\kappa$
Water	997.1	4179	0.613
Silver	10500	235	429

To minimise the complexity of the governing equations, the following non-dimension variables and parameters are initiated in the present research.

$$\begin{aligned}X &= \frac{x}{h}; \quad Y = \frac{y}{h}; \quad U = \frac{u}{U_h} = \frac{hu}{\nu_f}; \quad \tau = \frac{t\nu_f}{h^2}; \quad \theta = \frac{T - T_0}{T_a - T_0}; \quad F = \frac{C}{C_0}; \\ \bar{P} &= \frac{h^2}{\rho_f \nu_f^2} P; \quad Bi = \frac{h_f h}{\kappa_f}; \quad A = \frac{h A_0}{\rho_f \nu_f \omega_p}; \quad \Omega = \frac{\omega_p h^2}{\nu_f}; \quad \beta = m(T_a - T_0); \\ N_B &= \frac{\tau_{nf} D_B C_0}{\alpha_f}; \quad N_t = \frac{\tau_{nf} D_T (T_a - T_0)}{\alpha_f T_a}; \quad Pr = \frac{\nu_f}{\alpha_f}; \quad Le = \frac{\nu_f}{D_B}; \\ Ec &= \frac{\nu_f^2}{C_p (T_a - T_0) h^2}; \quad M = \frac{\sigma B_0^2 h^2}{\mu_f};\end{aligned}\quad (4.8)$$

The non-dimensional transformed equations, together with the boundary conditions, can be written as:

$$\frac{\partial U}{\partial \tau} = \frac{\rho_f}{\rho_{nf}} A \Omega (1 + \varepsilon \text{Cos}(\Omega \tau)) + \frac{\rho_f \mu_{nf}}{\rho_{nf} \mu_f} e^{-\beta \theta} \left( \frac{\partial^2 U}{\partial Y^2} - \beta \frac{\partial \theta}{\partial Y} \frac{\partial U}{\partial Y} \right) - \frac{\rho_f}{\rho_{nf}} M U \quad (4.9)$$

$$\frac{\partial \theta}{\partial \tau} = \frac{\kappa_{nf}(\rho C_p)_f}{\kappa_f(\rho C_p)_{nf} \text{Pr}} \frac{\partial^2 \theta}{\partial Y^2} + \frac{\mu_{nf}(\rho C_p)_f}{\mu_f(\rho C_p)_{nf}} e^{-\beta \theta} Ec \left( \frac{\partial U}{\partial Y} \right)^2 + \frac{N_b}{\text{Pr}} \left( \frac{\partial \theta}{\partial Y} \frac{\partial F}{\partial Y} \right) + \frac{N_t}{\text{Pr}} \left( \frac{\partial \theta}{\partial Y} \right)^2 \quad (4.10)$$

$$\frac{\partial F}{\partial \tau} = \frac{1}{Le} \left[ \frac{\partial^2 f}{\partial Y^2} + \frac{N_t}{N_B} \frac{\partial^2 \theta}{\partial Y^2} \right] \quad (4.11)$$

with the corresponding dimensionless boundary conditions,

$$\left. \begin{aligned} U = \gamma; \quad \theta = 0; \quad F = 1 \quad \text{at } Y = 0 \\ U = 1; \quad \frac{\partial \theta}{\partial Y} = -\frac{\kappa_f}{\kappa_{nf}} Bi(\theta - 1); \quad \frac{\partial F}{\partial Y} = -\frac{N_t}{N_b} \frac{\partial \theta}{\partial Y} \quad \text{at } Y = 1 \end{aligned} \right\} \quad (4.12)$$

Here  $A$ ,  $\Omega$ ,  $\beta$ ,  $M$ ,  $N_b$ ,  $N_t$ ,  $\text{Pr}$ ,  $Le$ ,  $Ec$ ,  $\gamma$  and  $Bi$  are the dimensionless steady pressure gradient, phase angle, non-dimensional viscosity variation parameter, magnetic field parameter, Brownian motion parameter, thermophoresis diffusion parameter, Prandtl number, Lewis number, Eckert number, the stretching parameter, and Biot number, respectively. The physical attentions in the existing study are the skin friction coefficient  $C_f$  and the local Nusselt number  $Nu$ , defined at wall as

$$C_f = \frac{e^{-\beta \theta} \mu_{nf}}{\mu_f} \frac{\partial U}{\partial Y} \quad \text{and} \quad Nu = -\frac{\kappa_{nf}}{\kappa_f} \frac{\partial \theta}{\partial Y} \quad (4.13)$$

Here the lower plate is at  $Y = 0$  and the upper plate is at  $Y = 1$ .



### 4.3 Numerical Analysis

Equations (4.9)–(4.12) are clearly a system of nonlinear boundary value problem (BVP) and can be solved numerically using the discretisation of the forward finite difference method. Grid-independence studies show that the computational domain  $0 \leq Y \leq 1$  is partitioned into equal parts, and the grid size is given as  $\Delta Y = 1/N$  with the grid points  $Y_j = (j - 1)\Delta Y$ ,  $1 \leq j \leq N + 1$ . The discretisation is based on a linear Cartesian mesh and uniform grid on which finite differences are taken. The first and second spatial derivatives in equations (4.9)–(4.11) are approximated with second order forward finite differences. Convergence of the scheme is assumed when the values of every one of the unknowns  $U$ ,  $\theta$ ,  $F$  and their gradients differ by less than  $10^{-5}$  for the last two time steps for all values of  $Y$ .

Let  $U(Y_j, t)$ ,  $\theta(Y_j, t)$ ,  $F(Y_j, t)$  are approximated by  $U_j$ ,  $\theta_j$ ,  $F_j$ , respectively. Then considering superscript  $n + 1$  as a new time approximation, the finite difference system for the current problem becomes

$$\begin{aligned} \frac{U_j^{n+1} - U_j^n}{\Delta \tau} &= \frac{\rho_f}{\rho_{nf}} A \Omega (1 + \varepsilon \text{Cos}(\Omega \tau)) + \frac{\rho_f \mu_{nf}}{\rho_{nf} \mu_f} e^{-\beta \theta_j^n} \frac{U_{j+1}^n - 2U_j^n + U_{j-1}^n}{\Delta Y^2} \\ &\quad - \frac{\rho_f \mu_{nf}}{\rho_{nf} \mu_f} \beta e^{-\beta \theta_j^n} \left( \frac{\theta_{j+1}^n - \theta_j^n}{\Delta Y} \frac{U_{j+1}^n - U_j^n}{\Delta Y} \right) - \frac{\rho_f}{\rho_{nf}} M U_j^n \end{aligned} \quad (4.14)$$

$$\begin{aligned} \frac{\theta_j^{n+1} - \theta_j^n}{\Delta \tau} &= \frac{\kappa_{nf}(\rho C_p)_f}{\kappa_f(\rho C_p)_{nf} \text{Pr}} \frac{\theta_{j+1}^n - 2\theta_j^n + \theta_{j-1}^n}{\Delta Y^2} + \frac{\mu_{nf}(\rho C_p)_f}{\mu_f(\rho C_p)_{nf}} e^{-\beta \theta} E_c \left( \frac{U_{j+1}^n - U_j^n}{\Delta Y} \right)^2 \\ &\quad + \frac{n_b}{\text{Pr}} \left( \frac{\theta_{j+1}^n - \theta_j^n}{\Delta Y} \frac{F_{j+1}^n - F_j^n}{\Delta Y} \right) + \frac{n_t}{\text{Pr}} \left( \frac{\theta_{j+1}^n - \theta_j^n}{\Delta Y} \right)^2 \end{aligned} \quad (4.15)$$

$$\frac{F_j^{n+1} - F_j^n}{\Delta \tau} = \frac{F_{j+1}^n - 2F_j^n + F_{j-1}^n}{Le \Delta Y^2} + \frac{n_t}{Le n_B} \frac{\theta_{j+1}^n - 2\theta_j^n + \theta_{j-1}^n}{\Delta Y^2} \quad (4.16)$$

Corresponding to the grid points, the difference equations are customised to represent the

boundary conditions as follows

$$\left. \begin{aligned} U_1 &= \gamma; & \theta_1 &= 0; & F_1 &= 1 \\ U_{N+1} &= 1; & \theta_{N+1} &= \theta_N - \frac{\kappa_f}{\kappa_{nf}} Bi \Delta Y (\theta_N - 1); & F_{N+1} &= F_N - \frac{N_i}{N_b} (\theta_{N+1} - \theta_N) \end{aligned} \right\} \quad (4.17)$$

Finally, discretisation in space can be made based on backward finite difference approximation to obtain the skin friction and Nusselt number and results can be estimated at  $Y = 0$  for the lower plate as follows

$$C_f = \frac{e^{-\beta\theta_1} \mu_{nf} (U_2^n - \gamma)}{\mu_f \Delta Y} \quad \text{and} \quad Nu = -\frac{\kappa_{nf} \theta_2^n}{\kappa_f \Delta Y} \quad (4.18)$$

Consequently, for the upper plate at  $Y = 1$

$$C_f = \frac{e^{-\beta\theta_{N+1}} \mu_{nf} (U_{N+1}^n - U_N^n)}{\mu_f \Delta Y} \quad \text{and} \quad Nu = -\frac{\kappa_{nf} (\theta_{N+1}^n - \theta_N^n)}{\kappa_f \Delta Y} \quad (4.19)$$

Table 4.2: Comparison of different values of  $Bi$  and  $\beta$  taking  $\varphi = 0$ ,  $\varepsilon = 0$ ,  $\gamma = 0$ ,  $M = 0$

$\tau$	$Bi$	$\beta$	Skin Friction $C_f$		Nusselt number $Nu$	
			[142]	Present work	[142]	Present work
10	1	0.1	0.397	0.395	0.512	0.511
10	1	0.5	0.145	0.146	0.223	0.221
10	3	0.1	0.406	0.405	0.79	0.784

#### 4.4 Results and Siscussion

This study considers pure water as base fluid and water-based Newtonian nanofluids containing silver ( $Ag$ ) as nanoparticles. The Prandtl number of the base fluid (water) is kept constant at 6.2, and the effect of solid volume fraction is investigated in the range of  $0 \leq \varphi \leq 0.3$ . To obtain

$\varphi = 0.1\%$  volume fraction of  $W_f = 100ml$  water-based nanofluid,  $W_s = 1.0541gm$  silver ( $Ag$ ) is to be mixed in the base fluid where  $r_s = 10500kg/m^3$  and  $r_f = 997.1kg/m^3$  which is measured from the following equation [145]

$$\varphi = \left( \frac{W_s/\rho_s}{W_s/\rho_s + W_f/\rho_f} \right) \times 100 \quad (4.20)$$

Table 4.3: Physical properties of  $Ag$ -water nanofluid for different  $\varphi$

$\varphi$	$\rho_{nf}$	$(\rho C_p)_{nf}$	$\kappa_{nf}$	$\mu_{nf}$
0.1	1947.39	$3.9959 \times 10^6$	0.816	0.001340
0.2	2897.68	$3.8249 \times 10^6$	1.070	0.001799
0.3	3847.97	$3.6539 \times 10^6$	1.396	0.002512

Numerical solutions for the representative velocity field, temperature field, concentration field, skin friction, and Nusselt number have been carried out by assigning arbitrary chosen specific values to various thermophysical parameters controlling the flow system (see Figures 4.2–4.13).

Figures 4.2–4.5 illustrate the parametric effects on the nanofluid velocity profiles where solid and dash lines represent the fluid flow driven by pulsatile and steady pressure gradients, respectively. Figure 4.2 shows the velocity profiles against time at different spaces across the channel. All the quantities have attained their steady state for a steady pressure gradient at  $\tau = 5$ . From the Table 4.3, it is seen that there is a rise in the density  $\rho_{nf}$  as well as the dynamic viscosity  $\mu_{nf}$  of nanofluid when nanoparticles volume fraction  $\varphi$  increases.

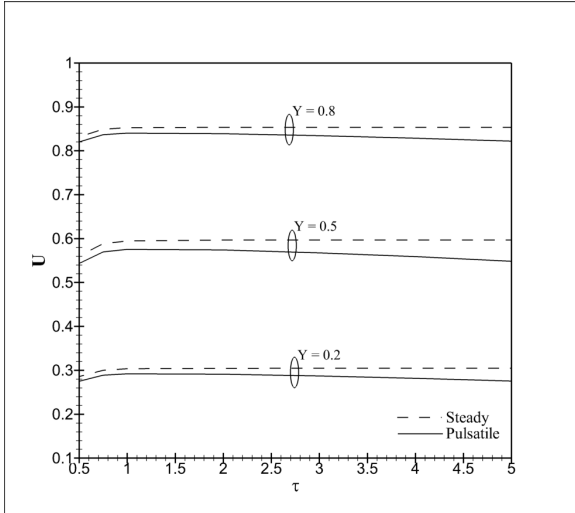


Figure 4.2: Velocity profiles for  $\tau$  at different space

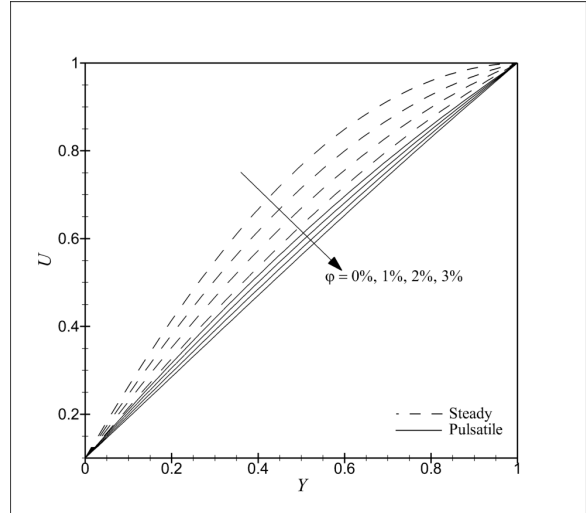


Figure 4.3: Velocity profiles for different  $\varphi$

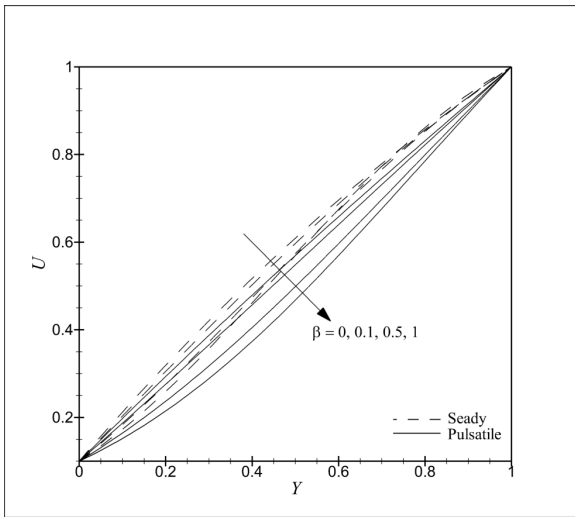


Figure 4.4: Velocity profiles for different  $\beta$

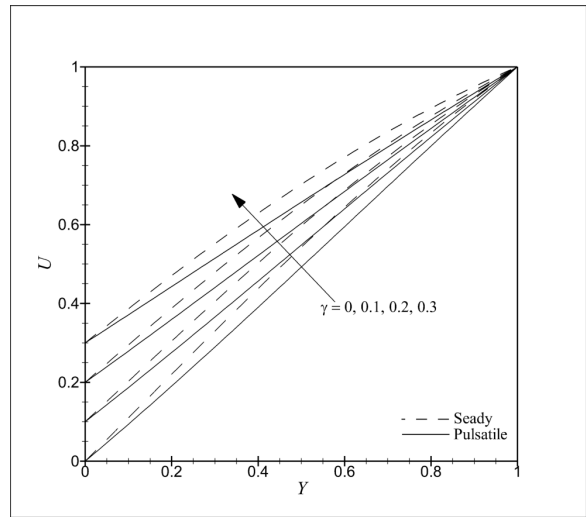


Figure 4.5: Velocity profiles for different  $\gamma$

Higher nanofluid viscosity results in a falling environment in the fluid velocity profiles, which are precisely found in figure 4.3 from this present research. The temperature-dependent viscosity is the phenomenon of a fluid by which viscosity reduces as its temperature enhances. When the temperature rises, the molecular interchange enlarges as molecules move faster in higher temperatures; consequently, the fluid becomes lighter and flows more quickly.

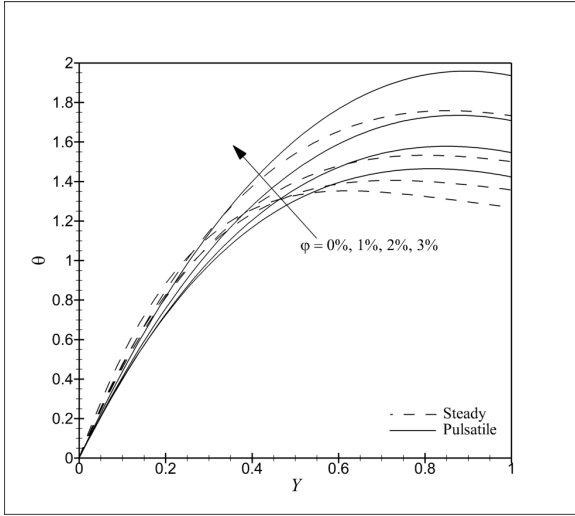


Figure 4.6: Temperature profiles for different  $\varphi$

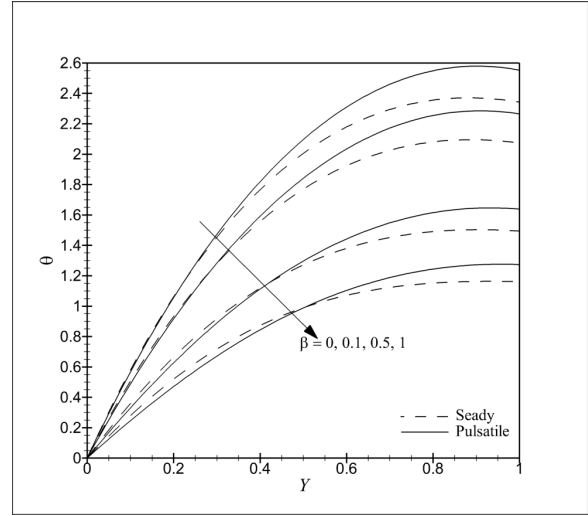


Figure 4.7: Temperature profiles for different  $\beta$

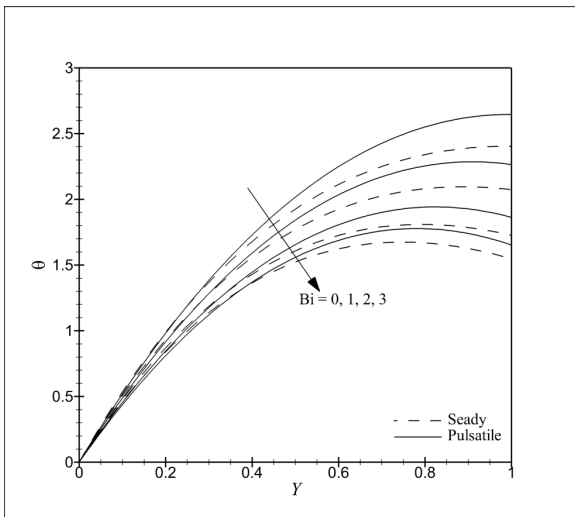


Figure 4.8: Temperature profiles for different  $Bi$

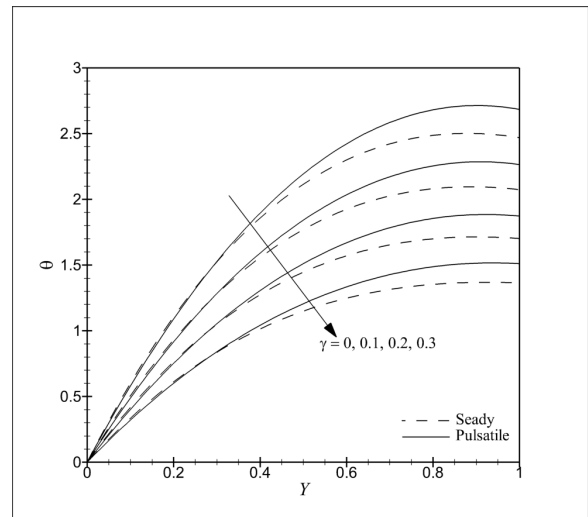


Figure 4.9: Temperature profiles for different  $\gamma$

In figure 4.4, for constant pressure gradient, we discover that the velocity profiles of the nanofluid increase with the decreasing viscosity due to the enhancement of viscosity variation parameter  $\beta$ . But because of pulsatile flow, the environment reverses, and the velocity decreases with the increase of  $\beta$ . The effects of stretching parameter  $\gamma$  are plotted in figure 4.5. As

$\gamma$  increases, the thickness of the momentum boundary layer increases for both pulsatile and constant pressure gradients.

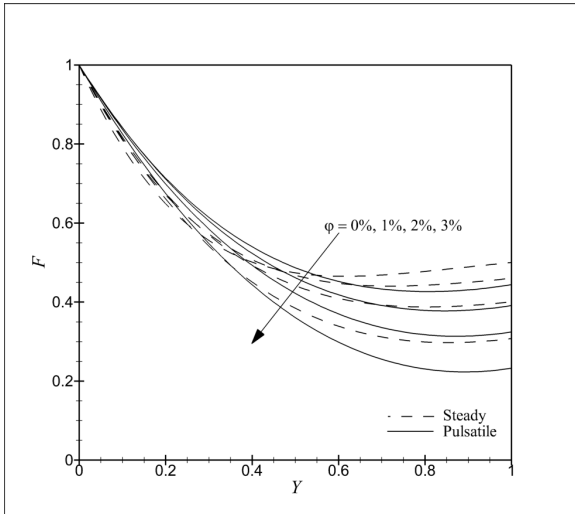


Figure 4.10: Concentration profiles for different  $\varphi$

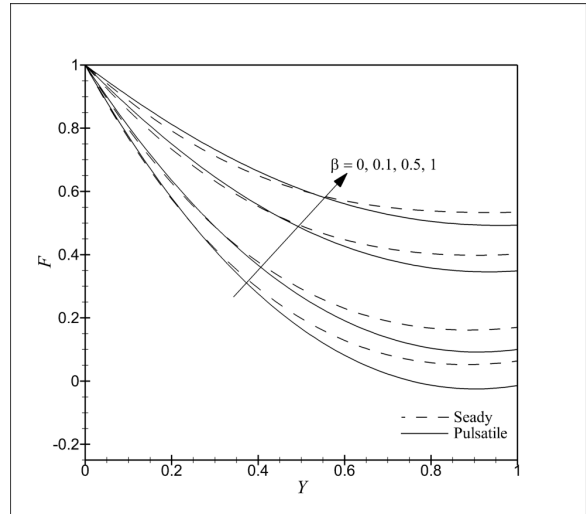


Figure 4.11: Concentration profiles for different  $\beta$

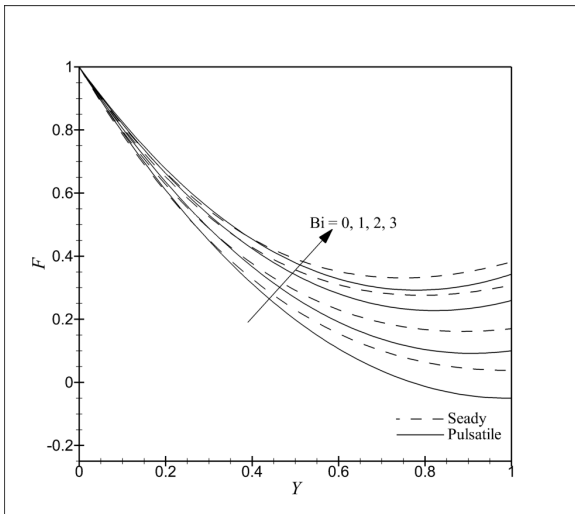


Figure 4.12: Concentration profiles for different  $Bi$

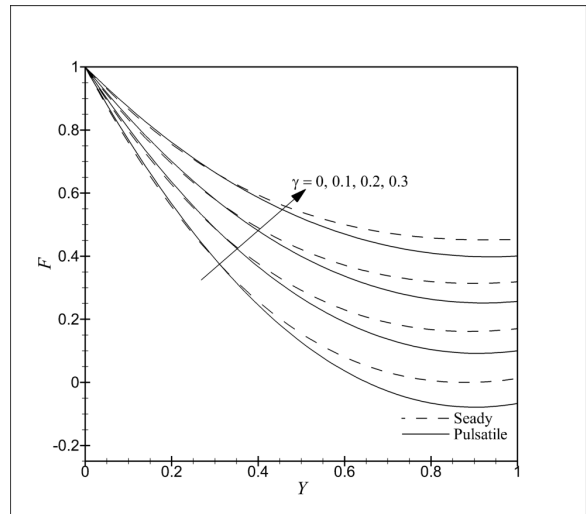


Figure 4.13: Concentration profiles for different  $\gamma$

When nanoparticles volume fraction  $\varphi$  increases, there is a rise in the thermal conductivity  $\kappa_{nf}$  of nanofluid, for which increasing nanoparticle volume fraction results in an enhanced

environment in the fluid temperature profiles, which are found in figure 4.6 obtained from this present research for both pulsatile and constant pressure gradient. With the increase of  $\beta$ , the nanofluid viscosity decreases; as a result, the kinetic viscosity of nanoparticles increases and a rise in the temperature is examined, as shown in Fig. 4.7. Figure 4.8 depicts that the temperature profile decreases across the channel with the increasing convective cooling as Biot number increases at the upper channel wall due to increasing heat loss toward the ambient surrounding from the walls. Figure 4.9 demonstrates that the temperature profile decreases across the channel with the rising stretching parameter  $\gamma$  at the lower channel wall. Figures 4.10-4.13 illustrate the various parametric effects on concentration profiles. When nanoparticle volume fraction  $\varphi$  increases, nanofluid concentration profiles fall, as shown in figure 4.10, where rising situations are detected for increasing viscosity variation parameter  $\beta$ , Biot number  $Bi$  and stretching parameter  $\gamma$  at the lower wall displayed in figures 4.11–4.13, respectively.

Table 4.4: Skin Friction and Nusselt Number with parameters variations:  $Pr = 6.2$ ,  $Le = 1$ ,  $Nb = 0.4$ ,  $Nt = 0.16$ ,  $Ec = 1$ ,  $Bi = 1$ ,  $M = 0.5$ ,  $\gamma = 0.1$ ,  $A = 2$ ,  $\varepsilon = 2$ ,  $\Omega = 15^\circ$  for different values of  $\varphi$  and  $\beta$  for pulsatile pressure gradient

	Pulsatile pressure gradient				Steady pressure gradient			
$\varphi$	$C_{f_{Y=0}}$	$Nu_{Y=0}$	$C_{f_{Y=0}}$	$Nu_{Y=1}$	$C_{f_{Y=0}}$	$Nu_{Y=0}$	$C_{f_{Y=0}}$	$Nu_{Y=1}$
0	1.1154	4.0607	0.5921	0.3597	1.6866	5.5547	0.0402	0.2152
0.1	1.269	4.9001	0.7693	0.6525	1.8242	6.2485	0.2439	0.4514
0.2	1.4731	6.0915	0.9977	1.0759	2.0112	7.3167	0.504	0.8253
0.3	1.7472	7.811	1.2958	1.701	2.2672	8.9351	0.8401	1.41
$\beta$	$C_{f_{Y=0}}$	$Nu_{Y=0}$	$C_{f_{Y=0}}$	$Nu_{Y=1}$	$C_{f_{Y=0}}$	$Nu_{Y=0}$	$C_{f_{Y=0}}$	$Nu_{Y=1}$
0	1.3893	5.4507	0.9015	0.7868	1.93	6.7194	0.3606	0.5592
0.1	1.269	4.9001	0.7693	0.6525	1.8242	6.2485	0.2439	0.4514
0.5	0.9914	3.6385	0.4672	0.317	1.5584	5.1722	-0.0329	0.2004
1	0.823	2.8954	0.2843	0.1002	1.3665	4.6064	-0.2127	0.0849

## 4.5 Conclusions

From the overall analysis, we can conclude that the nanoparticles volume fraction  $\varphi$  has a decreasing effect on velocity and nanofluid concentration while increasing impact on temperature. Again viscosity variation parameter  $\beta$  has an increasing outcome on momentum for steady pressure gradient, whereas it has a reverse effect for pulsatile pressure gradient. Moreover, the Biot number significantly impacts temperature and concentration, and the consequence of stretching parameter  $\gamma$  is very considerable.



## CHAPTER 5

### ANALYSIS FOR ELASTICO-VISCOUS NANOFLUID FLOW IN A CHANNEL INTEGRATING THERMAL RELAXATION TIME USING TWO PARAMETERS LIE GROUP TRANSFORMATION

**Abstract.** The present research is an arrangement of heat transfer investigation of the unsteady viscoelastic nanofluid slip flow in a porous channel that incorporates stress and thermal relaxation time factors. The Lie group analysis of two parameters, which provides an appropriate method to address non-linear equations, is carried out to transform the mathematical model into a system of non-linear ODEs that are numerically solved. The consequences of flow control parameters are studied for the momentum, temperature and diffusion profiles, taking the shear stress and heat transfer into account. The domino effects are finally described from the material point of view. A comparison of the Cattaneo-Christov heat flux (CCHF) model and Fourier's law is an exciting feature of this homework. The CCHF model introduced the thermal relaxation phase in the manifestation of the energy distribution in preference to the conventional Fourier's law. In addition, a noteworthy conclusion of the current research can be expressed by stating that the stress relaxation parameter improves the nanofluid viscosity that resists flow while the heat transfer is enhanced. In contrast, thermal relaxation depreciates heat transfer.

**Keywords:** Maxwell parameter, Nanofluid, Lie group analysis, Elastico-viscous fluid, Convective surface

#### 5.1 Introduction

An attractive and highly uncertain tribological substance concerns the elastico-viscosity effect on lubrication features in thin film flows. The addition of polymers to crystal oils, recognised as multi-grade oils, has been familiar since the mid-1990s [146, 52, 50, 147]. These accom-

paniments reinforce the consequential lubricants to convert non-Newtonian and viscoelastic, employing a shear rate-dependent viscosity [51, 148, 149]. The actual non-linear affiliation concerning shear stress and strain rate of elastico-viscous liquids could anticipate time-dependent effects. Still, the conventional Newtonian fluid attaching Navier-Stokes equations is unable to establish this relationship [150, 151]. Polymer solutions, paints, colloidal solutions, clay, blood, melt, mud, condensed milk, glues, printing ink, soaps, emulsions, shampoos, and tomato paste are the models of the non-Newtonian liquids and contain both elasticity and viscosity characteristics. But the central obstruction is to model a particular constitutive equation that exposes all the salient properties of such viscoelastic fluids. For this reason, investigators have projected several viscoelastic fluid models integrating different characteristics of non-Newtonian liquids [152, 153, 154]. The elastico-viscous fluid Models, together with second-order fluids, are perfect for the slow indication of low elastic solutions [155]. However, these types of fluids with a high Deborah number that measure the time-dependent effects do not give significant results for highly viscoelastic polymers, so the weight of these fluid models is limited for the polymer industry [156, 157]. The Maxwell model, the most representative and practical elastico-viscous model, should be taken into account for efficient analysis to carry out operative and hypothetical work in the industrial sector [158]. Elastico-Viscous fluids are generally classified as differential-, integral- and rate-type fluids. The Maxwell model is a simple feature of rate-type viscoelastic material that possesses the physiognomies of the relaxation phase of fluid, namely the viscosity ratio to the modulus of elasticity. It eradicates the multifaceted effects of shear-reliant viscosity and permits someone to emphasise the fluids' elasticity influence on its boundary layer physiognomies [159]. Harris [49] initially established the constitutive equation of the upper convected Maxwell (UCM) model to exert the lubricant behaviour of the elastico-viscous fluid. Plastic manufacturing, food processing, paper production, and aerodynamic extrusion of plastic films are the applications of elastico-viscous fluids in industrial, bioengineering, and production procedures. Because of escalating usage, academics have paid greater attention to studying boundary layer flows of non-Newtonian fluids [160, 161].

Heat transfer phenomena captivate the researcher's attention because they influence technical and industrial purposes, including conserving space and nuclear apparatuses, biomedical processes, heat transmission in tissues, pasteurisation of milk, and the magnetic direction of drugs, etc. Fourier [162] recommended a heat flux feature, heat conduction law, to portray heat transfer behaviour. However, the classical Fourier's law yields a parabolic thermal equation that supports an immediate modification in the energy transport of the deliberated scheme at the start of any procedure. The principle of causality in the continuum is therefore denied, which is visible in the transient problems in a particularly short phase of time, a shallow temperature or an extremely high heat flux. To conquer this matter, Cattaneo [163] hosted the thermal relaxation phase to construct the hyperbolic thermal energy equation, allowing heat transfer through thermal waves' transmission with finite speed. The concept of Cattaneo was again enhanced by Christov [164], who swapped the time derivative in Cattaneo's model with Oldroyd's upper-convective derivative that maintained the material-invariant construction and finally converted to the renowned Cattaneo-Christov heat flux model. The strength and exceptionality of the CCHF model clarification are evaluated by Ciarletta and Straughan [165]. The thermal moderation phase can be understood by the time phase required to gather the energy to form heat flux. In other words, it represents an evaluation of the thermal inertial of a material. This factor means the resistive environment of the changed system, instigated by the external temperature gradient applied, thus causing a thermal delay in the model structure. The thermal inertial in heat transfer affects the heat transfer in nanofluids and various spaces of ballistics and astrophysics [166, 167, 168]. There are excellent practical applications of heat transmission designed by the CCHF model, such as demonstration of skin burns injury [169, 170, 171].

The squeeze flow problem is an acute transient flow problem for channels where containment surfaces possess a transverse motion. Stefan [172] introduced this ground-breaking work and formulated the flow phenomena. So far, the exploration of the squeeze flow progression is getting extensive attention from researchers because of its purposes in chemical engineering and biomechanics. Reciprocating engine bearing performance, injection and compression mould-

ing, polymer processing, food processing, modelling of synthetics transportation inside living bodies, and modelling of lubrication systems are realistic applications of squeezing flows [173, 174, 175, 176]. Nanofluids are the new-generation heat transfer fluids with higher thermal conductivity at deficient particle concentrations than conventional fluids. They are engineered by stably suspending and uniformly dispersing a small amount of nanometer-sized (between 1 and 100 nm in diameter) ultrafine metallic, nonmetallic or ceramic particles in ordinary heat transfer fluids. Choi [25] first established the concept of nanofluid. Recent researchers have identified that substituting usual coolants with nanofluids may be advantageous in improving heat transfer efficiency in nuclear space and engineering, domestic refrigerators/freezers, and cooling of engines and micro-electronics, Wong and Leon [96]. Moreover, electromagnetic nanoparticles play an essential role in bio-medicinal applications compared to other metallic particles because these can be used to control and manipulate the nanofluid through magnetic force, Uddin *et al.* [139, 121]. As a part of these researches, Buongiorno [41] composed a mathematical scheme to describe the convective heat transfer in nanofluids, taking two crucial effects, namely the Brownian and thermophoretic diffusions, into account.

The boundary velocity, proportional to the shearing stress at the solid surface, plays a vital role in boundary value problems. The dimension of the proportionality constant, known as the slip parameter, is the length. For viscoelastic fluids, the slip condition is considerably significant [177]. This feature has many medical science applications, such as polishing artificial heart valves [178]. Several situations include polymer fluids with high-weight molecules, heavy suspensions, and lubrication problems flowing through multiple interfaces. Navier [179] initially proposed the general boundary condition, illustrating the surface's fluid slip. Moreover, magneto-hydrodynamics (MHD) is the relation between the conducting fluids and electromagnetic fields. It has plentiful applications in science, manufacturing and engineering, mainly in the design of heat exchanger devices, MHD accelerators and generators, thermal insulation systems, plasma confinement and others [180, 181].

Norwegian mathematician Sophus Lie developed a classic scheme called the Lie group trans-

formation to discover invariants and similarities of solutions [182, 183, 184, 185]. Lie group analysis provides an appropriate method to address non-linear equations. The Lie group transformation proposes a precise mathematical interpretation of perceptive thoughts of symmetry and offers beneficial techniques for the analytical resolution of non-linear ODEs. Lie group analysis is an emergent field of mathematics with many applications [186, 187, 188].

So far, few efforts have been formulated to review the heat and mass transfer through compression flow. Therefore, the current research aims to explore the flow flux of the time-dependent Maxwell viscoelastic nanofluid pressed into two parallel walls with stretched porous surfaces by integrating the CCHF theory to describe the thermal temporal relaxation factor.

## 5.2 Model Equations

The viscoelastic activities will be gathered if elastic stress is functional to the liquid. The resultant strain will be time-dependent, regarded as the relaxation phase. The constitutive equation considering unsteady stress relaxation [159] is

$$\rho \frac{d\mathbf{V}}{dt} = -\nabla p + \nabla \cdot \mathbf{S} \quad (5.1)$$

Here the extra stress tensor  $\mathbf{S}$  follows the UCM model [189] given by

$$\mathbf{S} + \lambda_S \left( \frac{d\mathbf{S}}{dt} + \mathbf{V} \cdot \nabla \mathbf{S} - \mathbf{L} \mathbf{S} - \mathbf{S} \mathbf{L}^{tr} \right) = \mu (\mathbf{L} + \mathbf{L}^{tr}) \quad (5.2)$$

Here  $\mathbf{L}^{tr} = \nabla \mathbf{V}$  is the velocity gradient, and the superscript *tr* indicates a transpose,  $L_{ij} = \partial u_i / \partial x_j$ ,  $\lambda_S > 0$  is the stress relaxation time of non-Newtonian fluids, and  $\lambda_S = 0$  provides Newtonian fluids. The CCHF model is anticipated by hosting the thermal relaxation phase in Fourier's model, also called the modified Fourier heat conduction law, offered by [175]

$$\mathbf{q} + \lambda_T \left[ \frac{\partial \mathbf{q}}{\partial t} + \mathbf{V} \cdot \nabla \mathbf{q} - \mathbf{q} \cdot \nabla V + (\nabla \cdot V) \mathbf{q} \right] = -\kappa_{nf} \nabla T \quad (5.3)$$

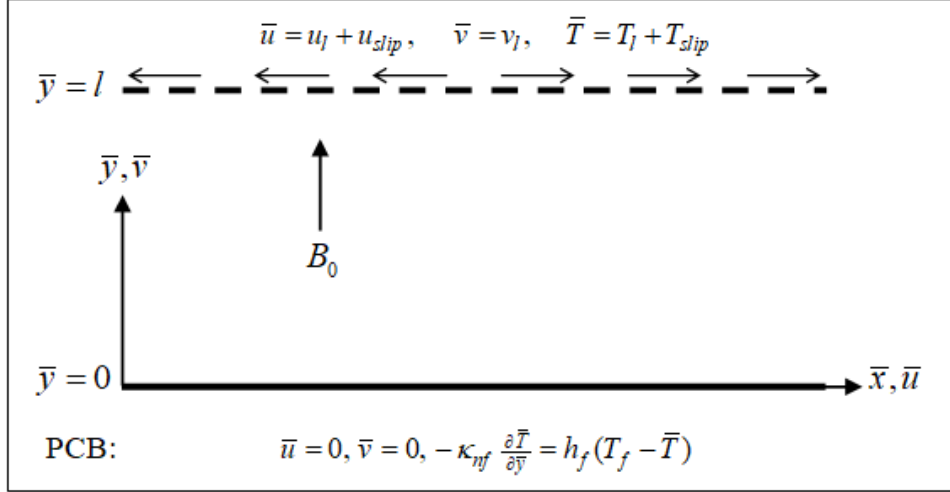


Figure 5.1: Physical model

Here  $\lambda_T = 0$  converts the expression (5.3) to conventional Fourier's law.

The liquid flow is laminar, unsteady and three-dimensional to express the physical model. An incompressible ( $\nabla \cdot V = 0$ ), electrically conducting Maxwell nanofluid is clutched between two parallel walls. The Cartesian coordinate system explains the physical configuration so that the  $x$ -axis is taken along the plate surface, and the  $y$ -axis is vertical to the plates. An identical magnetic field of strength  $B_0$  is functional along the  $y$ -direction, and the exterior electric field is assumed to be zero, as shown in Fig.5.1. Moreover, the viscous dissipation effect is preserved, and thermal resistance may also be associated with heat transfer by convection at the surface. The governing model equations consisting of conservation of mass, momentum and energy are given by

$$\frac{\partial \bar{u}}{\partial \bar{x}} + \frac{\partial \bar{v}}{\partial \bar{y}} = 0 \quad (5.4)$$

$$\begin{aligned} \frac{\partial \bar{u}}{\partial \bar{t}} + \bar{u} \frac{\partial \bar{u}}{\partial \bar{x}} + \bar{v} \frac{\partial \bar{u}}{\partial \bar{y}} + \lambda_S \left( \frac{\partial^2 \bar{u}}{\partial \bar{t}^2} + 2\bar{u} \frac{\partial^2 \bar{u}}{\partial \bar{t} \partial \bar{x}} + 2\bar{v} \frac{\partial^2 \bar{u}}{\partial \bar{t} \partial \bar{y}} + \bar{u}^2 \frac{\partial^2 \bar{u}}{\partial \bar{x}^2} + \bar{v}^2 \frac{\partial^2 \bar{u}}{\partial \bar{y}^2} \right. \\ \left. + 2\bar{u}\bar{v} \frac{\partial^2 \bar{u}}{\partial \bar{x} \partial \bar{y}} \right) = -\frac{1}{\rho_{nf}} \frac{\partial \bar{p}}{\partial \bar{x}} + \nu_{nf} \frac{\partial^2 \bar{u}}{\partial \bar{y}^2} - \frac{\sigma_{nf} B_0^2}{\rho} \left( \bar{u} + \lambda_S \left( \frac{\partial \bar{u}}{\partial \bar{t}} + \bar{v} \frac{\partial \bar{u}}{\partial \bar{y}} \right) \right) \end{aligned} \quad (5.5)$$

$$\begin{aligned}
& \frac{\partial \bar{T}}{\partial t} + \bar{u} \frac{\partial \bar{T}}{\partial \bar{x}} + \bar{v} \frac{\partial \bar{T}}{\partial \bar{y}} + \lambda_T \left( \frac{\partial^2 \bar{T}}{\partial t^2} + 2\bar{u} \frac{\partial^2 \bar{T}}{\partial t \partial \bar{x}} + 2\bar{v} \frac{\partial^2 \bar{T}}{\partial t \partial \bar{y}} + \bar{u}^2 \frac{\partial^2 \bar{T}}{\partial \bar{x}^2} + \bar{v}^2 \frac{\partial^2 \bar{T}}{\partial \bar{y}^2} \right. \\
& + 2\bar{u}\bar{v} \frac{\partial^2 \bar{T}}{\partial \bar{x} \partial \bar{y}} + \frac{\partial \bar{u}}{\partial t} \frac{\partial \bar{T}}{\partial \bar{x}} + \frac{\partial \bar{v}}{\partial t} \frac{\partial \bar{T}}{\partial \bar{y}} + \left( \bar{u} \frac{\partial \bar{u}}{\partial \bar{x}} + \bar{v} \frac{\partial \bar{u}}{\partial \bar{y}} \right) \frac{\partial \bar{T}}{\partial \bar{x}} + \left( \bar{u} \frac{\partial \bar{v}}{\partial \bar{x}} + \bar{v} \frac{\partial \bar{v}}{\partial \bar{y}} \right) \frac{\partial \bar{T}}{\partial \bar{y}} \Big) \\
& = \frac{\kappa_{nf}}{(\rho c_p)_{nf}} \frac{\partial^2 \bar{T}}{\partial \bar{y}^2} + \frac{\mu_{nf}}{(\rho c_p)_{nf}} \left( \frac{\partial \bar{u}}{\partial \bar{y}} \right)^2
\end{aligned} \tag{5.6}$$

Newton's cooling law in convection, describing the thermal resistance at the lower surface, is a restatement of the differential equation given by Fourier's law. So, assuming convective feature at the lower plate, the boundary conditions are prescribed as

$$\left. \begin{aligned}
& \bar{u} = u_l + u_{slip}, \quad \bar{v} = v_l, \quad \bar{T} = T_l + T_{slip} \quad \text{at } \bar{y} = l \\
& \bar{u} = 0, \quad \bar{v} = 0, \quad -\kappa_{nf} \frac{\partial \bar{T}}{\partial \bar{y}} = h_f (T_f - \bar{T}) \quad \text{at } \bar{y} = 0
\end{aligned} \right\} \tag{5.7}$$

Here  $\lambda_S$  is the stress relaxation time factor;  $p$  is the nanofluid pressure;  $\lambda_T$  is the thermal relaxation time factor;  $u_l = u_w \gamma/h$  is the stretching velocity;  $u_{slip} = \delta_u \frac{\partial \bar{u}}{\partial \bar{y}}$  is the slip velocity;  $v_l$  is the suction velocity;  $T_{slip} = \delta_T \frac{\partial \bar{T}}{\partial \bar{y}}$  is the thermal slip;  $T_f = T_l + (T_0 - T_l) \frac{x}{(1-t)^2}$  is the convective temperature supposed to vary along the surface and in time;  $h_f$  is the coefficient of convective heat transfer. Relations among the nanofluids' physical properties are given by

$$\begin{aligned}
\mu_{nf} &= \frac{\mu_f}{(1-\varphi)^{2.5}}, \quad \alpha_{nf} = \frac{\kappa_{nf}}{(\rho c_p)_{nf}}, \quad (\rho c_p)_{nf} = (1-\varphi)(\rho c_p)_f + \varphi(\rho c_p)_s \\
\frac{\kappa_{nf}}{\kappa_f} &= \frac{(\kappa_s + (n-1)\kappa_f) - (n-1)\varphi(\kappa_f - \kappa_s)}{(\kappa_s + (n-1)\kappa_f) + \varphi(\kappa_f - \kappa_s)}, \\
\rho_{nf} &= (1-\varphi)\rho_f + \varphi\rho_s, \quad \frac{\sigma_{nf}}{\sigma_f} = 1 + \frac{3(\sigma_s/\sigma_f - 1)\varphi}{(\sigma_s/\sigma_f + 2) - (\sigma_s/\sigma_f - 1)\varphi}
\end{aligned} \tag{5.8}$$

Here the nanoparticles volume fraction is represented by  $\varphi$ . Here  $n = 3$  is the nanoparticle spherical shape factor for thermal conductivity, defined by Maxwell [139, 81, 87]. The

thermophysical features of water and various solid nanoparticles [139] are given in Table 5.1.

Table 5.1: Thermophysical properties of water and different nanoparticles

Materials	$\rho$	$c_p$	$\kappa$	$\sigma$
Water	997.1	4179	0.613	0.05
<i>Ag</i>	10500	235	429	$6.3 \times 10^7$
<i>Cu</i>	8933	386	401	$5.96 \times 10^7$
<i>Al<sub>2</sub>O<sub>3</sub></i>	3970	765	40	$1.0 \times 10^{-10}$
<i>TiO<sub>2</sub></i>	4250	686.2	8.9538	$1.0 \times 10^{-12}$

Now to find the approximate solutions to the model, it is essential to make the model equations dimensionless using the following non-dimensional variables [174]

$$t = \frac{\bar{t}u_w}{h}, \quad x = \frac{\bar{x}}{h}, \quad y = \frac{\bar{y}}{h}, \quad u = \frac{\bar{u}}{u_w}, \quad v = \frac{\bar{v}}{u_w}, \quad p = \frac{\bar{p}}{p_0}, \quad T = \frac{\bar{T} - T_l}{T_0 - T_l} \quad (5.9)$$

Then the dimensionless PDE model is given by the following equations

$$\frac{\partial u}{\partial x} + \frac{\partial v}{\partial y} = 0 \quad (5.10)$$

$$\begin{aligned} & \frac{\partial u}{\partial t} + u \frac{\partial u}{\partial x} + v \frac{\partial u}{\partial y} + \beta_{S_x} \left( \frac{\partial^2 u}{\partial t^2} + 2u \frac{\partial^2 u}{\partial t \partial x} + 2v \frac{\partial^2 u}{\partial t \partial y} + u^2 \frac{\partial^2 u}{\partial x^2} + v^2 \frac{\partial^2 u}{\partial y^2} + 2uv \frac{\partial^2 u}{\partial x \partial y} \right) \\ & = -\frac{p_0}{u_w^2 \rho_{nf}} \frac{\partial p}{\partial x} + \frac{\nu_{nf}}{\nu_f} \frac{1}{\text{Re}} \frac{\partial^2 u}{\partial y^2} - \frac{\sigma_{nf} \rho_f}{\sigma_f \rho_{nf}} M_x \left( u + \beta_{S_x} \left( \frac{\partial u}{\partial t} + v \frac{\partial u}{\partial y} \right) \right) \end{aligned} \quad (5.11)$$



$$\begin{aligned}
& \frac{\partial T}{\partial t} + u \frac{\partial T}{\partial x} + v \frac{\partial T}{\partial y} + \beta_{T_x} \left( \frac{\partial^2 T}{\partial t^2} + 2u \frac{\partial^2 T}{\partial t \partial x} + 2v \frac{\partial^2 T}{\partial t \partial y} + u^2 \frac{\partial^2 T}{\partial x^2} \right. \\
& \left. + v^2 \frac{\partial^2 T}{\partial y^2} + 2uv \frac{\partial^2 T}{\partial x \partial y} + \frac{\partial u}{\partial t} \frac{\partial T}{\partial x} + \frac{\partial v}{\partial t} \frac{\partial T}{\partial y} + \left( u \frac{\partial u}{\partial x} + v \frac{\partial u}{\partial y} \right) \frac{\partial T}{\partial x} + \left( u \frac{\partial v}{\partial x} + v \frac{\partial v}{\partial y} \right) \frac{\partial T}{\partial y} \right) \\
& = \frac{\kappa_{nf}(\rho c_p)_f}{\kappa_f(\rho c_p)_{nf} \text{PrRe}} \frac{\partial^2 T}{\partial y^2} + \frac{\mu_{nf}(\rho c_p)_f E c_x}{\mu_f(\rho c_p)_{nf} \text{Re}} \left( \frac{\partial u}{\partial y} \right)^2 \quad (5.12)
\end{aligned}$$

Here  $\text{Re} = \frac{u_w h}{\nu_f}$  is the Reynolds number;  $\beta_{s_x} = \frac{u_w \lambda_s}{h}$  is the Maxwell parameter;  $M_x = \frac{\sigma_f B_0^2 h}{\rho_f u_w}$  is the magnetic field parameter;  $\text{Pr} = \frac{\nu_f(\rho c_p)_f}{\kappa_f}$  is the Prandtl number;  $E c_x = \frac{u_w^2}{(c_p)_f(T_w - T_i)}$  is the Eckert number.

Let  $\psi$  be the stream function. Set  $u = \frac{\partial \psi}{\partial y}$  and  $v = -\frac{\partial \psi}{\partial x}$  in the above equations to get

$$\begin{aligned}
& \frac{\partial^2 \psi}{\partial t \partial y} + \frac{\partial \psi}{\partial y} \frac{\partial^2 \psi}{\partial x \partial y} - \frac{\partial \psi}{\partial x} \frac{\partial^2 \psi}{\partial y^2} + \beta_{s_x} \left( \frac{\partial^3 \psi}{\partial t^2 \partial y} + 2 \frac{\partial \psi}{\partial y} \frac{\partial^3 \psi}{\partial t \partial x \partial y} - 2 \frac{\partial \psi}{\partial x} \frac{\partial^3 \psi}{\partial t \partial y^2} + \left( \frac{\partial \psi}{\partial y} \right)^2 \frac{\partial^3 \psi}{\partial x^2 \partial y} \right. \\
& \left. + \left( \frac{\partial \psi}{\partial x} \right)^2 \frac{\partial^3 \psi}{\partial y^3} - 2 \frac{\partial \psi}{\partial x} \frac{\partial \psi}{\partial y} \frac{\partial^3 \psi}{\partial x \partial y^2} \right) = -\frac{p_0}{u_w^2 \rho_{nf}} \frac{\partial p}{\partial x} + \frac{\nu_{nf}}{\text{Re} \nu_f} \frac{\partial^3 \psi}{\partial y^3} - \frac{\sigma_{nf} \rho_f}{\sigma_f \rho_{nf}} M_x \\
& \cdot \left( \frac{\partial \psi}{\partial y} + \beta_{s_x} \left( \frac{\partial^2 \psi}{\partial t \partial y} - \frac{\partial \psi}{\partial x} \frac{\partial^2 \psi}{\partial y^2} \right) \right) \quad (5.13)
\end{aligned}$$

$$\begin{aligned}
& \frac{\partial T}{\partial t} + \frac{\partial \psi}{\partial y} \frac{\partial T}{\partial x} - \frac{\partial \psi}{\partial x} \frac{\partial T}{\partial y} + \beta_{T_x} \left( \frac{\partial^2 T}{\partial t^2} + 2 \frac{\partial \psi}{\partial y} \frac{\partial^2 T}{\partial t \partial x} - 2 \frac{\partial \psi}{\partial x} \frac{\partial^2 T}{\partial t \partial y} \right. \\
& \left. + \left( \frac{\partial \psi}{\partial y} \right)^2 \frac{\partial^2 T}{\partial x^2} + \left( \frac{\partial \psi}{\partial x} \right)^2 \frac{\partial^2 T}{\partial y^2} - 2 \frac{\partial \psi}{\partial y} \frac{\partial \psi}{\partial x} \frac{\partial^2 T}{\partial x \partial y} + \frac{\partial^2 \psi}{\partial t \partial y} \frac{\partial T}{\partial x} + \left( \frac{\partial \psi}{\partial y} \frac{\partial^2 \psi}{\partial x \partial y} - \frac{\partial \psi}{\partial x} \frac{\partial^2 \psi}{\partial y^2} \right) \frac{\partial T}{\partial x} \right. \\
& \left. - \frac{\partial^2 \psi}{\partial t \partial x} \frac{\partial T}{\partial y} + \left( \frac{\partial \psi}{\partial x} \frac{\partial^2 \psi}{\partial x \partial y} - \frac{\partial \psi}{\partial y} \frac{\partial^2 \psi}{\partial x^2} \right) \frac{\partial T}{\partial y} \right) = C_1 \frac{\partial^2 T}{\partial y^2} + C_2 \left( \frac{\partial^2 \psi}{\partial y^2} \right)^2 \quad (5.14)
\end{aligned}$$

Here  $C_1 = \frac{\kappa_{nf}(\rho c_p)_f}{\kappa_f(\rho c_p)_{nf} \text{PrRe}}$  and  $C_2 = \frac{\mu_{nf}(\rho c_p)_f E c_x}{\mu_f(\rho c_p)_{nf} \text{Re}}$ .

Dimensionless prescribed surface temperature (PST) boundary conditions are given by

$$\left. \begin{aligned}
& \text{at } y = \frac{l}{h} : \\
& \frac{\partial \psi}{\partial y} = \gamma_h + \varepsilon_{u_h} \frac{\partial^2 \psi}{\partial y^2}, \quad \frac{\partial \psi}{\partial x} = -fw_h, \quad T = \varepsilon_{T_h} \frac{\partial T}{\partial y} \\
& \text{at } y = 0 : \\
& \frac{\partial \psi}{\partial y} = 0, \quad \frac{\partial \psi}{\partial x} = 0, \quad \frac{\partial T}{\partial y} = -\frac{\kappa_f}{\kappa_{nf}} Bi_h \left( \frac{x}{(1-t)^2} - T \right)
\end{aligned} \right\} \quad (5.15)$$

Here  $\gamma_h$  is the stretching parameter;  $fw_h$  is the suction parameter;  $\varepsilon_{u_h} = \frac{\delta_u}{h}$  is the momentum slip parameter;  $\varepsilon_{T_h} = \frac{\delta_T}{h}$  is the thermal slip parameter;  $Bi_h = \frac{h_f h}{\kappa_f}$  is the Biot numbers for convective heat transfer.

### 5.3 Method of Transformations

The significance of similarity solutions in many areas of research is limitless. Looking for a universal symmetric approach that can be useful to specific mathematical models is obligatory. The Lie group analysis transformation procedure is a sound technique for the theory of the continuous symmetry of numerical structures, which is immensely functional for various fields of contemporary modern mathematical physics. This analysis is anticipated to deliver a new methodology for studying the continuous symmetries of model equations governing the heat transfer fluxes in Maxwell nanofluids. In the process, this theory trims down the number of independent parameters of the governing PDEs considered for the physical model and maintains the invariant structure of the model with the corresponding initial and boundary conditions. Due to the unsteady flow ( $0 < t < 1$ ) of fluid in a channel, the following two parameters linear groups of transformations are to consider for the Lie group analysis [188]:

$$\begin{aligned}
\Gamma : \hat{t} &= (1-t)e^{\alpha_1}, \hat{x} = xe^{\beta_1}, \hat{\psi} = \psi e^{\alpha_2} e^{\beta_2}, \hat{y} = ye^{\alpha_3} e^{\beta_3}, \hat{T} = Te^{\alpha_4} e^{\beta_4}, \hat{p} = pe^{\alpha_5} e^{\beta_5}, \\
\hat{M}_x &= M_x e^{\alpha_6} e^{\beta_6}, \hat{\beta}_{S_x} = \beta_{S_x} e^{\alpha_7} e^{\beta_7}, \hat{E}c = Ec_x e^{\alpha_8} e^{\beta_8}, \hat{\beta}_{T_x} = \beta_{T_x} e^{\alpha_9} e^{\beta_9}, \\
\hat{l} &= le^{\alpha_{10}} e^{\beta_{10}}, \hat{\gamma}_h = \gamma_h e^{\alpha_{11}} e^{\beta_{11}}, \hat{f}_{w_h} = f_{w_h} e^{\alpha_{12}} e^{\beta_{12}}, \hat{\varepsilon}_{u_h} = \varepsilon_{u_h} e^{\alpha_{13}} e^{\beta_{13}} \\
\hat{\varepsilon}_{T_h} &= \varepsilon_{T_h} e^{\alpha_{14}} e^{\beta_{14}}, \hat{B}i_h = Bi_h e^{\alpha_{15}} e^{\beta_{15}}
\end{aligned} \tag{5.16}$$

Here  $\alpha_i, \beta_i$  ( $i = 1, 2, \dots, 15$ ) are constants. We seek the values of  $\alpha_i, \beta_i$  such that the forms of Eqns. (5.2) – (5.15) are invariant under the transformations connected by the following relations

$$\begin{aligned}
\alpha_2 &= -\frac{1}{2}\alpha_1, \alpha_3 = \frac{1}{2}\alpha_1, \alpha_4 = -2\alpha_1, \alpha_5 = -2\alpha_1, \alpha_6 = -\alpha_1, \alpha_7 = \alpha_1, \alpha_8 = 0 \\
\alpha_9 &= \alpha_1, \alpha_{10} = \frac{1}{2}\alpha_1, \alpha_{11} = -\alpha_1, \alpha_{12} = -\frac{1}{2}\alpha_1, \alpha_{13} = \frac{1}{2}\alpha_1, \alpha_{14} = \frac{1}{2}\alpha_1, \alpha_{15} = -\frac{1}{2}\alpha_1, \\
\beta_2 &= \beta_1, \beta_3 = 0, \beta_4 = \beta_1, \beta_5 = \beta_1, \beta_6 = 0, \beta_7 = 0, \beta_8 = -\beta_1, \beta_9 = 0, \\
\beta_{10} &= 0, \beta_{11} = \beta_1, \beta_{12} = 0, \beta_{13} = 0, \beta_{14} = 0, \beta_{15} = 0
\end{aligned} \tag{5.17}$$

With these relationships of  $\alpha_i$  and  $\beta_i$ , Eqn. (5.3) turns into

$$\begin{aligned}
\Gamma : \hat{t} &= (1-t)e^{\alpha_1}, \hat{x} = xe^{\beta_1}, \hat{\psi} = \psi e^{-\frac{1}{2}\alpha_1} e^{\beta_1}, \hat{y} = ye^{\frac{1}{2}\alpha_1}, \hat{T} = Te^{-2\alpha_1} e^{\beta_1}, \hat{p} = pe^{-2\alpha_1} e^{2\beta_1}, \\
\hat{M}_x &= M_x e^{-\alpha_1} e^0, \hat{\beta}_{S_x} = \beta_{S_x} e^{\alpha_1} e^0, \hat{E}c = Ec_x e^0 e^{-\beta_1}, \hat{\beta}_{T_x} = \beta_{T_x} e^{\alpha_1} e^0, \\
\hat{l} &= le^{\frac{1}{2}\alpha_1} e^0, \hat{\gamma}_h = \gamma_h e^{-\alpha_1} e^{\beta_1}, \hat{f}_{w_h} = f_{w_h} e^{-\frac{1}{2}\alpha_1} e^0, \hat{\varepsilon}_{u_h} = \varepsilon_{u_h} e^{\frac{1}{2}\alpha_1} e^0, \\
\hat{\varepsilon}_{T_h} &= \varepsilon_{T_h} e^{\frac{1}{2}\alpha_1} e^0, \hat{B}i_h = Bi_h e^{-\frac{1}{2}\alpha_1} e^0
\end{aligned} \tag{5.18}$$

From the absolute invariants, the similarity parameters are described as

$$\begin{aligned}
\eta &= (1-t)^{-\frac{1}{2}}y, \quad \psi = (1-t)^{-\frac{1}{2}}xf(\eta), \quad T = (1-t)^{-2}x\theta(\eta), \quad p = (1-t)^{-2}x^2p_\eta, \\
M_x &= (1-t)^{-1}M, \quad \beta_{S_x} = (1-t)\beta_S, \quad Ec_x = (x)^{-1}Ec, \quad \beta_{T_x} = (1-t)\beta_T, \\
l &= \sqrt{1-t}h, \quad \gamma_h = (1-t)^{-1}x\gamma, \quad f_{w_h} = (1-t)^{-\frac{1}{2}}f_w, \quad \varepsilon_{u_h} = \sqrt{1-t}\varepsilon_u, \\
\varepsilon_{T_h} &= \sqrt{1-t}\varepsilon_T, \quad Bi_h = (1-t)^{-\frac{1}{2}}Bi
\end{aligned} \tag{5.19}$$

Using the above similarity transformations into Eqns. (5.2)–(5.15), we obtain the following similarity equations,

$$\begin{aligned}
&\left( \frac{\nu_{nf}}{\nu_f \text{Re}} - \frac{\beta_S}{4}(\eta^2 - 4\eta f + 4f^2) \right) f^{iv} - \frac{1}{2}(\eta f''' + 3f'' + 2f'f'' - 2ff''') \\
&- \frac{\beta_S}{4} \left( 9\eta f''' + 4\eta f''^2 - 16ff''' + 8f'f'' - 8ff''^2 - 8f'^2f'' + 15f'' \right) - \frac{\sigma_{nf}\rho_f}{\sigma_f\rho_{nf}}M \\
&\quad \times \left( f'' + \frac{\beta_S}{2}(\eta f''' + 3f'' - 2ff''' - 2f'f'') \right) = 0
\end{aligned} \tag{5.20}$$

$$\begin{aligned}
&\left( \frac{\kappa_{nf}(\rho c_p)_f}{\kappa_f(\rho c_p)_{nf}\text{Re Pr}} - \frac{\beta_T}{4}(\eta^2 - 4\eta f + 4f^2) \right) \theta'' - \left( \frac{\eta}{2}\theta' + 2\theta + f'\theta - f\theta' \right) + \frac{\mu_{nf}(\rho c_p)_f Ec}{\mu_f(\rho c_p)_{nf}\text{Re}} f''^2 \\
&- \frac{\beta_T}{4} (2\eta f'\theta' + 2\eta f''\theta + 9\eta\theta' + 20f'\theta - 22f\theta' + 4f'^2\theta - 4ff'\theta' - 4ff''\theta + 24\theta) = 0
\end{aligned} \tag{5.21}$$

Following a similar procedure, the PCB boundary conditions take the form

$$\left. \begin{aligned}
f' &= \gamma + \varepsilon_u f'', \quad f = f_w, \quad \theta = \varepsilon_T \theta' \quad \text{at } \eta = 1 \\
f' &= 0, \quad f = 0, \quad \theta' = -\frac{\kappa_f}{\kappa_{nf}} Bi(1-\theta) \quad \text{at } \eta = 0
\end{aligned} \right\} \tag{5.22}$$

Finally, the physical attentions in the existing study are the skin friction coefficient  $C_f$  and the local Nusselt number  $Nu$  defined as

$$C_f \propto \frac{\mu_{nf}}{\mu_f} f'' \quad \text{and} \quad Nu \propto -\frac{\kappa_{nf}}{\kappa_f} \theta' \quad (5.23)$$

#### 5.4 Numerical Method

Equations (5.3)–(5.3) (7.20)–(7.21) combined with the boundary conditions (5.22) are solved numerically using the collocation method. The analysis is prepared for various influences like nanoparticle volume fraction parameter  $\varphi$ , Maxwell parameter  $\beta_S$ , magnetic field parameter  $M$ , Prandtl number  $Pr$ , Eckert number  $Ec$ , thermal relaxation parameter  $\beta_T$ , stretching parameter  $\gamma$ , suction parameter  $f_w$ , velocity slip parameter  $\varepsilon_u$  and thermal slip parameter  $\varepsilon_T$ . The mesh size is  $\eta = 0.01$ , and the tolerance factor is  $10^{-6}$ . Based on the present model, we are considering  $[0, 1]$  as the domain of the channel problem. First, an assessment of the current analysis is arranged with Raza *et al.* [190], shown in Table 5.2, when  $Pr = 6.2$ ,  $M = 0.5$ ,  $Re = 4$ ,  $f_w = 1$ ,  $\varepsilon_u = 0.1$ ,  $\varepsilon_T = 0.1$ , and all others are zero.

Table 5.2: Comparison of local Nusselt number for several values of  $\varphi$

	Raza <i>et al.</i> [190]	Present work
$\varphi$	$\theta'(0)$	$\theta'(0)$
0.01	-4.964682800390394	-4.965132
0.03	-4.795613667915525	-4.796557
0.05	-4.629249877087038	-4.629878

#### 5.5 Results and Discussion

The renovation of the model equations trims down the mathematical work extensively. Graphical representations of consequences are very constructive in discussing the physical features offered

by the solutions.

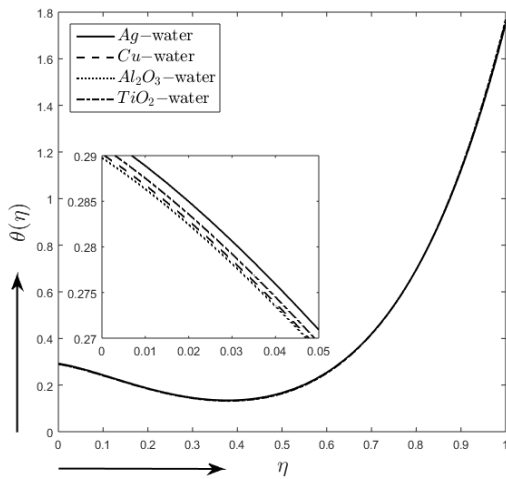


Figure 5.2: Temperature profiles for different water-based nanofluids

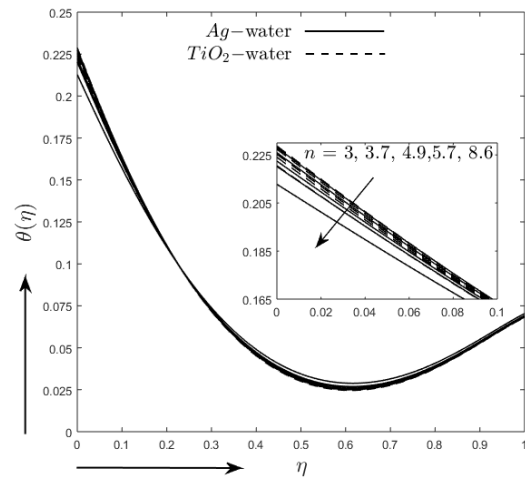


Figure 5.3: Temperature profiles for nanoparticle shape factor  $n$

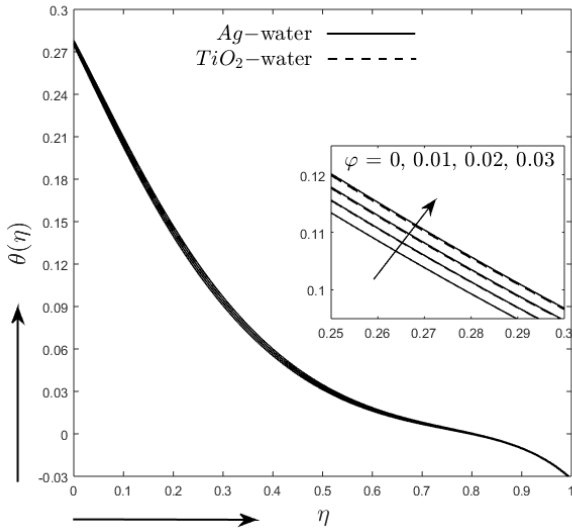


Figure 5.4: Temperature profiles for nanoparticle volume fraction  $\varphi$

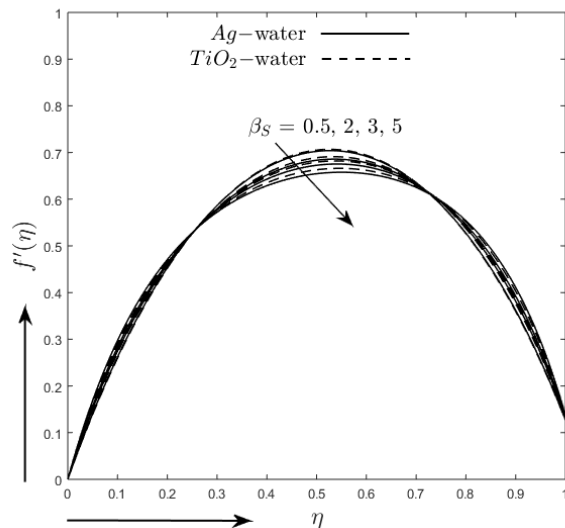


Figure 5.5: Velocity profile for Maxwell number  $\beta_S$

First, the energy distribution analysis is prepared for water-based viscoelastic nanofluid hosting  $Ag$  and  $TiO_2$  solid nanoparticles, separately, flowing in a parallel plate incorporating the

CCHF model, portrayed in Fig. 5.2. The temperature distribution profile is higher for *Ag*-water compares other water-based nanofluids. Figure 5.3 displays the thermal distributions, taking different shape factors of solid nanoparticles, for 4% *Ag*-water (solid line) and *TiO<sub>2</sub>*-water (dashed line) nanofluids, respectively. The impacts of solid nanoparticles of spherical shape ( $n = 3$ ) [87] are prominent for *Ag*-water (solid line) and *TiO<sub>2</sub>*-water (dashed line) nanofluids near the lower surface. But away from the lower surface after  $\eta = 0.23$  these profiles reverse the trend for both nanofluids. The nanoparticle volume fraction effect on *Ag*-water (solid line) and *TiO<sub>2</sub>*-water (dashed line) nanofluids are represented in Fig. 5.4 for a range of volume fractions from 0% to 3%. The temperature profile rises with the increasing  $\varphi$ . It is a vital phenomenon that the nanoparticle volume fraction improves the thermal transport in the traditional fluid.

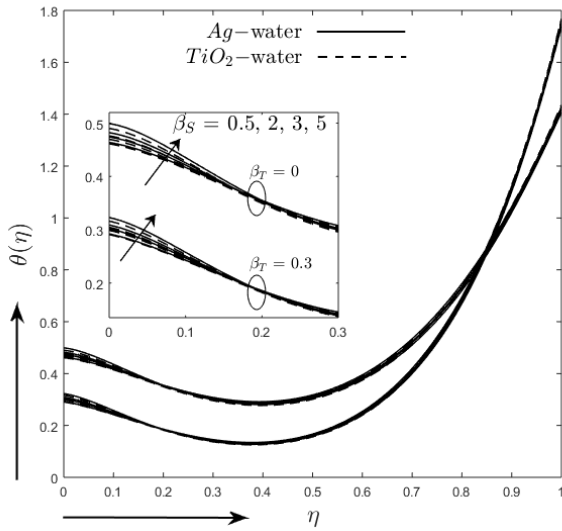


Figure 5.6: Temperature profile for Maxwell number  $\beta_S$

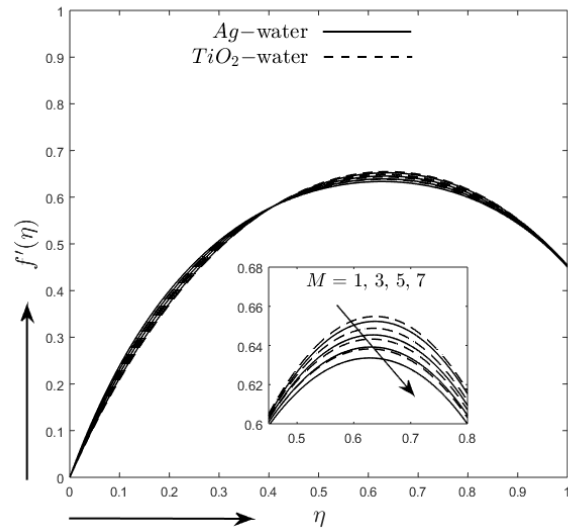


Figure 5.7: Velocity profile for magnetic field parameter  $M$

When the elastic stress is functional in a liquid, the time during which it achieves stability is the relaxation phase, which is more significant for highly viscous fluids. The Maxwell number/ Deborah number ( $\beta_S$ ) trades with the fluid relaxation phase to its characteristic time scale. Here  $\beta_S = 0$  gives the result for a Newtonian viscous incompressible fluid. The fluid with a trivial

Deborah number exhibits liquid-like activities, but a large Deborah number communicates with solid-like materials able to conduct and retain heat better. Therefore, it is found that progressively increasing the Maxwell parameter raises the fluid viscosity, which improves resistance to flow. Consequently, the hydrodynamic boundary layer thickness for Maxwell fluid declines, as shown in Fig. 5.5, for both 4% *Ag*-water (solid line) and *TiO<sub>2</sub>*-water (dashed line) nanofluids. Additionally, it is realised that the momentum contour of *Ag*-water (solid line) is more controlled than that of *TiO<sub>2</sub>*-water (dashed line) nanofluid.

Figure 5.6 shows the enhanced consequence of  $\beta_S$  on the thermal boundary layer near the convective lower wall mutually for conventional Fourier heat flux ( $\beta_T = 0$ ) and  $\beta_T = 0.3$ . A different fact is seen at  $\eta = 0.19$  where there is no parametric effect due to the variation of  $\beta_S$  on the energy profile, and after  $\eta = 0.19$  the temperature profiles decrease. From this probe, it is established that the elastic force endorses the energy transfer in Maxwell fluid.

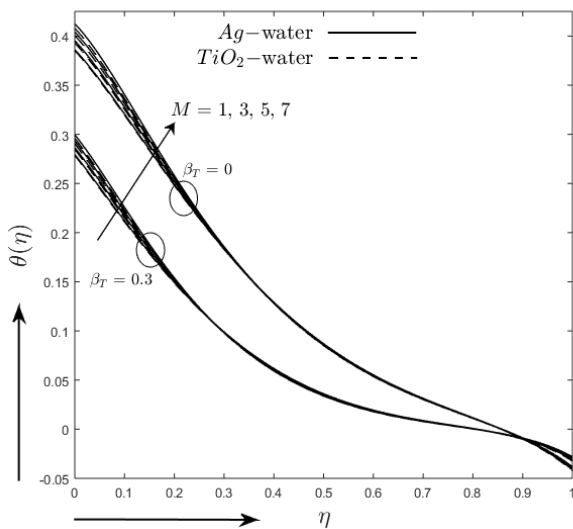


Figure 5.8: Temperature profile for magnetic field parameter  $M$

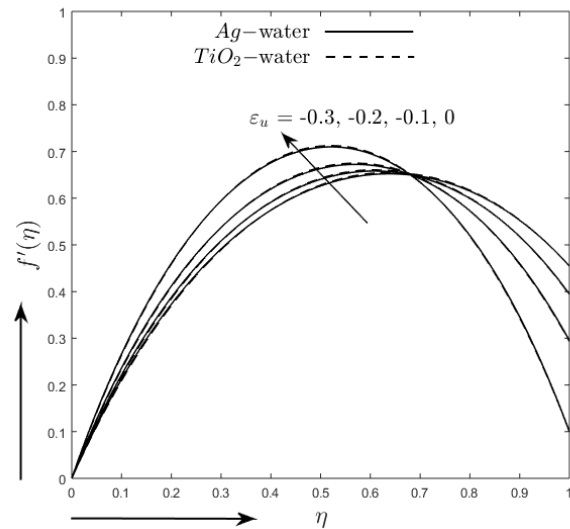


Figure 5.9: Velocity profile for momentum slip parameter  $\epsilon_u$

It is detected in Fig. 5.7 that an acceleration in the magnetic parameter ( $M$ ) diminishes the momentum distribution profile. This reduction is introduced by the magnetic field effect



imposed on an electrically conductive fluid, which generates a drag force termed Lorentz force against the flow route along the wall to slow down velocity. The consequential fact is that the magnetic field is accountable for reducing velocity. Figure 5.8 depicts that the thermal contours are affected proportionally by the increase of  $M$  for classical Fourier heat flux ( $\beta_T = 0$ ) and CCHF ( $\beta_T = 0.3$ ).

The outcome of Fig. 5.9 expresses that the momentum increases with the mounting rate of the slip parameter  $\varepsilon_u$  in the opposite track to the flow. In Fig. 5.10, it is established that the temperature increases with the higher slip parameter  $\varepsilon_u$  for both classical Fourier heat flux ( $\beta_T = 0$ ) and CCHF ( $\beta_T = 0.3$ ).

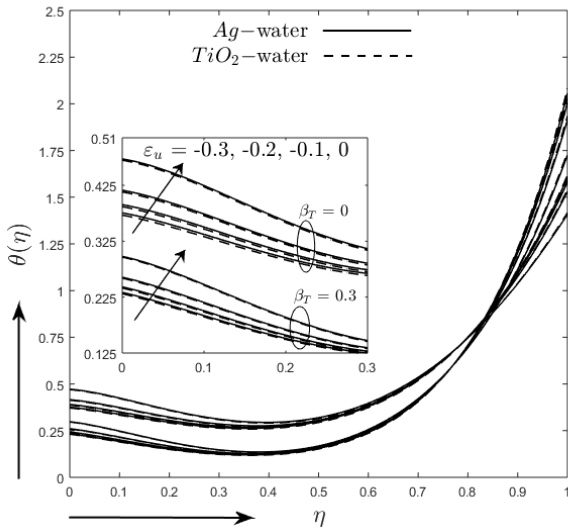


Figure 5.10: Temperature profile for momentum slip parameter  $\varepsilon_u$

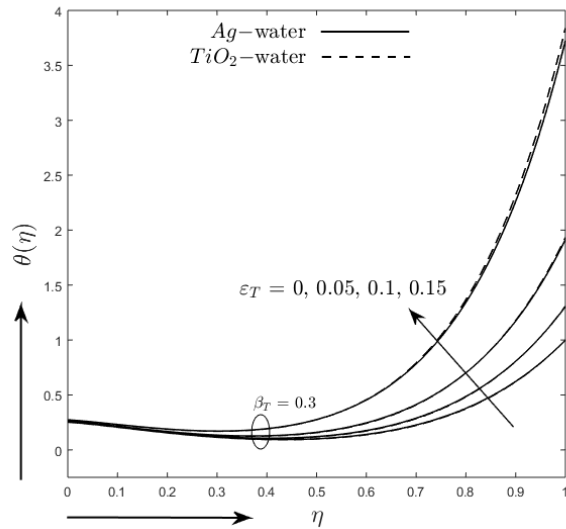


Figure 5.11: Temperature profile for thermal slip parameter  $\varepsilon_T$

The consequence of Fig. 5.11 expresses that the thermal energy increases with the escalating rate of the thermal slip parameter  $\varepsilon_T$  for CCHF ( $\beta_T = 0.3$ ). The convective parameter as Biot number comes up only in the lower surface boundary condition (5.22) [ $\theta'(0) = -\frac{\kappa_f}{\kappa_n f} Bi(1 - \theta(0))$ ]. When  $Bi = 0$ , an insulated boundary condition is attained at the surface. It is motivating to remind that if  $Bi$  is higher, the thermal energy profiles are improved, as seen in Fig. 5.12. The

uniform temperature boundary condition is achieved. Convective boundary condition arises in some factual situations, such as the nanofluid flow around the micro-electromechanical system (MEMS) [191].

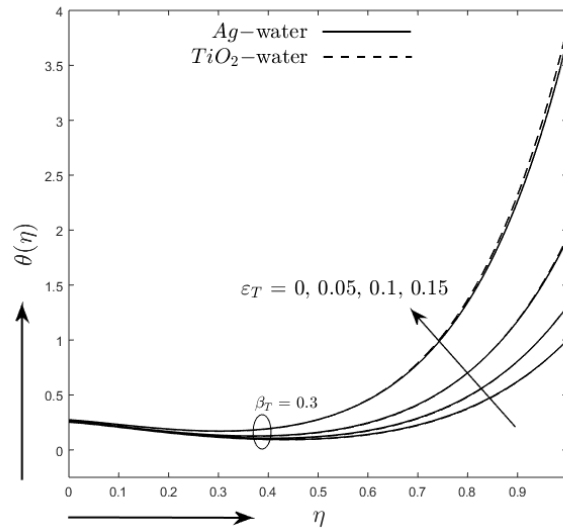


Figure 5.12: Temperature profile for Biot number  $Bi$

**Parametric effects on Nusselt number at the boundaries:** Nusselt numbers ( $Nu$ ) for some different values of Maxwell number ( $\beta_S$ ) and thermal relaxation parameter ( $\beta_T$ ) considering  $\varphi = 4\%$ ;  $n = 3$ ;  $M = 1$ ;  $Re = 1$ ;  $Ec = 0.1$ ;  $f_w = 0.5$ ;  $\gamma = 0.1$ ;  $\varepsilon_u = -0.1$ ;  $\varepsilon_T = 0.3$ ;  $Bi = 1$  are displayed in Table 5.3 for  $Ag$ -water and 5.4 for  $TiO_2$ -water nanofluids, respectively..

Table 5.3: Heat transfer ( $Nu$ ) in  $Ag$ -water nanofluid for different values of  $\beta_S$  and  $\beta_T$

$\beta_S$	$\beta_T$	$\eta = 0$	$\eta = 1$
0.1	0.3	0.686497	-0.136659
0.3		0.686001	-0.136231
0.5		0.685488	-0.135799
0.7		0.684961	-0.135364
0.1	0.2	0.668544	-0.16676
	0.1	0.644361	-0.218067
	0	0.608476	-0.323434

Table 5.4: Heat transfer ( $Nu$ ) in  $TiO_2$ -water nanofluid for different values of  $\beta_S$  and  $\beta_T$

$\beta_S$	$\beta_T$	$\eta = 0$	$\eta = 1$
0.1	0.3	0.700083	-0.136228
0.3		0.699665	-0.135883
0.5		0.699234	-0.135534
0.7		0.698793	-0.135182
0.1	0.2	0.681731	-0.16589
	0.1	0.657041	-0.216224
	0	0.620503	-0.318984

From these tabular data, an assessment of the CCHF model ( $\beta_T \neq 0$ ) and Fourier's model ( $\beta_T = 0$ ) is presented graphically in Figure 5.13 for the lower plate and Figure 5.14 for the upper plate, respectively. The impact of the thermal relaxation parameter ( $\beta_T$ ) on the Nusselt number at the edges are calculated for water-based nanofluid hosting silver and Titania solid nanoparticles,

as revealed in Figures 5.13 and 5.14. Here *Ag*-water and *TiO<sub>2</sub>*-water nanofluids are indicated by the solid line and dashed line, respectively. The Nusselt number correlates with the energy transmission rate at the boundary. The energy transmission rates of both nanofluids at the lower convective surface ( $\eta = 0$ ) are upward with the enlarged  $\beta_T$ . An outstanding assessment of the CCHF model ( $\beta_T \neq 0$ ) and Fourier's model ( $\beta_T = 0$ ), a noteworthy feature of recent research, is also portrayed in the above diagrams.

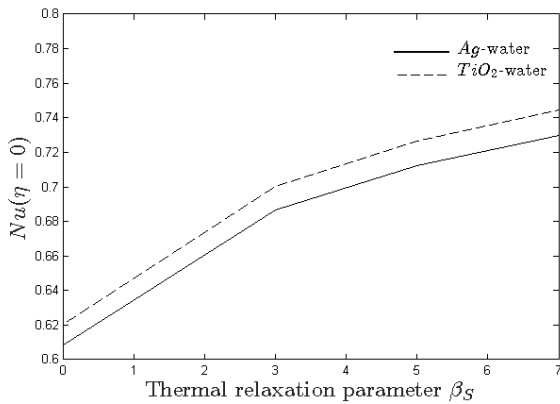


Figure 5.13: Nusselt number at  $\eta = 0$  for thermal relaxation parameter ( $\beta_T$ )

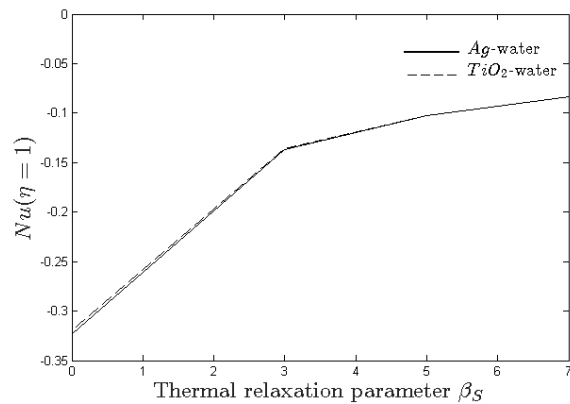


Figure 5.14: Nusselt number at  $\eta = 1$  for thermal relaxation parameter ( $\beta_T$ )

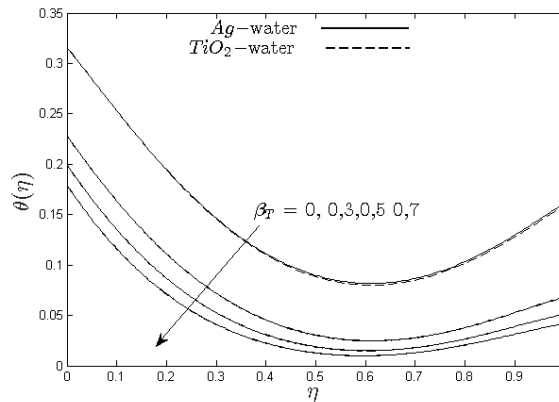


Figure 5.15: Temperature profile for thermal relaxation parameter ( $\beta_T$ )

The higher  $\beta_T$  parameter creates a resistive environment of the changed system, as shown in Figure 5.15, thus causing a thermal delay through a higher energy transmission rate. Therefore,

silver-water nanofluid can play an essential role in developing the mechanical systems of various spaces of ballistics and astrophysics.

## **5.6 Conclusions**

The recent analysis illustrates the flow feature of time-dependent Maxwell viscoelastic water-based nanofluids squeezed in parallel surfaces with the stretched upper surface. All the precise results are deliberated from the physical perspective, and the major findings of the research can be listed as follows:

1. Silver–water nanofluid provides comparatively higher energy transport.
2. The higher nanoparticle volume concentration enhances the energy transport.
3. The consequence of spherical-shaped solid nanoparticles with thermal slip is outstanding for thermal energy transfer.
4. Maxwell viscoelasticity parameter improves heat transfer.
5. CCHF delays energy transmission.
6. The combined influence of Maxwell viscoelasticity and Magnetic strength parameters with the velocity slip feature shows noteworthy control on the velocity profiles.

In conclusion, it can be affirmed that this model presenting phenomena of velocity control and enhancement of the transfer of heat in the Ag-water nanofluid can be an excellent opportunity to extend the mechanical systems' cooling performances.

## CHAPTER 6

### EFFECT OF BROWNIAN DIFFUSION ON SQUEEZING ELASTICO-VISCOUS NANOFUID FLOW WITH CATTANEO-CHRISTOV HEAT FLUX MODEL IN A CHANNEL WITH DOUBLE SLIP EFFECT

**Abstract.** The present study deals with the analysis of heat transfer of the unsteady Maxwell nanofluid flow in a squeezed rotating channel of a porous extensible surface subject to the velocity and thermal slip effects incorporating the theory of heat flow intensity of Cattaneo-Christov model for the expression of the energy distribution in preference to the classical Fourier's law. A set of transformations is occupied to renovate the current model in a system of nonlinear ordinary differential equations that are numerically decoded with the help of MATLAB integrated function *bvp4c*. The effects of various flow control parameters are investigated for the momentum, temperature and diffusion profiles, as well as for the wall shearing stress and the heat and mass transfer. The results are finally described from the material point of view. A comparison of heat flux models of Cattaneo-Christov and Fourier is also performed. An important result from the present work is that the squeezing parameter is strong enough in the middle of the channel to retard the fluid flow.

**Keywords:** Maxwell fluid model; squeezing flow; elastico-viscous; nanofluid; channel; rotation.

#### 6.1 Introduction

The heat transfer phenomena is of great concern because of its impact on industrial applications, including cooling of space and nuclear reactors, heat conduction in tissues pasteurization of milk, magnetic targeting of drugs, etc. Fourier [162] proposed a heat flux model, named as heat conduction law that produces a parabolic energy equation that advocates an instantaneous change in the temperature of considered system at the beginning of any process. Cattaneo

[163] introduced thermal relaxation time so as to produce the hyperbolic energy equation which permitted the heat transport through the transmission of thermal waves with finite speed. The theory of Cattaneo was further improved by Christov [164] who replaced the time derivative in the Cattaneo's model by the Oldroyd's upper-convective derivative [192] that preserved the material-invariant formulation and that became prominent as Cattaneo-Christov heat flux. Ciavarella and Straughan [165] analyzed the stability and uniqueness of the solution of the energy equation for Cattaneo-Christov heat flux model. Thermal relaxation time can be interpreted physically as the time needed for accumulating the thermal energy essential for generating heat flux [167, 168]. Inclusion of the thermal inertia in heat propagation has effects in the heat transport in nano-material, nanofluids and many areas of ballistics and astrophysics [169, 170, 171].

The practice of adding polymers to mineral oils, known as multi-grade oils, has become recognized since the middle of 1990s [146, 52, 50]. These additions force the resulting lubricants to become non-Newtonian and viscoelastic exerting shear-rate dependent viscosity [148, 149]. The highly non-linear relationship between shear stress and strain rate of non-Newtonian fluids cannot be demonstrated by the classical Newtonian fluid model enclosing Navier-Stokes equations [150, 151]. The non-Newtonian fluids include polymer solutions, certain lubricants and oils, suspension and colloidal solutions, blood, melts, condensed milk, emulsions, soaps, shampoos, tomato paste, and many others containing the properties of both elasticity and viscosity. Researchers have proposed several viscoelastic fluid models incorporating different features of non-Newtonian fluids [55, 153, 154]. Models of viscoelastic fluids, including second-order fluids and / or Walter-B fluids, are ideal for slow motion of low elastic fluids [155]. To carry out an effective theoretical work in the industrial sector, the most realistic and practical viscoelastic fluid models, such as the Maxwell fluid or the Oldroyd-B fluid, should be considerable for efficient analysis [156, 193]. The Maxwell fluid, a simple class of rate-type viscoelastic material, eliminates the complex effects of shear-reliant viscosity and accordingly permits one to highlight the influence of fluids elasticity on the characteristics of its boundary layer [159]. Harris [49] first developed the constitutive equation of upper convected Maxwell (UCM) fluid to model

the lubricant behavior of the non-Newtonian fluid. Due to the rising practical applications in industrial and manufacturing procedures, researchers have paid their attention to the study of boundary layer flow of non-Newtonian fluids [161, 160].

Nanofluids are the new-generation heat transfer fluids which containing higher thermal conductivity at very low particle concentrations than the conventional fluids. This idea of nanofluid was first developed by Choi [25]. Recent researchers have identified that the substitution of usual coolants with nanofluids may be advantageous in processes like improving heat transfer efficiency in nuclear space and engineering, domestic refrigerators/freezers; and cooling of engine and micro-electronics [96]. Moreover, electromagnetic nanoparticles are playing important role in bio-medicinal applications as compared to other metallic particles because these can be used to control and manipulate the nanofluid through magnetic force[139, 121]. As a part of these researches, Buongiorno [41] composed a mathematical model to study the convective heat transfer in nanofluids taking two important effects, namely the Brownian and thermophoresis diffusions into account.

While Stefan [172] carried out this pioneering work and basic formulations on flow phenomena, so far the analysis of the compression flow process is receiving considerable attention by the researchers because of its purposes in the fields of biomechanics and chemical engineering [173]. Reciprocating engine bearing performance, injection and compression molding, polymer processing, and modeling of lubrication system are realistic applications of squeezing flows [174, 175].

The boundary velocity, proportional to the shearing stress at the solid surface, is playing an important role in boundary value problems. For viscoelastic fluids, the slip condition is considerably important [177]. This feature has many applications in medical science, for example, polishing artificial heart valves [178]. There are several situations that include polymer fluids with high weight molecules, heavy suspensions, and lubrication problems flowing through multiple interfaces. Navier [179] initially proposed the general boundary condition which illustrates the fluid slip at the surface.



So far, few attempts have been made to study the transfer of heat and mass through a three-dimensional compression flow in a rotating channel, and therefore, the objective of the current work is to analyze the effect of thermal relaxation factor on the flow flux of time dependent Maxwell viscoelastic nanofluid that is squeezed in rotating parallel plates with porous stretched surface incorporating Cattaneo-Christov heat flux model.

## 6.2 Mathematical Model

The governing model equations consisting of conservation of mass, momentum, energy and concentration are given by

$$\frac{\partial \rho}{\partial t} + \nabla \cdot (\rho \mathbf{V}) = 0 \quad (6.1)$$

$$\rho \frac{d\mathbf{V}}{dt} = \nabla \cdot \boldsymbol{\tau} \quad (6.2)$$

$$\rho c_p \frac{dT}{dt} = -\nabla \cdot \mathbf{q} - p \nabla \cdot \mathbf{V} - c_p \mathbf{J}_s \cdot \nabla T + \Phi + S_Q \quad (6.3)$$

$$\frac{dC}{dt} = -\frac{1}{\rho} \nabla \cdot \mathbf{J}_s \quad (6.4)$$

Here,  $\mathbf{V} = (u, v, w)$  is the three-dimensional velocity of the viscous fluid,  $\boldsymbol{\tau}$  is the Cauchy stress tensor,  $T$  is the temperature of the fluid,  $\mathbf{q}$  is the heat flux,  $\Phi$  is the viscous dissipation term that describes the conversion of mechanical energy to heat. Also,  $S_Q$  represents the heat sources,  $\mathbf{J}_s$  is the sum of Brownian and thermophoresis diffusions,  $\rho$  and  $c_p$  are the density and specific heat respectively.

The elasto-viscous behavior of fluid will be realized if elastic stress is applied to the fluid, and the resulting strain will be time dependent characterized by relaxation time. The constitutive

equation considering time dependent stress relaxation is [173]

$$\tau = -pI + \mathbf{S} \quad (6.5)$$

The extra stress tensor  $\mathbf{S}$  satisfies the upper convected Maxwell model given by

$$\mathbf{S} + \lambda_S \left( \frac{d\mathbf{S}}{dt} + \mathbf{V} \cdot \nabla \mathbf{S} - \mathbf{L}\mathbf{S} - \mathbf{S}\mathbf{L}^{\text{tr}} \right) = \mu (\mathbf{L} + \mathbf{L}^{\text{tr}}) \quad (6.6)$$

Here,  $\mathbf{L}^{\text{tr}} = \nabla \mathbf{V}$  (*i.e.*,  $L_{ij} = \partial u_i / \partial x_j$ ) is the velocity gradient and the superscript tr indicates a transpose,  $\mu$  is the viscosity,  $\lambda_S > 0$  is the stress relaxation time where  $\lambda_S = 0$  describes the Newtonian fluids.

Cattaneo–Christov model is proposed by adding thermal relaxation time in Fourier’s Law, also called the modified Fourier heat conduction law, presented by [168]

$$\mathbf{q} + \lambda_T \left( \frac{\partial \mathbf{q}}{\partial t} + \mathbf{V} \cdot \nabla \mathbf{q} - \mathbf{q} \cdot \nabla \mathbf{V} + (\nabla \cdot \mathbf{V})\mathbf{q} \right) = -\kappa \nabla \mathbf{T} \quad (6.7)$$

Here,  $\kappa$  is the thermal conductivity and  $\lambda_T$  is the thermal relaxation time parameter for the heat flux where  $\lambda_T = 0$  simplifies the expression (7) to classical Fourier’s law.

Buongiorno [41] disclosed the combination of Brownian and thermophoresis diffusions given by

$$\mathbf{J}_s = -\rho D_B \nabla C - \rho D_T \frac{\nabla T}{T_a} \quad (6.8)$$

Here,  $D_B$  is the Brownian diffusion coefficient,  $D_T$  is the thermal diffusion coefficient and  $T_a$  is the reference temperature.

To demonstrate the physical model of present analysis, it is considered that the flow is laminar, unsteady and three dimensional. An incompressible ( $\nabla \cdot \mathbf{V} = 0$ ), electrically conducting elasto-viscous Maxwell nanofluid is being squeezed between two infinite parallel plates rotating about  $y$ -axis. To explain the physical configuration, the Cartesian coordinate system is introduced such a way that  $x$ -axis is measured along the plate surface and  $y$ -axis is perpendic-

ular to the plates, shown in Fig. 6.1. There is a vital consideration that fluid properties will not deviate of in the  $z$ -direction *i.e.*,  $\frac{\partial}{\partial z} = 0$ . The gap width between those plates in the minimal separation region is taken as time dependent given by  $h(t) = l\sqrt{1 - \alpha t}$ , where  $l$  is the steady gap width and  $\alpha$  is a constant having dimension  $\text{time}^{-1}$ . For  $\alpha > 0$  the two plates are squeezed until they touch  $t = 1/\alpha$  and for  $\alpha < 0$  the two plates are always separated. The upper plate placed at  $y = h(t)$  is squeezing towards the lower plate with a vertical velocity  $v_h = \frac{dh(t)}{dt}$ . This plate is stretched with a velocity  $u_h = \alpha_h x / (1 - \alpha t)$  in the positive  $x$ - direction with velocity slip parameter  $r_1$  and thermal slip parameter  $r_2$ . The lower plate is fixed at  $y = 0$  assumed to be porous in which the fluid flows with suction velocity  $v_0 = -V_0 / (1 - \alpha t)$ . A uniform magnetic field of density  $B_0$  is applied to along  $y$ - direction and the external electric field is assumed zero.

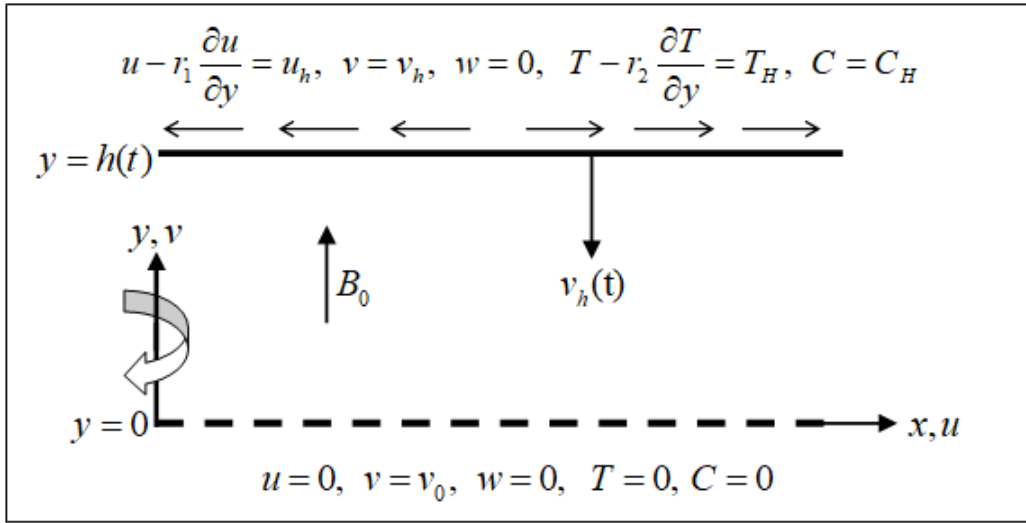


Figure 6.1: Physical model

The boundary conditions of the present physical models are

$$\left. \begin{aligned} u - r_1 \frac{\partial u}{\partial y} = u_h, \quad v = v_h, \quad w = 0, \quad T - r_2 \frac{\partial T}{\partial y} = T_H, \quad C = C_H \quad \text{at } y = h(t) \\ u = 0, \quad v = v_0, \quad w = 0, \quad T = 0, \quad C = 0, \quad \text{at } y = 0 \end{aligned} \right\} \quad (6.9)$$

Now in order to find the approximate solutions of the model it is essential to make the model

equations dimensionless using the following non-dimensional variables [174, 175]:

$$\begin{aligned}\eta &= \frac{y}{l(1-\alpha t)^{\frac{1}{2}}}, \quad u = \frac{\alpha x}{2(1-\alpha t)} f', \quad v = \frac{-\alpha l}{2(1-\alpha t)^{\frac{1}{2}}} f, \\ w &= \frac{\alpha x}{2(1-\alpha t)} g, \quad T = T_H \theta, \quad C = C_H F\end{aligned}\quad (6.10)$$

Using the above transformations, the equation (6.1) is satisfied and the equations (6.2)-(6.4) are reduced to

$$\begin{aligned}(1 - Sq\beta_S (\eta^2 - 2\eta f + f^2)) f^{iv} - Sq\beta_S (9\eta f''' + 2\eta f''^2 - 2f f''^2 - 2f'^2 f'' \\ - 8f f''' + 4f' f'' + 15f'') - M (f'' + \beta_S (\eta f''' + 3f'' - f f''' - f' f'')) \\ - Sq (\eta f''' + 3f'' + f' f'' - f f''' + 2\omega g') = 0\end{aligned}\quad (6.11)$$

$$\begin{aligned}(1 - Sq\beta_S (\eta^2 - 2\eta f + f^2)) g'' - Sq\beta_S (7\eta g' + 2\eta f' g' + 4f' g - 6f g' - 2f f' g' + 8g) \\ - Sq (\eta g' + 2g + f' g - f g' - 2\omega f') - M (g + \beta_S (\eta g' + 2g - f g')) = 0\end{aligned}\quad (6.12)$$

$$\begin{aligned}(1 - Pr Sq\beta_T (\eta^2 - 2\eta f + f^2)) \theta'' - Sq Pr (\eta \theta' - f \theta') \\ - Sq Pr \beta_T (3\eta \theta' - \eta f' \theta' - 3f \theta' + f f' \theta') + Pr (N_B \theta' F' + N_T \theta'^2) \\ + Ec Pr (4\delta^2 f'^2 + f''^2 + g'^2 + \delta^2 g^2) = 0\end{aligned}\quad (6.13)$$

$$F'' - Sq Le (\eta F' - f F') + \frac{Nt}{Nb} \theta'' = 0\quad (6.14)$$

The dimensionless boundary conditions are

$$\left. \begin{aligned} f = 1, \quad f' = \gamma_u + \varepsilon_u f'', \quad g = 0, \quad \theta = 1 + \varepsilon_u \theta', \quad F = 1, \quad \text{at } \eta = 1 \\ f = f_w, \quad f' = 0, \quad g = 0, \quad \theta = 0, \quad F = 0 \quad \text{at } \eta = 0 \end{aligned} \right\} \quad (6.15)$$

Here,  $\omega = \frac{2(1-\alpha t)}{\alpha} \Omega$  is the rotation parameter;  $\beta_S = \frac{\lambda_S \alpha}{2(1-\alpha t)}$  is the Maxwell parameter;  $Sq = \frac{\alpha l^2}{2\nu}$  is the squeeze number;  $M = \frac{\sigma B_0^2 h^2}{\mu}$  is the Magnetic field parameter;  $Pr = \frac{\nu \rho C_p}{\kappa_f}$  is the Prandtl number;  $Ec = \frac{\rho u_a^2}{\rho C_p T_H}$  is the Eckert number;  $\gamma_u = \frac{\alpha h}{\alpha}$  is the stretching parameter;  $\varepsilon_u = \frac{r_1}{h}$  is the velocity slip parameter;  $\varepsilon_T = \frac{r_2}{h}$  is the thermal slip parameter;  $\delta = \frac{h}{x}$  is the characteristic length ratio;  $fw = \frac{2V_0}{\alpha h}$  is the suction parameter.

Finally, the physical attentions in the existing study are the skin friction coefficient  $C_f$ , the local Nusselt number  $Nu$  and the Sherwood number ( $Sh$ ) defined as

$$C_f \propto f'', \quad Nu \propto -\theta' \quad \& \quad Sh \propto -F' \quad (6.16)$$

### 6.3 Numerical Method

Equations (6.11)-(6.14) combined with the boundary conditions (6.15) are solved numerically using finite difference code developed by a MATLAB boundary value problem solver, known as bvp4c. The analysis is made for various values of the pertinent parameters such as Brownian motion parameter  $N_B$ , squeezing parameter  $Sq$ , Maxwell parameter  $\beta_S$ , thermal relaxation parameter  $\beta_T$ , rotation parameter  $\omega$ , stretching parameter  $\gamma_u$ , velocity slip parameter  $\varepsilon_u$  and thermal slip parameter  $\varepsilon_T$ . The step size is taken as  $\eta = 0.01$  and the tolerance criteria are set to  $10^{-6}$ . On the basis of the present model,  $[0, 1]$  is measured as the domain of a channel. First of all, comparison of the current model is arranged with [174], shown in Table 6.1.

Table 6.1: Comparison for skin friction coefficient, local Nusselt number and local Sherwood numbers for different values of  $Sq$  when  $Pr = Ec = \gamma_u = 1.0$ ,  $\delta = 0.1$ .

Pr	Mustafa <i>et al.</i> [174]			Present work		
	$-f'(1)$	$-\theta'(1)$	$F'$	$-f'(1)$	$-\theta'(1)$	$F'$
-1.0	3.026324	3.02632355855	3.026323	2.170091	3.319899	0.804559
-0.5	5.98053	5.98053039715	5.98053	2.617404	3.129491	0.781402
0.01	14.43941	14.4394132325	14.439411	3.007133	3.047091	0.761225
0.5	1.513162	1.51316180648	1.513161	3.336448	3.026327	0.744224
2.0	3.631588	3.63158826816	3.631587	4.167387	3.118553	0.701813

#### 6.4 Results and Siscussion

Figures 6.2(a) and 6.2(b) are devoted to the analysis of the impact of the Brownian motion parameter  $N_B$  on the temperature and concentration profiles, respectively. These figures allow us to conclude that the temperature and concentration distributions are enhanced with  $N_B$ . The Brownian motion parameter illustrates a significant variation in temperature profiles, while compared to concentration profiles. These outcomes express a similar result remarkable with the work of Reddy *et al.* [194]. These figures also reveals that the temperature of the fluid is lifted and the concentration is reduced for thermal relaxation parameter  $\beta_T$ .

Figures 6.3(a), 6.3(b) and 6.4(a), 6.4(b) express the behavior of squeezing parameter  $Sq$ . When plates are coming closer the values of  $Sq$  are considered positive. Figure 6.3(a) shows that, with the increase of the values of  $Sq$  fluid velocity decreases. Clearly the flow velocity decreases in the channel when fluid is clutched inside. But the secondary velocity profiles increase with  $Sq$ , shown in Fig. 6.3(b). Furthermore, there is no variation in velocity profiles due to the classical Fourier's heat flux model ( $\beta_T = 0$ ) and the Cattaneo-Christov heat flux model ( $\beta_T = 0.3$ ). Figures 6.4(a) and 6.4(b) demonstrate the influence of  $Sq$  parameter on the heat and solutal distributions respectively. From the above representations, it can be revealed that

the deviation of the fluid properties for the classical Fourier and Cattaneo-Christov heat fluxes approaches for the higher value of squeezing parameter.

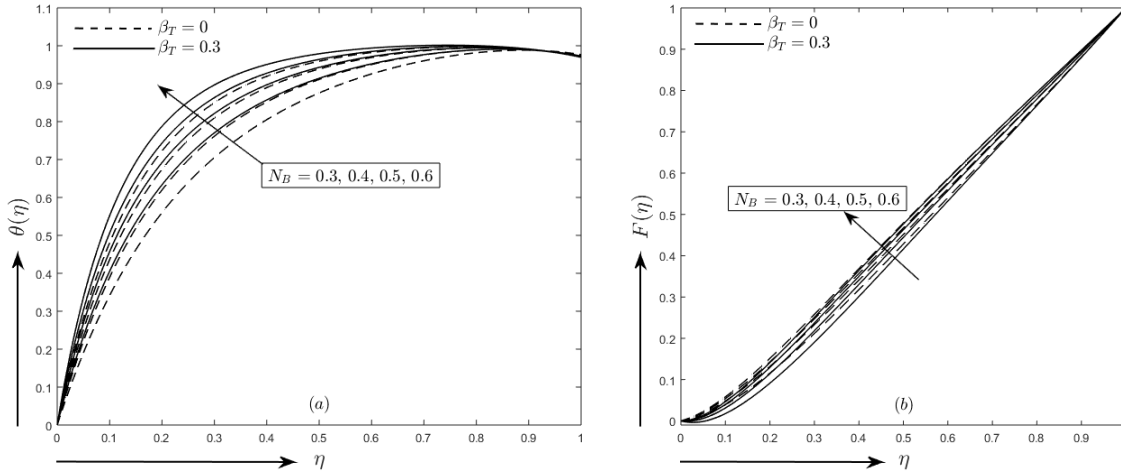


Figure 6.2:  $N_B$  effect on the profiles of (a) temperature and (b) concentration

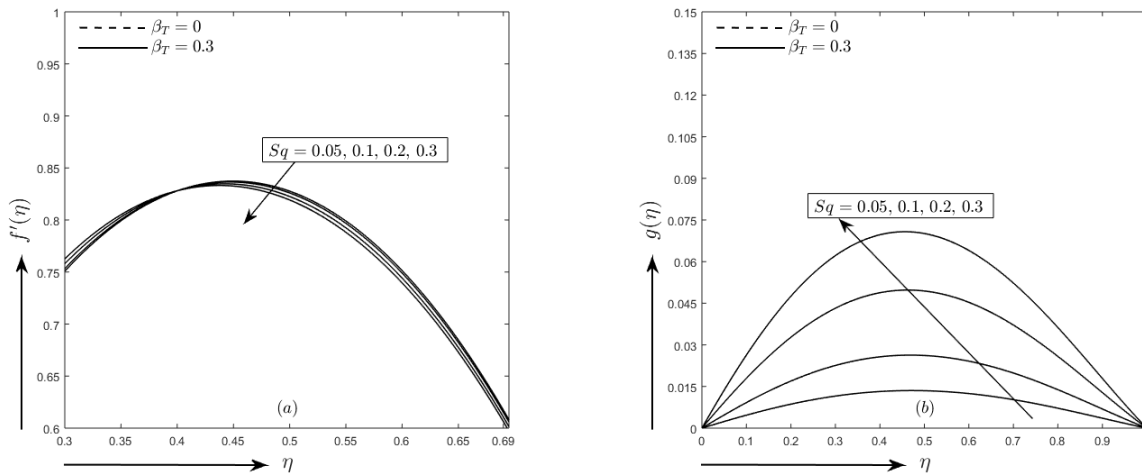


Figure 6.3:  $Sq$  effect on the profiles of (a) primary velocity and (b) transverse velocity.

When the elastic stress is applied to the non-Newtonian fluid, the time during which the fluid achieves its stability is the relaxation time, which is greater for highly viscous fluids. The Maxwell parameter  $\beta_S$  deals with the fluid relaxation time to its characteristic time scale. Here  $\beta_S = 0$  gives the result for Newtonian viscous incompressible fluid. The fluid with a small

Maxwell parameter exhibits liquid-like activities but large Maxwell parameter communicates with solid-like materials able to conduct and retain heat better. Therefore, it is observed physically that gradually increasing the Maxwell parameter can increase the fluid viscosity, which enhances resistance to flow and, as a result, the hydrodynamic boundary layer thickness reduces for Maxwell fluid, as shown in Fig. 6.5(a). There is also declining effect of  $\beta_S$  on the secondary velocity, displayed in Fig. 6.5(b).

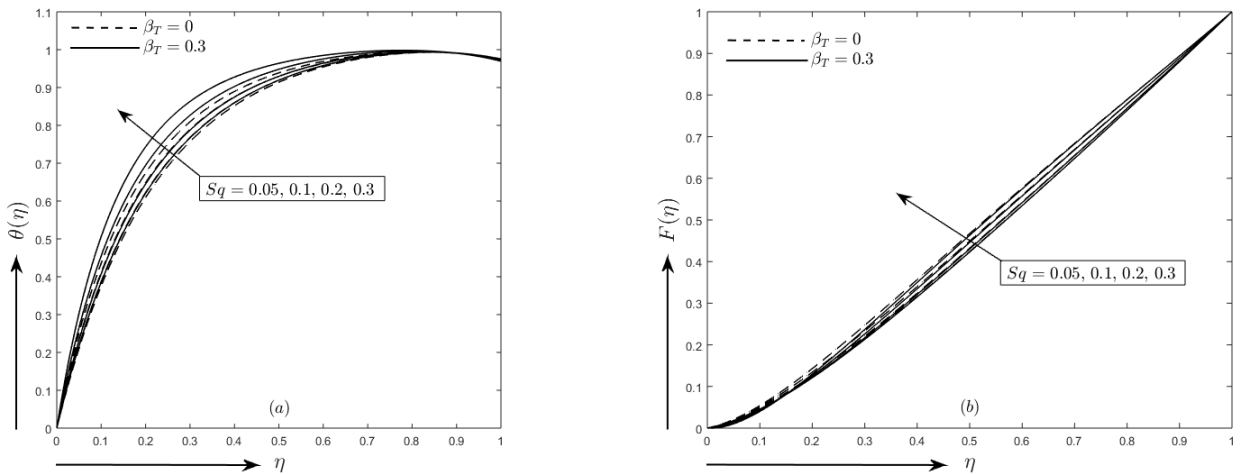


Figure 6.4:  $Sq$  effect on the profiles of (a) temperature and (b) concentration.

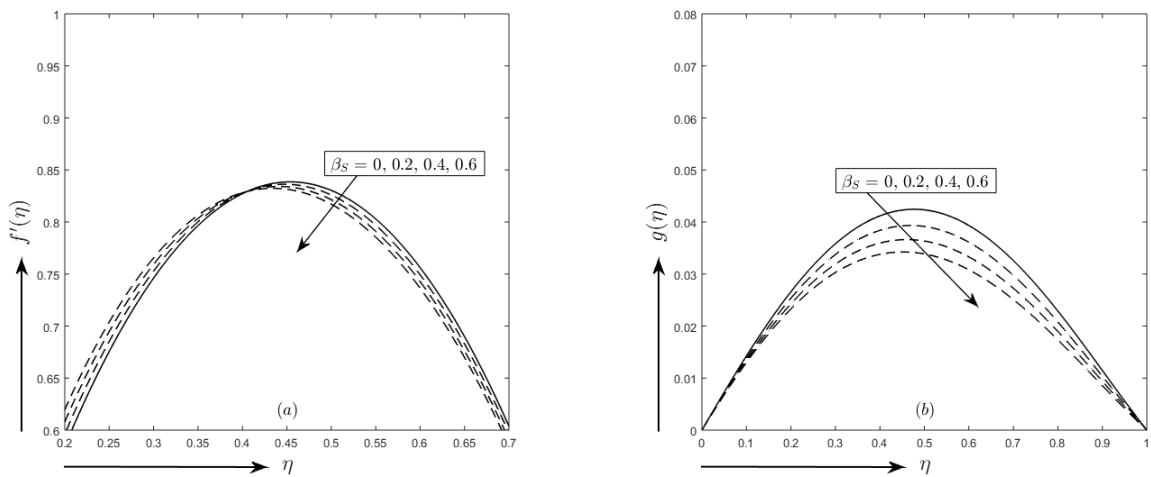


Figure 6.5:  $\beta_S$  effect on the profiles of (a) primary velocity and (b) secondary velocity.



Figure 6.6(a) presents the significant effect of rotation parameter  $\omega$  on secondary velocity. The rotation of the plates generates higher  $z$ -momentum. Figures 6.6(b) and 6.7(a), 6.7(b) depict the stretching parameter  $\gamma_u$  effects on  $x$ -momentum,  $z$ -momentum and energy distributions, respectively. From Fig. 6.6(b), it is observed that the stretching velocity enhances strength to the fluid velocity to increase the  $x$ -momentum distribution with the increase of stretching effect  $\gamma_u$  at the stretching upper surface. Figure 6.7(a) expresses that the  $z$ -momentum decreases with the higher values of stretching parameter  $\gamma_u$ . Figure 6.7(b) exhibits the fact that The energy distribution is an increasing function of  $\gamma_u$ .

The result found from Fig. 6.8(a) expresses the fact that the velocity increases with the mounting value of velocity slip parameter  $\varepsilon_u$  but after the cross flow situated at  $\eta = 0.656$  the velocity reverses the flow tendency and decreases at the upper wall indicated in the Fig. 6.8(a). In Fig. 6.8(b), it is found that the secondary velocity increases with the positive values of slip parameter  $\varepsilon_u$ . A significant depiction, portrayed from the above observations, the fluid velocity is higher for the velocity slip parameter  $\varepsilon_u$ . The energy distribution rises with the velocity slip parameter  $\varepsilon_u$ , found in Fig. 6.9(a). But Fig. 6.9(b) shows that the temperature profile is a decreasing function of the thermal slip parameter  $\varepsilon_T$ .

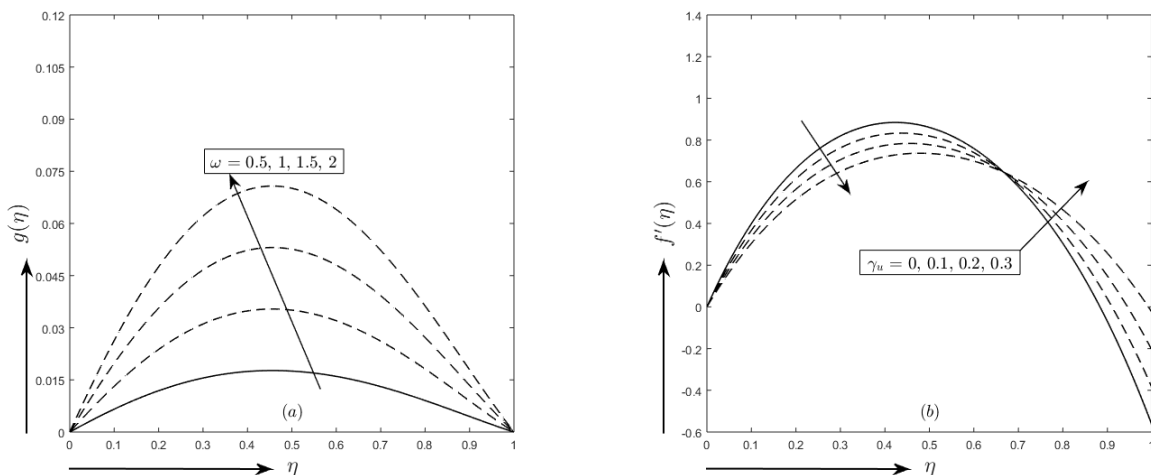


Figure 6.6: (a)  $\varepsilon_u$  effect on transverse velocity profile and (b)  $\gamma_u$  effect on primary velocity profile.

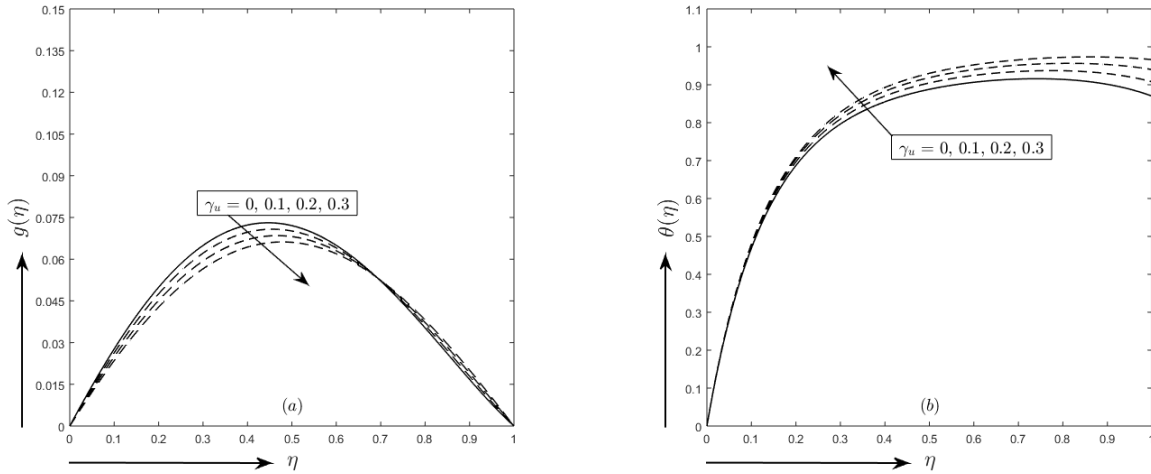


Figure 6.7:  $\gamma_u$  effect on the profiles of (a) transverse velocity and (b) temperature.

Finally, from the point of view of physical interest, the skin friction coefficient is useful to estimate the total frictional drag exerted on the surface. The Nusselt Number is used to characterize the heat flux from a heated solid surface to a fluid. Additionally, Table 6.2 displays the skin friction ( $C_f$ ) for squeezing parameters and Maxwell parameter at the upper ( $\eta = 1$ ) and lower ( $\eta = 0$ ) plates for classical Fourier ( $\beta_T = 0$ ) and Cattaneo-Christov ( $\beta_T = 0.3$ ) heat fluxes. The effect of squeezing parameter  $Sq$  and Maxwell parameter  $\beta_T$  on the local Nusselt number  $Nu$  and are arranged in the Table 6.3 classical Fourier ( $\beta_T = 0$ ) and Cattaneo-Christov ( $\beta_T = 0.3$ ) heat fluxes considering  $M = 1$ ;  $\omega = 2$ ;  $\delta = 0.1$ ;  $Pr = 6.838$ ;  $Ec = 0.02$ ;  $\gamma_u = 0.1$ ;  $\varepsilon_u = 0.1$ .

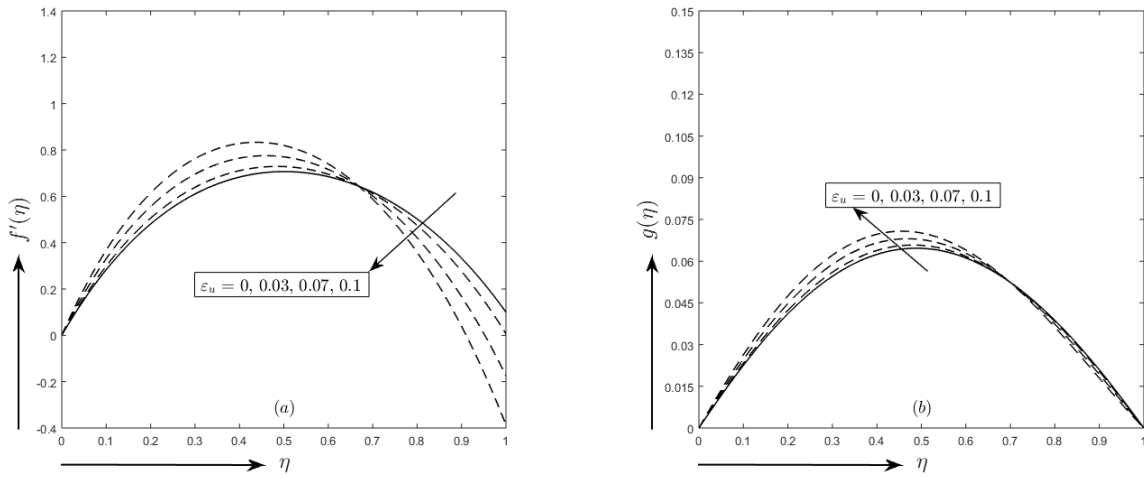


Figure 6.8:  $\varepsilon_u$  effect on the profiles of (a) primary velocity and (b) secondary velocity.

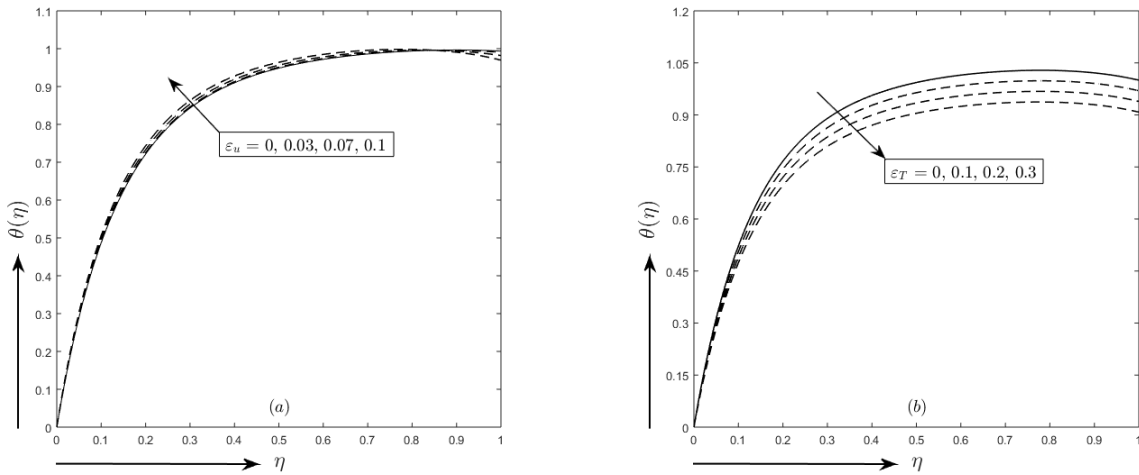


Figure 6.9: (a)  $\varepsilon_u$  effect on the temperature profile and (b)  $\varepsilon_T$  effect on the temperature profile.

Table 6.2: Skin friction ( $C_f$ ) for different values of  $Sq$  and  $\beta_S$  at the upper ( $\eta = 1$ ) and lower ( $\eta = 0$ ) plates for classical Fourier ( $\beta_T = 0$ ) and Cattaneo Christov ( $\beta_T = 0.3$ ) heat fluxes

		$\beta_T = 0$		$\beta_T = 0.3$	
$Sq$	$\beta_S$	$C_{f_{\eta=1}}$	$C_{f_{\eta=0}}$	$C_{f_{\eta=1}}$	$C_{f_{\eta=0}}$
0.1	0.5	-4.659543	4.056332	-4.659543	4.056332
0.2		-4.757606	4.214218	-4.757606	4.214218
0.3		-4.861431	4.377962	-4.861431	4.377962
	0.6	-4.921623	4.486911	-4.921623	4.486911
	0.7	-4.983358	4.598035	-4.983358	4.598035

Table 6.3: Nussult number ( $Nu$ ) for different values of  $Sq$  and  $\beta_S$  at the upper ( $\eta = 1$ ) and lower ( $\eta = 0$ ) plates for classical Fourier ( $\beta_T = 0$ ) and Cattaneo Christov ( $\beta_T = 0.3$ ) heat fluxes

		$\beta_T = 0$		$\beta_T = 0.3$	
$Sq$	$\beta_S$	$Nu_{\eta=1}$	$Nu_{\eta=0}$	$Nu_{\eta=1}$	$Nu_{\eta=0}$
0.1	0.5	0.253098	-4.942629	0.261092	-5.325179
0.2		0.269455	-5.387022	0.283571	-6.271893
0.3		0.286328	-5.861222	0.304701	-7.396247
	0.6	0.290002	-5.867768	0.308438	-7.405840
	0.7	0.293886	-5.874447	0.312386	-7.415598

## 6.5 Conclusions

The present paper is to study the effect of thermal relaxation factor on the flow of Maxwell nanofluid squeezing in the parallel rotating plates with porous stretched surface incorporating Cattaneo-Christov heat flux model. The major outcomes drawn from the study of the present model can be summarized as follows:

1. The thermal boundary layer thickness rises for the Brownian motion parameter, squeezing parameter, stretching parameter and velocity slip parameter.
2. The thermal boundary layer thickness decreases for the thermal slip parameter.
3. The hydrodynamic boundary layer thickness is reduced for the squeezing parameter, Maxwell parameter and stretching parameter.
4. The velocity distributions are higher for the velocity slip parameter.
5. The concentration is elevated for Brownian motion parameter and squeezing parameter.

In conclusion of the current study, it can be argued that the squeezing parameter and the stretching parameter that have the velocity control phenomena, can improve the heat transfer in the nanofluid. This study will provide a great opportunity to develop the cooling performance of mechanical system like automotive radiators and nuclear reactors.

## CHAPTER 7

### CONCLUSION

#### 7.1 Summary

Throughout this thesis, the dynamics of a nanofluid boundary layer flowing over a convectively heated surface are investigated. After considering the complex dynamic between the electrical conductivity of the conventional base fluids and that of the nanoparticles, the resulting dimensionless nonlinear differential equations are solved numerically with the help of the well-known finite difference method and a MATLAB package. This is done in order to take into account the complex dynamic that occurs between the two things being considered. Similarity transformation is used to generate the governing equations for mass, momentum, and energy and then turn them into non-similar equations. Effects of relevant parameter settings on velocity and temperature profiles, skin-friction coefficient, and Nusselt number are investigated and graphically shown using numerical data.

Compared to ordinary base fluids, our findings showed that nanofluids are incredibly susceptible to the influence of magnetic fields due to the complicated interaction of the electrical conductivity of nanoparticles with that of the base fluid. A magnetic field effect on nanofluids plays an essential role in both the cooling and heating processes, as an increase in the nanoparticle volume fraction and magnetic strength causes the temperature to rise and the velocity to fall.

This research is crucial because it shows how essential nanofluids are for a wide variety of fields, including heat transmission, cleaning, medicine, and biomedicine. Engineering applications where heat augmentation is crucial include next-generation solar film collectors, heat exchanger technology, geothermal energy storage, and many more. Heat transfer, chemical and bioprocessing, medicine (drug administration and functional tissue cell inter-

action), and many more are only some of the many uses for nanofluids. Nanofluid research has the potential to greatly advance the current state-of-the-art in nanotechnology due to its interdisciplinary character.

## **7.2 Future study**

Nanofluid thermal conductivity data is inconsistent. These inconsistencies must be overcome to use nanofluids in heat transfer devices. Clustering, pH value, and ultrasonic vibration affect thermal conductivity, although little is known about their effects. The relative importance of thermal conductivity enhancement techniques in nanofluid theoretical investigations is unknown. New theoretical models incorporating the impacts of many enhancement processes and comparing their predictions with systematic experimental data will help explain anomalous thermal conductivity enhancement with nanofluids.

Nanofluid convective heat transport is analysed using several theoretical methods. Numerical studies on this topic are insufficient to assess approach accuracy. Numerical evaluations of the offered methodologies help determine their validity. However, forced convection heat transfer of nanofluids has little experimental data, making comparing computational results with actual results challenging.

Like thermal conductivity, convective heat transmission of nanofluids is governed by particle volume fraction, particle size, particle material, temperature, and base fluid type. Most of these parameters have not been tested for heat transfer effects. Comprehensive investigations of nanofluid heat transfer will help optimise nanofluid heat transfer enhancement.

Finally, the influence of a magnetic field on hybrid nanofluid flow in industrial tubes or pipes needs more study.

# Appendices



## APPENDIX A

### NOMENCLATURE

<p><u>A</u></p> <p><math>A</math> Unsteadiness parameter</p> <p><math>A_1</math> Rivlin Ericksen tensor</p> <p><u>B</u></p> <p><math>b</math> Initial stretching rate</p> <p><math>bf</math> Base fluid</p> <p><math>B</math> Magnetic field applied normal to the surface</p> <p><math>B_0</math> Magnetic field strength</p> <p><math>Bi</math> Biot number for convective heat transfer</p> <p><math>Bi_h</math> Biot number</p> <p><math>Bi^*</math> Biot number for convective mass transfer</p> <p><u>C</u></p> <p><math>C_f</math> Skin friction coefficient</p> <p><math>c_p</math> Heat capacitance</p> <p><math>C_0</math> Concentration at the bottom plate</p>	<p><math>C_l</math> Concentration at the upper plate</p> <p><math>C_w</math> Concentration at surface</p> <p><math>C_\infty</math> Concentration apart from surface</p> <p><u>D</u></p> <p><math>D_B</math> Brownian diffusion coefficient</p> <p><math>D_T</math> Thermophoresis diffusion coefficient</p> <p><u>E</u></p> <p><math>E</math> Electromagnetic strength</p> <p><math>Ec</math> Eckert number</p> <p><u>F</u></p> <p><math>f</math> Dimensionless velocity</p> <p><math>F</math> Dimensionless concentration</p> <p><math>f_w</math> Suction parameter</p> <p><u>H</u></p> <p><math>h_f</math> Convective heat transfer coefficient</p> <p><math>h_f^*</math> Convective mass transfer coefficient</p> <p><u>K</u></p> <p><math>k</math> Relaxation time <math>&gt; 0</math></p>
--	--

$k_0$	Initial relaxation time at $t = 0$	$\underline{\mathbb{T}}$	
$\underline{L}$		$T_0$	Temperature at bottom the plate
$Le$	Lewis number	$T_l$	Temperature at the upper plate
$L^{tr}$	Velocity gradient	$t$	Time
$\underline{M}$		$T_w$	Initial surface temperature
$M$	Magnetic field parameter	$T_\infty$	Free stream temperature
$\underline{N}$		$T_{slip}$	Thermal slip
$Nb$	Brownian motion parameter	$T_f$	Convective temperature
$Nt$	Thermophoresis parameter	$\underline{U-Z}$	
$n$	Nanoparticles shape factor	$u_l$	Stretching velocity
$N$	Slip variation constant	$u_{slip}$	Slip velocity
$Nu$	Nusselt number	$u_w$	Surface velocity
$\underline{P}$		$U_a$	Fluid flow
$p$	Pressure	$V$	Velocity Vector
$Pr$	Prandtl number	$v_l$	Suction velocity
$\underline{R}$		$(x, y)$	2D-Cartesian Coordinates
$Re$	Reynolds number	$\underline{\text{Greek}}$	
$R$	Chemical reaction	$\alpha$	Thermal diffusivity
$\underline{S}$		$\beta$	Deborah number
$S$	Stress tensor	$\beta_S$	Deborah number/Maxwell number
$Sh$	Sherwood number	$\gamma_h$	Stretching parameter

$\lambda_S$	Stress relaxation time factor $> 0$	$\kappa_{cr}$	Chemical reaction parameter
$\lambda_T$	Thermal relaxation time factor $> 0$	$\nu$	Kinematic viscosity
$\mu$	Viscosity of the nanofluid	$\theta$	Dimensionless temperature
$\mu_0$	Dynamic viscosity	$\rho$	Density
$\delta_u$	Velocity slip ratio	$\sigma$	Electrical conductivity
$\delta_T$	Temperature slip ratio	$\psi$	Stream function
$\varepsilon$	Local electromagnetic field parameter	$\Psi$	Shape factor
		CCHF	Cattaneo-Christov Heat Flux
$\varepsilon_{u_h}$	Velocity slip parameter	UCM	Upper convected Maxwell
$\varepsilon_{T_h}$	Thermal slip parameter		<u>Sub/Superscript</u>
$\eta$	Dimensionless length	$f$	Base fluid
$\varphi$	Nanoparticle volume fraction parameter	$nf$	Nanofluid
		$s$	Solid nanoparticles
$\kappa$	Thermal conductivity	tr	Transpose of a matrix

## APPENDIX B

### RESEARCH CONTRIBUTION FROM THE CURRENT THESIS

List of published papers:

1. M. E. Karim, M. A. Samad, & M. Ferdows (2017, June). Magneto hall-effect on unsteady elastico-viscous nanofluid slip flow in a channel in presence of thermal radiation and heat generation with Brownian motion. In AIP Conference Proceedings (Vol. 1851, No. 1, p. 020052). AIP Publishing LLC. DOI: 10.1063/1.4984681
2. M. E. Karim, M. A. Samad, & M. Ferdows (2019, July). Numerical study of the effect of variable viscosity on unsteady pulsatile nanofluid flow through a Couette channel of stretching wall with convective heat transfer. In AIP Conference Proceedings (Vol. 2121, No. 1, p. 070005). AIP Publishing LLC. DOI: 10.1063/1.5115912
3. M. E. Karim, & M. A. Samad (2020, February). Numerical Study on Time Dependent Maxwell Nanofluid Slip Flow over Porous Stretching Surface with Chemical Reaction. Research Journal of Applied Sciences, Engineering and Technology, 17(1): 24-34. DOI: 10.19026/rjaset.17.6031
4. M. A. Samad & M. E. Karim (2020, January). Effect of Heat Generation and Thermal Radiation on the Slip Flow of Time Dependent Elastico-viscous Maxwell Nanofluid Flow over a Porous Stretching Inclined Surface. Dhaka Univ. J. Sci. 68(1): 19- 28.
5. M. E. Karim, & M. A. Samad (2020). Effect of Brownian Diffusion on Squeezing Elastico-Viscous Nanofluid Flow with Cattaneo-Christov Heat Flux Model in a Channel with Double Slip Effect. Applied Mathematics, 11(4), 277-291. DOI: 10.4236/am.2020.114021
6. M. E. Karim, & M. A. Samad (2020). Lie group analysis for Elastico-viscous Maxwell nanofluid flow in a channel of stretching surface with convective boundary condition. AIJR Proceedings, 34-44. DOI: 10.21467/proceedings.100.4

List of attending conferences:

1. 21st BMS International Mathematics Conference 2019, Department of Applied Mathematics, University of Dhaka, Dhaka-1000, Bangladesh. December 6–8, 2019
2. International Conference on Applied Mathematics and Computational Sciences (icamcs-2019), Department of Mathematics, DIT University, Dehradun-248009, India. October 17–19, 2019
3. 8th BSME International Conference on Thermal Engineering, BUET, Dhaka-1000, Bangladesh. December 19–21, 2018
4. 7th BSME International Conference on Thermal Engineering, BUET, Dhaka-1000, Bangladesh. December 22–24, 2016
5. 2nd International Bose Conference: Recent trends in physical sciences, University of Dhaka, Dhaka-1000, Bangladesh. December 3–4, 2015
6. 19th BMS International Math Conference, Department of Mathematics and Natural Sciences BRAC University, 66 Mohakhali, Dhaka-1212, Bangladesh. December 18–20, 2015

List of departmental seminars:

1. Title of the 1st seminar: "Pulsatile Nanofluid Flow Through a Couette Channel Stretching Sheet with Convective Heat Transfer", Dated: 16 May 2018.
2. Title of the 2nd seminar: "Numerical Analysis of Elastico-viscous Ethylene Glycol Based Nanofluid Slip Flow between Rotating and Squeezing Channel", Dated: 21 March, 2022.

## REFERENCES

- [1] M. Faraday, "Experimental researches in electricity," *Philosophical transactions of the Royal Society of London*, no. 122, pp. 125–162, 1832.
- [2] H. Alfvén, "Existence of electromagnetic-hydrodynamic waves," *Nature*, vol. 150, no. 3805, pp. 405–406, 1942.
- [3] J. Larmor and S. Joseph, "Possible rotational origin of magnetic fields of sun and earth," *Elec. Rev*, vol. 85, p. 412, 1919.
- [4] S. Ostrach, "An analysis of laminar free-convection flow and heat transfer about a flat plate parallel to the direction of the generating body force," NASA Report, Lewis Flight Propulsion Laboratory, Cleveland, Ohio, Washington, Tech. Rep., 1952, pp. 1–48.
- [5] R. Goody, "The influence of radiative transfer on cellular convection," *Journal of Fluid Mechanics*, vol. 1, no. 4, pp. 424–435, 1956.
- [6] V. J. Rossow, "On flow of electrically conducting fluids over a flat plate in the presence of a transverse magnetic field," Tech. Rep., 1958, pp. 1–54.
- [7] B. C. Sakiadis, "Boundary-layer behavior on continuous solid surfaces: I. Boundary-layer equations for two-dimensional and axisymmetric flow," *AIChE Journal*, vol. 7, no. 1, pp. 26–28, 1961.
- [8] L. J. Crane, "Flow past a stretching plate," *Zeitschrift für angewandte Mathematik und Physik ZAMP*, vol. 21, no. 4, pp. 645–647, 1970.
- [9] E. M. Sparrow and R. D. Cess, "Radiation heat transfer, augmented edition, hemisphere publ," *Crop.*, Washington, DC, 1978.
- [10] V. M. Soundalgekar, N. V. Vighnesam, and I. Pop, "Combined free and forced convection flow past a vertical porous plate," *International Journal of Energy Research*, vol. 5, no. 3, pp. 215–226, 1981.
- [11] A. Raptis and C. Perdikis, "Unsteady flow through a porous medium in the presence of free convection," *International communications in heat and mass transfer*, vol. 12, no. 6, pp. 697–704, 1985.

- [12] M. A. Mansour, "Radiative and free-convection effects on the oscillatory flow past a vertical plate," *Astrophysics and space science*, vol. 166, no. 2, pp. 269–275, 1990.
- [13] C.-R. Lin and C.-K. Chen, "Exact solution of heat transfer from a stretching surface with variable heat flux," *Heat and mass transfer*, vol. 33, no. 5, pp. 477–480, 1998.
- [14] B. K. Jha, "Natural convection in unsteady MHD couette flow," *Heat and mass transfer*, vol. 37, no. 4, pp. 329–331, 2001.
- [15] S. R. Pop, I Pop, and T Grosan, "Radiation effects on the flow near the stagnation point of a stretching sheet," *Technische Mechanik-European Journal of Engineering Mechanics*, vol. 25, no. 2, pp. 100–106, 2005.
- [16] M. Ferdows, M. Ota, A. Sattar, and M. Alam, "Similarity solution for MHD flow through vertical porous plate with suction," *Journal of Computational and Applied Mechanics*, vol. 6, no. 1, pp. 15–25, 2005.
- [17] J. Z. Jordán, "Network simulation method applied to radiation and viscous dissipation effects on MHD unsteady free convection over vertical porous plate," *Applied Mathematical Modelling*, vol. 31, no. 9, pp. 2019–2033, 2007.
- [18] M. A. Samad and M. Mohebujjaman, "MHD heat and mass transfer free convection flow along a vertical stretching sheet in presence of magnetic field with heat generation," *Research Journal of Applied Sciences, Engineering and Technology*, vol. 1, no. 3, pp. 98–106, 2009.
- [19] O. D. Makinde, "On MHD heat and mass transfer over a moving vertical plate with a convective surface boundary condition," *The Canadian Journal of Chemical Engineering*, vol. 88, no. 6, pp. 983–990, 2010.
- [20] P. Pavar, L Harikrishna, and M. S. Reddy, "Heat transfer over a stretching porous surface on a steady MHD fluid flow," *International Journal of Ambient Energy*, pp. 1–8, 2021.
- [21] Y.-M. Li, I. Ullah, N Ameer Ahammad, I. Ullah, T. Muhammad, and S. A. Asiri, "Approximation of unsteady squeezing flow through porous space with slip effect: DJM approach," *Waves in Random and Complex Media*, pp. 1–15, 2022.
- [22] S. K. Das, S. U. S. Choi, W. Yu, and T Pradeep, "Nanofluids-science and technology. A John Wiley & Sons," *Inc., Hoboken*, 2008.

- [23] C. N. R. Rao, A. Müller, and A. K. Cheetham, *The chemistry of nanomaterials: synthesis, properties and applications*. John Wiley & Sons, 2006.
- [24] D. P. Kulkarni, D. K. Das, and R. S. Vajjha, “Application of nanofluids in heating buildings and reducing pollution,” *Applied Energy*, vol. 86, no. 12, pp. 2566–2573, 2009.
- [25] S. U. S. Choi and J. A. Eastman, “Enhancing thermal conductivity of fluids with nanoparticles,” Argonne National Lab., IL (United States), Tech. Rep., 1995.
- [26] A. R. I. Ali and B. Salam, “A review on nanofluid: Preparation, stability, thermophysical properties, heat transfer characteristics and application,” *SN Applied Sciences*, vol. 2, no. 10, pp. 1–17, 2020.
- [27] S. Lee, S. U. S. Choi, S. Li, and J. A. Eastman, “Measuring thermal conductivity of fluids containing oxide nanoparticles,” vol. 121, no. 2, 280–289, 1999.
- [28] S. K. Das, N. Putra, P. Thiesen, and W. Roetzel, “Temperature dependence of thermal conductivity enhancement for nanofluids,” *J. Heat Transfer*, vol. 125, no. 4, pp. 567–574, 2003.
- [29] S. M. S. Murshed, K. C. Leong, and C Yang, “Investigations of thermal conductivity and viscosity of nanofluids,” *International journal of thermal sciences*, vol. 47, no. 5, pp. 560–568, 2008.
- [30] S. Das and R. N. Jana, “Natural convective magneto-nanofluid flow and radiative heat transfer past a moving vertical plate,” *Alexandria Engineering Journal*, vol. 54, no. 1, pp. 55–64, 2015.
- [31] M. Lomascolo, G. Colangelo, M. Milanese, and A. De Risi, “Review of heat transfer in nanofluids: Conductive, convective and radiative experimental results,” *Renewable and Sustainable Energy Reviews*, vol. 43, pp. 1182–1198, 2015.
- [32] M. Rashidi, N. V. Ganesh, A. A. Hakeem, and B Ganga, “Buoyancy effect on MHD flow of nanofluid over a stretching sheet in the presence of thermal radiation,” *Journal of Molecular liquids*, vol. 198, pp. 234–238, 2014.
- [33] M Turkyilmazoglu, “Unsteady convection flow of some nanofluids past a moving vertical flat plate with heat transfer,” *Journal of heat transfer*, vol. 136, no. 3, p. 031 704,



- [34] S. Dinarvand, R. Hosseini, and I. Pop, “Unsteady convective heat and mass transfer of a nanofluid in Howarth’s stagnation point by Buongiorno’s model,” *International Journal of Numerical Methods for Heat & Fluid Flow*, vol. 25, no. 5, pp. 1176–1197, 2015.
- [35] L. Nakharintr and P. Naphon, “Magnetic field effect on the enhancement of nanofluids heat transfer of a confined jet impingement in mini-channel heat sink,” *International Journal of Heat and Mass Transfer*, vol. 110, pp. 753–759, 2017.
- [36] R. K. Tiwari and M. K. Das, “Heat transfer augmentation in a two-sided lid-driven differentially heated square cavity utilizing nanofluids,” *International Journal of heat and Mass transfer*, vol. 50, no. 9-10, pp. 2002–2018, 2007.
- [37] S Baag and S. R. Mishra, “Heat and mass transfer analysis on MHD 3 –  $D$  water-based nanofluid,” *Journal of Nanofluids*, vol. 4, no. 3, pp. 352–361, 2015.
- [38] M. M. Bhatti, S. R. Mishra, T. Abbas, and M. M. Rashidi, “A mathematical model of MHD nanofluid flow having gyrotactic microorganisms with thermal radiation and chemical reaction effects,” *Neural Computing and Applications*, vol. 30, no. 4, pp. 1237–1249, 2018.
- [39] O. D. Makinde and S. R. Mishra, “On stagnation point flow of variable viscosity nanofluids past a stretching surface with radiative heat,” *International Journal of Applied and Computational Mathematics*, vol. 3, no. 2, pp. 561–578, 2017.
- [40] T. Thumma and S. R. Mishra, “Effect of viscous dissipation and joule heating on magnetohydrodynamic Jeffery nanofluid flow with and without multi slip boundary conditions,” *Journal of Nanofluids*, vol. 7, no. 3, pp. 516–526, 2018.
- [41] J. Buongiorno, “Convective transport in nanofluids,” *Journal of heat transfer*, vol. 128, no. 3, pp. 240–250, 2006.
- [42] M Goodarzi *et al.*, “Investigation of nanofluid mixed convection in a shallow cavity using a two-phase mixture model,” *International Journal of Thermal Sciences*, vol. 75, pp. 204–220, 2014.
- [43] A. M. Aly and Z. A. S. Raizah, “Double-diffusive natural convection in an enclosure filled with nanofluid using ISPH method,” *Alexandria Engineering Journal*, vol. 55, no. 4, pp. 3037–3052, 2016.

- [44] A. I. Alsabery, M. A. Sheremet, A. J. Chamkha, and I Hashim, “Conjugate natural convection of  $Al_2O_3$ -water nanofluid in a square cavity with a concentric solid insert using Buongiorno’s two-phase model,” *International Journal of Mechanical Sciences*, vol. 136, pp. 200–219, 2018.
- [45] S. Y. Motlagh and H. Soltanipour, “Natural convection of  $Al_2O_3$ -water nanofluid in an inclined cavity using Buongiorno’s two-phase model,” *International Journal of Thermal Sciences*, vol. 111, pp. 310–320, 2017.
- [46] M Sheikholeslami and D. D. Ganji, “Magnetohydrodynamic flow in a permeable channel filled with nanofluid,” *Scientia Iranica. Transaction B, Mechanical Engineering*, vol. 21, no. 1, p. 203, 2014.
- [47] J. I. Ramos and N. S. Winowich, “Magnetohydrodynamic channel flow study,” *The Physics of Fluids*, vol. 29, no. 4, pp. 992–997, 1986.
- [48] A. Belhocine, N. Stojanovic, and O. I. Abdullah, “Numerical simulation of laminar boundary layer flow over a horizontal flat plate in external incompressible viscous fluid,” *European Journal of Computational Mechanics*, pp. 337–386, 2021.
- [49] J. Harris, *Rheology and non-Newtonian flow*. Longman Publishing Group, 1977.
- [50] A. Cameron and C. M. Mc Ettles, “Basic lubrication theory,” 1981.
- [51] H. A. Barnes, J. F. Hutton, and K. Walters, *An introduction to rheology*. Elsevier, Amsterdam, 1989.
- [52] J. G. Oldroyd, “On the formulation of rheological equations of state,” *Proceedings of the Royal Society of London. Series A. Mathematical and Physical Sciences*, vol. 200, no. 1063, pp. 523–541, 1950.
- [53] D. W. Beard and K. Walters, “Elastico-viscous boundary-layer flows i. two-dimensional flow near a stagnation point,” in *Mathematical Proceedings of the Cambridge Philosophical Society*, Cambridge University Press, vol. 60, 1964, pp. 667–674.
- [54] K. R. Rajagopal and A. S. Gupta, “An exact solution for the flow of a non-Newtonian fluid past an infinite porous plate,” *Meccanica*, vol. 19, no. 2, pp. 158–160, 1984.
- [55] K. R. Rajagopal, T. Y. Na, and A. S. Gupta, “Flow of a viscoelastic fluid over a stretching sheet,” *Rheologica Acta*, vol. 23, no. 2, pp. 213–215, 1984.

- [56] M. Ramzan and M. Bilal, “Time dependent MHD nano-second grade fluid flow induced by permeable vertical sheet with mixed convection and thermal radiation,” *PloS one*, vol. 10, no. 5, e0124929, 2015.
- [57] A. Majeed, T. Javed, and A. Ghaffari, “Numerical investigation on flow of second grade fluid due to stretching cylinder with solet and dufour effects,” *Journal of Molecular Liquids*, vol. 221, pp. 878–884, 2016.
- [58] M. Yavuz, N. Sene, and M. Yıldız, “Analysis of the influences of parameters in the fractional second-grade fluid dynamics,” *Mathematics*, vol. 10, no. 7, p. 1125, 2022.
- [59] A. Stubhaug, *The Mathematician Sophus Lie: It was the audacity of my thinking*. Springer, 2002.
- [60] M. Akgül and M Pakdemirli, “Lie group analysis of a non-Newtonian fluid flow over a porous surface,” *Scientia Iranica*, vol. 19, no. 6, pp. 1534–1540, 2012.
- [61] M. Jalil and S. Asghar, “Flow and heat transfer of powell–eyring fluid over a stretching surface: A lie group analysis,” *Journal of fluids engineering*, vol. 135, no. 12, 2013.
- [62] K. U. Rehman, N. U. Saba, M. Y. Malik, and A. A. Malik, “Encountering heat and mass transfer mechanisms simultaneously in powell-erying fluid through lie symmetry approach,” *Case studies in thermal engineering*, vol. 10, pp. 541–549, 2017.
- [63] A. A. Afify and M. A. El-Aziz, “Lie group analysis of flow and heat transfer of non-Newtonian nanofluid over a stretching surface with convective boundary condition,” *Pramana*, vol. 88, no. 2, pp. 1–10, 2017.
- [64] N. C. Roşca, A. V. Roşca, and I. Pop, “Lie group symmetry method for MHD double-diffusive convection from a permeable vertical stretching/shrinking sheet,” *Computers & mathematics with applications*, vol. 71, no. 8, pp. 1679–1693, 2016.
- [65] H. A. Ogunseye, H. Mondal, P. Sibanda, and H. Mambili-Mamboundou, “Lie group analysis of a powell–eyring nanofluid flow over a stretching surface with variable properties,” *SN Applied Sciences*, vol. 2, no. 1, pp. 1–12, 2020.

- [66] M. E. Karim, M. A. Samad, and M Ferdows, “Magneto Hall effect on unsteady elasto-viscous nanofluid slip flow in a channel in presence of thermal radiation and heat generation with Brownian motion,” in *AIP Conference Proceedings*, AIP Publishing LLC, vol. 1851, 2017, p. 020 052.
- [67] M. E. Karim, M. A. Samad, and M Ferdows, “Numerical study of the effect of variable viscosity on unsteady pulsatile nanofluid flow through a Couette channel of stretching wall with convective heat transfer,” in *AIP Conference Proceedings*, AIP Publishing LLC, vol. 2121, 2019, p. 070 005.
- [68] M. E. Karim and M. A. Samad, “Effect of Brownian diffusion on squeezing elasto-viscous nanofluid flow with Cattaneo-Christov heat flux model in a channel with double slip effect,” *Applied Mathematics*, vol. 11, no. 4, pp. 277–291, 2020.
- [69] J. W. Daily, W James, D. R. Harleman, *et al.*, *Fluid dynamics*. Addison-Wesley, 1966.
- [70] L. Prandtl, “Über flüssigkeitsbewegung bei sehr kleiner reibung,” *Verhandl. III, Internat. Math.-Kong., Heidelberg, Teubner, Leipzig, 1904*, pp. 484–491, 1904.
- [71] C.-G. Falthammar, “Plasma physics from laboratory to cosmos-the life and achievements of hannes alfven,” *IEEE transactions on plasma science*, vol. 25, no. 3, pp. 409–414, 1997.
- [72] E. F. Northrup, “Some newly observed manifestations of forces in the interior of an electric conductor,” *Physical Review (Series I)*, vol. 24, no. 6, p. 474, 1907.
- [73] P. Sporn and A. Kantrowitz, “Magnetohydrodynamics: Future power process?” *Power*, vol. 103, no. 11, pp. 62–65, 1959.
- [74] L. Steg and G. W. Sutton, “The prospects of MHD power generation,” *Astronautics*, vol. 5, pp. 22–25, 1960.
- [75] M. Faraday, “Vi. the bakerian lecture.-experimental researches in electricity.-second series,” *Philosophical Transactions of the Royal Society of London*, no. 122, pp. 163–194, 1832.
- [76] J. A. Shercliff, *The theory of electromagnetic flow-measurement*. CUP Archive, 1962.

- [77] A Kolin, "An electromagnetic flowmeter. principle of the method and its application to bloodflow measurements," *Proceedings of the Society for Experimental Biology and Medicine*, vol. 35, no. 1, pp. 53–56, 1936.
- [78] A. F. Kolesnichenko, "Electromagnetic processes in liquid material in the USSR and east european countries," *ISIJ international*, vol. 30, no. 1, pp. 8–26, 1990.
- [79] R. B. Bird, "Transport phenomena," *Appl. Mech. Rev.*, vol. 55, no. 1, R1–R4, 2002.
- [80] D. W. Green and M. Z. Southard, *Perry's chemical engineers' handbook*. McGraw-Hill Education, 2019.
- [81] J. C. Maxwell, *A treatise on electricity and magnetism*. Clarendon press, 1873, vol. 1.
- [82] C. G. Granqvist and R. A. Buhrman, "Ultrafine metal particles," *Journal of applied Physics*, vol. 47, no. 5, pp. 2200–2219, 1976.
- [83] S. U. S. Choi, Z. G. Zhang, W. Yu, F. E. Lockwood, and E. A. Grulke, "Anomalous thermal conductivity enhancement in nanotube suspensions," *Applied physics letters*, vol. 79, no. 14, pp. 2252–2254, 2001.
- [84] S Yatsuya, Y Tsukasaki, K Mihama, and R Uyeda, "Preparation of extremely fine particles by vacuum evaporation onto a running oil substrate," *Journal of Crystal Growth*, vol. 45, pp. 490–494, 1978.
- [85] S. K. Das, S. U. S. Choi, and H. E. Patel, "Heat transfer in nanofluids—a review," *Heat transfer engineering*, vol. 27, no. 10, pp. 3–19, 2006.
- [86] J. A. Eastman, S. U. S. Choi, S. Li, W Yu, and L. J. Thompson, "Anomalously increased effective thermal conductivities of ethylene glycol-based nanofluids containing copper nanoparticles," *Applied physics letters*, vol. 78, no. 6, pp. 718–720, 2001.
- [87] R. L. Hamilton and O. K. Crosser, "Thermal conductivity of heterogeneous two component systems," *Industrial & Engineering chemistry fundamentals*, vol. 1, no. 3, pp. 187–191, 1962.
- [88] X. Wang, X. Xu, and S. U. S. Choi, "Thermal conductivity of nanoparticle-fluid mixture," *Journal of thermophysics and heat transfer*, vol. 13, no. 4, pp. 474–480, 1999.

- [89] M Chopkar, S Sudarshan, P. K. Das, and I Manna, "Effect of particle size on thermal conductivity of nanofluid," *Metallurgical and materials transactions A*, vol. 39, no. 7, pp. 1535–1542, 2008.
- [90] H. Xie, J. Wang, T. Xi, and Y. Liu, "Thermal conductivity of suspensions containing nanosized *SiC* particles," *International Journal of Thermophysics*, vol. 23, no. 2, pp. 571–580, 2002.
- [91] H. C. Brinkman, "The viscosity of concentrated suspensions and solutions," *The Journal of chemical physics*, vol. 20, no. 4, pp. 571–571, 1952.
- [92] B. C. Pak and Y. I. Cho, "Hydrodynamic and heat transfer study of dispersed fluids with submicron metallic oxide particles," *Experimental Heat Transfer an International Journal*, vol. 11, no. 2, pp. 151–170, 1998.
- [93] K Vafayi, M Calandra, and O Gunnarsson, "Electronic thermal conductivity at high temperatures: Violation of the Wiedemann-franz law in narrow-band metals," *Physical Review B*, vol. 74, no. 23, p. 235 116, 2006.
- [94] S. Ganguly, S. Sikdar, and S. Basu, "Experimental investigation of the effective electrical conductivity of aluminum oxide nanofluids," *Powder Technology*, vol. 196, no. 3, pp. 326–330, 2009.
- [95] L. Wang and J. Fan, "Nanofluids research: Key issues," *Nanoscale research letters*, vol. 5, no. 8, pp. 1241–1252, 2010.
- [96] K. V. Wong and O. De Leon, "Applications of nanofluids: Current and future," *Advances in mechanical engineering*, vol. 2, p. 519 659, 2010.
- [97] S Senthilraja, M Karthikeyan, and R Gangadevi, "Nanofluid applications in future automobiles: Comprehensive review of existing data," *Nano-Micro Letters*, vol. 2, no. 4, pp. 306–310, 2010.
- [98] V. Trisaksri and S. Wongwises, "Critical review of heat transfer characteristics of nanofluids," *Renewable and sustainable energy reviews*, vol. 11, no. 3, pp. 512–523, 2007.
- [99] D. Wen, G. Lin, S. Vafaei, and K. Zhang, "Review of nanofluids for heat transfer applications," *Particuology*, vol. 7, no. 2, pp. 141–150, 2009.

- [100] J Routbort *et al.*, “Argonne national lab, michellin north america, st,” *Gobain Corp*, 2009.
- [101] I. C. Nelson, D. Banerjee, and R. Ponnappan, “Flow loop experiments using polyalphaolefin nanofluids,” *Journal of thermophysics and heat transfer*, vol. 23, no. 4, pp. 752–761, 2009.
- [102] S. Kim, I. C. Bang, J Buongiorno, and L. Hu, “Study of pool boiling and critical heat flux enhancement in nanofluids,” *Bulletin of the Polish Academy of Sciences: Technical Sciences*, vol. 55, no. 2, 2007.
- [103] J Buongiorno, L. Hu, G Apostolakis, R Hannink, T Lucas, and A Chupin, “A feasibility assessment of the use of nanofluids to enhance the in-vessel retention capability in light-water reactors,” *Nuclear Engineering and Design*, vol. 239, no. 5, pp. 941–948, 2009.
- [104] R. Saidur, K. Leong, and H. A. Mohammed, “A review on applications and challenges of nanofluids,” *Renewable and sustainable energy reviews*, vol. 15, no. 3, pp. 1646–1668, 2011.
- [105] S. P. Jang and S. U. Choi, “Cooling performance of a microchannel heat sink with nanofluids,” *Applied Thermal Engineering*, vol. 26, no. 17-18, pp. 2457–2463, 2006.
- [106] Y.-T. Chen, W.-C. Wei, S.-W. Kang, and C.-S. Yu, “Effect of nanofluid on flat heat pipe thermal performance,” in *2008 Twenty-fourth Annual IEEE Semiconductor Thermal Measurement and Management Symposium*, IEEE, 2008, pp. 16–19.
- [107] D Singh, J Toutbort, G Chen, *et al.*, “Heavy vehicle systems optimization merit review and peer evaluation,” *Annual Report, Argonne National Laboratory*, vol. 23, pp. 405–411, 2006.
- [108] C. Kleinstreuer, J. Li, and J. Koo, “Microfluidics of nano-drug delivery,” *International Journal of Heat and Mass Transfer*, vol. 51, no. 23-24, pp. 5590–5597, 2008.
- [109] J.-F. Yan and J. Liu, “Nanocryosurgery and its mechanisms for enhancing freezing efficiency of tumor tissues,” *Nanomedicine: Nanotechnology, Biology and Medicine*, vol. 4, no. 1, pp. 79–87, 2008.
- [110] R. S. Rivlin and J. L. Ericksen, “Stress-deformation relations for isotropic materials,” *Collected Papers of RS Rivlin*, pp. 911–1013, 1997.

- [111] W. Noll, "On the continuity of the solid and fluid states," *Journal of Rational Mechanics and Analysis*, vol. 4, pp. 3–81, 1955.
- [112] B. D. Coleman and W. Noll, "Foundations of linear viscoelasticity," *Reviews of modern physics*, vol. 33, no. 2, p. 239, 1961.
- [113] P. J. Olver and P. Rosenau, "The construction of special solutions to partial differential equations," *Physics Letters A*, vol. 114, no. 3, pp. 107–112, 1986.
- [114] L. V. Ovsiannikov, *Group analysis of differential equations*. Academic press, 2014.
- [115] G. W. Bluman, G. J. Reid, and S. Kumei, "New classes of symmetries for partial differential equations," *Journal of Mathematical Physics*, vol. 29, no. 4, pp. 806–811, 1988.
- [116] J. C. Strikwerda, *Finite difference schemes and partial differential equations*. SIAM, 2004.
- [117] A. R. Mitchell and D. F. Griffiths, "The finite difference method in partial differential equations," *A Wiley-Interscience Publication*, 1980.
- [118] L. F. Shampine and S. Thompson, "Solving ddes in matlab," *Applied Numerical Mathematics*, vol. 37, no. 4, pp. 441–458, 2001.
- [119] P. R. Nachtsheim and P. Swigert, "Satisfaction of the asymptotic boundary conditions in numerical solution of the system of non-linear equations of boundary layer type," Tech. Rep., 1965.
- [120] W. Khan and I Pop, "Boundary-layer flow of a nanofluid past a stretching sheet," *International journal of heat and mass transfer*, vol. 53, no. 11-12, pp. 2477–2483, 2010.
- [121] A. Kuznetsov and D. Nield, "Natural convective boundary-layer flow of a nanofluid past a vertical plate," *International Journal of Thermal Sciences*, vol. 49, no. 2, pp. 243–247, 2010.
- [122] R. S. R. Gorla, A. Chamkha, and A. M. Rashad, "Mixed convective boundary layer flow over a vertical wedge embedded in a porous medium saturated with a nanofluid," in *2010 3rd International Conference on Thermal Issues in Emerging Technologies Theory and Applications*, IEEE, 2010, pp. 445–451.



- [123] M. H. Matin, R Hosseini, M Simiari, and P Jahangiri, “Entropy generation minimization of nanofluid flow in a MHD channel considering thermal radiation effect,” *Mechanics*, vol. 19, no. 4, pp. 445–450, 2013.
- [124] N. A. Haroun, S. Mondal, and P. Sibanda, “Unsteady natural convective boundary-layer flow of MHD nanofluid over a stretching surfaces with chemical reaction using the spectral relaxation method: A revised model,” *Procedia Engineering*, vol. 127, pp. 18–24, 2015.
- [125] M. Rahman, A. V. Rosca, and I Pop, “Boundary layer flow of a nanofluid past a permeable exponentially shrinking surface with convective boundary condition using Buongiorno’s model,” *International Journal of Numerical Methods for Heat & Fluid Flow*, vol. 25, no. 2, pp. 299–319, 2015.
- [126] G. W. Sutton and A. Sherman, *Engineering magnetohydrodynamics*. Courier Dover Publications, NY, 2006.
- [127] A. O. Ali, O. D. Makinde, and Y. Nkansah-Gyekye, “Effect of Hall current on unsteady MHD couette flow and heat transfer of nano fluids in a rotating system,” *Appl. Comput. Math.*, vol. 4, pp. 232–244, 2015.
- [128] A. H. P. Skelland, *Non-Newtonian flow and heat transfer*. John Wiley and Sons, Inc., New York, 1967.
- [129] J. Hartnett, Y. Cho, and W Rohsenow, “Non-Newtonian fluids,” *Handbook of heat transfer*, vol. 5, pp. 126–131, 1998.
- [130] H. Kai-Long, “Unsteady mixed convection visco-elastic flow and heat transfer in a thin film flow over a porous stretching sheet with internal heat generation,” *International Journal of Physical Sciences*, vol. 6, no. 22, pp. 5080–5090, 2011.
- [131] M Mustafa and A. Mushtaq, “Model for natural convective flow of visco-elastic nanofluid past an isothermal vertical plate,” *The European Physical Journal Plus*, vol. 130, no. 9, pp. 1–9, 2015.
- [132] G. C. Rana and R. Chand, “Rayleigh-Bénard convection in an elastico-viscous Walters’ (model B’) nanofluid layer,” *Bulletin of the Polish Academy of Sciences. Technical Sciences*, vol. 63, no. 1, 235–244, 2015.

- [133] B. Coleman and W. Noll, “An approximation theorem for functionals, with applications in continuum mechanics,” *Arch. Rational Mech. Anal.*,
- [134] H. Markovitz and B. D. Coleman, “Incompressible second-order fluids,” *Advances in applied mechanics*, vol. 8, pp. 69–101, 1964.
- [135] Y.-L. Chen and K.-Q. Zhu, “Couette–poiseuille flow of Bingham fluids between two porous parallel plates with slip conditions,” *Journal of Non-Newtonian Fluid Mechanics*, vol. 153, no. 1, pp. 1–11, 2008.
- [136] S Srinivas, T Malathy, and A. S. Reddy, “A note on thermal-diffusion and chemical reaction effects on MHD pulsating flow in a porous channel with slip and convective boundary conditions,” *Journal of King Saud University-Engineering Sciences*, vol. 28, no. 2, pp. 213–221, 2016.
- [137] V. Sridhara and L. N. Satapathy, “ $Al_2O_3$ -based nanofluids: A review,” *Nanoscale research letters*, vol. 6, no. 1, pp. 1–16, 2011.
- [138] O. C. Farokhzad and R. Langer, “Nanomedicine: Developing smarter therapeutic and diagnostic modalities,” *Advanced drug delivery reviews*, vol. 58, no. 14, pp. 1456–1459, 2006.
- [139] M. Uddin, K. S. Al Kalbani, M. Rahman, M. Alam, N Al-Salti, and I. Eltayeb, “Fundamentals of nanofluids: Evolution, applications and new theory,” *International Journal of Biomathematics and Systems Biology*, vol. 2, no. 1, pp. 1–32, 2016.
- [140] C.-Y. Wang, “Pulsatile Flow in a Porous Channel,” *Journal of Applied Mechanics*, vol. 38, no. 2, pp. 553–555, Jun. 1971.
- [141] A. Bestman, “Pulsatile flow in heated porous channel,” *International Journal of Heat and Mass Transfer*, vol. 25, no. 5, pp. 675–682, 1982.
- [142] A. Ali and O. Makinde, “Modelling the effect of variable viscosity on unsteady Couette flow of nanofluids with convective cooling,” *Journal of Applied Fluid Mechanics*, vol. 8, no. 4, pp. 793–802, 2015.
- [143] M. H. Mkwizu and O. D. Makinde, “Entropy generation in a variable viscosity channel flow of nanofluids with convective cooling,” *Comptes Rendus Mécanique*, vol. 343, no. 1, pp. 38–56, 2015.

- [144] A Vijayalakshmi and S Srinivas, "A study on hydromagnetic pulsating flow of a nanofluid in a porous channel with thermal radiation," *Journal of Mechanics*, vol. 33, no. 2, pp. 213–224, 2017.
- [145] L. S. Sundar, M. H. Farooky, S. N. Sarada, and M. Singh, "Experimental thermal conductivity of ethylene glycol and water mixture based low volume concentration of  $Al_2O_3$  and  $CuO$  nanofluids," *International Communications in Heat and Mass Transfer*, vol. 41, pp. 41–46, 2013.
- [146] O Pinkus and B Sternlicht, "Theory of hydrodynamic lubrication, 1961," *MCGraw-Hm, New York*, pp. 81–85, 1949.
- [147] R. B. Bird, R. C. Armstrong, and O. Hassager, "Dynamics of polymeric liquids: Fluid mechanics. vol. 1," 1987.
- [148] M Brust *et al.*, "Rheology of human blood plasma: Viscoelastic versus Newtonian behavior," *Physical Review Letters*, vol. 110, no. 7, p. 078 305, 2013.
- [149] X. K. Li, Y. Luo, Y. Qi, and R. Zhang, "On non-Newtonian lubrication with the upper convected Maxwell model," *Applied Mathematical Modelling*, vol. 35, no. 5, pp. 2309–2323, 2011.
- [150] T. Sochi, "Flow of non-Newtonian fluids in porous media," *Journal of Polymer Science Part B: Polymer Physics*, vol. 48, no. 23, pp. 2437–2767, 2010.
- [151] V. Fox, L. Erickson, and L. Fan, "The laminar boundary layer on a moving continuous flat sheet immersed in a non-Newtonian fluid," *AIChE Journal*, vol. 15, no. 3, pp. 327–333, 1969.
- [152] K. R. Rajagopal and A. Gupta, "On a class of exact solutions to the equations of motion of a second grade fluid," *International Journal of Engineering Science*, vol. 19, no. 7, pp. 1009–1014, 1981.
- [153] H. Andersson, K. Bech, and B. Dandapat, "Magnetohydrodynamic flow of a power-law fluid over a stretching sheet," *International Journal of Non-Linear Mechanics*, vol. 27, no. 6, pp. 929–936, 1992.

- [154] K. Sadeghy and M. Sharifi, “Local similarity solution for the flow of a “second-grade” viscoelastic fluid above a moving plate,” *International Journal of Non-Linear Mechanics*, vol. 39, no. 8, pp. 1265–1273, 2004.
- [155] K. Bhattacharyya, T. Hayat, and R. S. R. Gorla, “Heat transfer in the boundary layer flow of Maxwell fluid over a permeable shrinking sheet,” *Therm. Energy Power Eng*, vol. 2, pp. 72–78, 2013.
- [156] T Hayat, Z Abbas, and M Sajid, “Series solution for the upper-convected Maxwell fluid over a porous stretching plate,” *Physics Letters A*, vol. 358, no. 5-6, pp. 396–403, 2006.
- [157] M. Pakdemirli, “Similarity analysis of boundary layer equations of a class of non-Newtonian fluids,” *International Journal of Non-Linear Mechanics*, vol. 29, no. 2, pp. 187–196, 1994.
- [158] M Bilal, M Sagheer, and S Hussain, “Three dimensional MHD upper-convected Maxwell nanofluid flow with nonlinear radiative heat flux,” *Alexandria engineering journal*, vol. 57, no. 3, pp. 1917–1925, 2018.
- [159] C. Fetecau and C. Fetecau, “A new exact solution for the flow of a Maxwell fluid past an infinite plate,” *International Journal of Non-Linear Mechanics*, vol. 38, no. 3, pp. 423–427, 2003.
- [160] N. Halim and N. F. M. Noor, “Analytical solution for Maxwell nanofluid boundary layer flow over a stretching surface,” in *AIP Conference Proceedings*, AIP Publishing, vol. 1682, 2015, p. 020 006.
- [161] M Mustafa, J. A. Khan, T Hayat, and A Alsaedi, “Simulations for Maxwell fluid flow past a convectively heated exponentially stretching sheet with nanoparticles,” *AIP Advances*, vol. 5, no. 3, p. 037 133, 2015.
- [162] J. Fourier, *Theorie analytique de la chaleur, par M. Fourier*. Chez Firmin Didot, père et fils, 1822.
- [163] C. Cattaneo, “Sulla conduzione del calore,” *Atti Sem. Mat. Fis. Univ. Modena*, vol. 3, pp. 83–101, 1948.

- [164] C. Christov, “On frame indifferent formulation of the Maxwell–cattaneo model of finite-speed heat conduction,” *Mechanics Research Communications*, vol. 36, no. 4, pp. 481–486, 2009.
- [165] M. Ciarletta and B. Straughan, “Uniqueness and structural stability for the Cattaneo–Christov equations,” *Mechanics Research Communications*, vol. 37, no. 5, pp. 445–447, 2010.
- [166] B. Straughan, “Thermal convection with the Cattaneo–Christov model,” *International Journal of Heat and Mass Transfer*, vol. 53, no. 1-3, pp. 95–98, 2010.
- [167] V. Tibullo and V. Zampoli, “A uniqueness result for the Cattaneo–Christov heat conduction model applied to incompressible fluids,” *Mechanics Research Communications*, vol. 38, no. 1, pp. 77–79, 2011.
- [168] S. Han, L. Zheng, C. Li, and X. Zhang, “Coupled flow and heat transfer in viscoelastic fluid with Cattaneo–Christov heat flux model,” *Applied Mathematics Letters*, vol. 38, pp. 87–93, 2014.
- [169] G. Layek and N. Pati, “Bifurcations and chaos in convection taking non-Fourier heat flux,” *Physics Letters A*, vol. 381, no. 41, pp. 3568–3575, 2017.
- [170] S. M. Upadhyaya, C. Raju, *et al.*, “Cattaneo-Christov heat flux model for magnetohydrodynamic flow in a suspension of dust particles towards a stretching sheet,” *Nonlinear Engineering*, vol. 7, no. 3, pp. 237–246, 2018.
- [171] F. Al Sulti, “Impact of Cattaneo–Christov heat flux model on stagnation-point flow toward a stretching sheet with slip effects,” *Journal of Heat Transfer*, vol. 141, no. 2, p. 022 003, 2019.
- [172] M. Stefan, “Versuch über die scheinbare adhäsion, sitzungsber,” *Abt. II, Österr.*, vol. 69, pp. 713–721, 1874.
- [173] N. Phan-Thien and R. Tanner, “Viscoelastic squeeze-film flows–Maxwell fluids,” *Journal of Fluid Mechanics*, vol. 129, pp. 265–281, 1983.
- [174] M. Mustafa, T. Hayat, and S. Obaidat, “On heat and mass transfer in the unsteady squeezing flow between parallel plates,” *Meccanica*, vol. 47, no. 7, pp. 1581–1589, 2012.

- [175] N Akmal, M Sagheer, and S Hussain, “Numerical study focusing on the entropy analysis of MHD squeezing flow of a nanofluid model using Cattaneo–Christov theory,” *AIP Advances*, vol. 8, no. 5, p. 055 201, 2018.
- [176] M. V. Krishna and A. J. Chamkha, “Hall effects on MHD squeezing flow of a water-based nanofluid between two parallel disks,” *Journal of porous media*, vol. 22, no. 2, 2019.
- [177] C. le Roux, “Existence and uniqueness of the flow of second-grade fluids with slip boundary conditions,” *Archive for Rational Mechanics and Analysis*, vol. 148, no. 4, pp. 309–356, 1999.
- [178] Y. Jiang, H. Qi, H. Xu, and X. Jiang, “Transient electroosmotic slip flow of fractional Oldroyd-B fluids,” *Microfluidics and Nanofluidics*, vol. 21, no. 1, p. 7, 2017.
- [179] C. Navier, “Memoirs de l’academie royale des sciences de l’institut de france, vol. 1,” *Royale des Sciences de l’Institut de France*, pp. 389–440, 1823.
- [180] M. E. Karim, M. A. Samad, and M. M. Hasan, “Dufour and sores effect on steady MHD flow in presence of heat generation and magnetic field past an inclined stretching sheet,” *Open journal of fluid dynamics*, vol. 2, no. 3, pp. 91–100, 2012.
- [181] H. M. Sithole, S. Mondal, P. Sibanda, and S. S. Motsa, “An unsteady MHD Maxwell nanofluid flow with convective boundary conditions using spectral local linearization method,” *Open Physics*, vol. 15, no. 1, pp. 637–646, 2017.
- [182] D. Levi, L. Vinet, and P. Winternitz, “Lie group formalism for difference equations,” *Journal of Physics A: Mathematical and General*, vol. 30, no. 2, p. 633, 1997.
- [183] M. Yürüsoy and M. Pakdemidotrliidot, “Symmetry reductions of unsteady three-dimensional boundary layers of some non-Newtonian fluids,” *International Journal of Engineering Science*, vol. 35, no. 8, pp. 731–740, 1997.
- [184] N. K. Ibragimov and N. K. Ibragimov, *Elementary Lie group analysis and ordinary differential equations*. Wiley New York, 1999, vol. 197.

- [185] A. Rosmila, R. Kandasamy, and I. Muhaimin, “Lie symmetry group transformation for MHD natural convection flow of nanofluid over linearly porous stretching sheet in presence of thermal stratification,” *Applied Mathematics and Mechanics*, vol. 33, no. 5, pp. 593–604, 2012.
- [186] C. Chen and Y.-L. Jiang, “Lie group analysis method for two classes of fractional partial differential equations,” *Communications in Nonlinear Science and Numerical Simulation*, vol. 26, no. 1-3, pp. 24–35, 2015.
- [187] M. J. Uddin, M. N. Kabir, and Y. M. Alginahi, “Lie group analysis and numerical solution of magnetohydrodynamic free convective slip flow of micropolar fluid over a moving plate with heat transfer,” *Computers & Mathematics with Applications*, vol. 70, no. 5, pp. 846–856, 2015.
- [188] M. Uddin, M. Rashidi, H. H. Alsulami, S Abbasbandy, and N Freidoonimeh, “Two parameters Lie group analysis and numerical solution of unsteady free convective flow of non-Newtonian fluid,” *Alexandria Engineering Journal*, vol. 55, no. 3, pp. 2299–2308, 2016.
- [189] C. Fetecau, D. Vieru, T. Abbas, and R. Ellahi, “Analytical solutions of upper convected Maxwell fluid with exponential dependence of viscosity under the influence of pressure,” *Mathematics*, vol. 9, no. 4, p. 334, 2021.
- [190] J. Raza, A. M. Rohni, and Z. Omar, “Numerical investigation of copper-water (Cu-water) nanofluid with different shapes of nanoparticles in a channel with stretching wall: Slip effects,” *Mathematical and Computational Applications*, vol. 21, no. 4, p. 43, 2016.
- [191] S. Kiwan and M. Al-Nimr, “Investigation into the similarity solution for boundary layer flows in microsystems,” *ASME J of Heat Transfer*, vol. 132, no. 4, p. 041 011, 2010.
- [192] S. Z. Alamri, A. A. Khan, M. Azeez, and R Ellahi, “Effects of mass transfer on MHD second grade fluid towards stretching cylinder: A novel perspective of Cattaneo–Christov heat flux model,” *Physics Letters A*, vol. 383, no. 2-3, pp. 276–281, 2019.
- [193] I. M. Alarifi *et al.*, “MHD flow and heat transfer over vertical stretching sheet with heat sink or source effect,” *Symmetry*, vol. 11, no. 3, p. 297, 2019.

- [194] J. R. Reddy, V Sugunamma, and N Sandeep, “Thermophoresis and brownian motion effects on unsteady MHD nanofluid flow over a slendering stretching surface with slip effects,” *Alexandria Engineering Journal*, vol. 57, no. 4, pp. 2465–2473, 2018.